DISSERTATION

How Brain Rhythms Guide Memory and Decisions

zur Erlangung des akademischen Grades
Doktor der Naturwissenschaften (Dr. rer. nat. / Ph. D.)
am Fachbereich Erziehungswissenschaften und Psychologie
der Freien Universität Berlin

von

HORST ALEXANDER VON LAUTZ

Berlin 2018

1. Gutachter: Prof. Dr. Felix Blankenburg
2. Gutachter: Dr. Radoslaw Cichy

Tag der Disputation: 13.02.2019

Acknowledgements

This thesis could not have been done without the help of many colleagues, friends, and family, who have supported me throughout the last years.

First of all, I want to thank Felix Blankenburg for all his time, guidance and the fact that he created such a nice atmosphere to do science in. My gratitude goes to Mark Stokes, for being such an approachable supervisor, always taking the time to have in-depth discussions, and believing in me. I also want to thank John-Dylan Haynes and Philipp Sterzer for having an open ear and guiding me especially in the beginning of this PhD.

Many thanks to my colleagues, both in Berlin at the NNU and in Oxford at OHBA. Without your day-to-day discussions, incredible support and overall good vibes, the last few years would not have been half the fun. Additionally, I want to thank the MEG team in Bennewitz and the Haus 6 residents for all their help.

I am grateful to Leonie, my family, Zwingli, and the gladiators for always being there for me, supporting me through the ups and downs, and always having my back.

Finally, I want to recognize all the institutions that have funded this research. First of all, the Bernstein Center, who beyond giving me financial support has introduced me to a dynamic and interactive research community. Many thanks also to the Oxford Centre for Human Brain Activity, the Studienstiftung des Deutschen Volkes, the DAAD, the Ernst-Reuter Gesellschaft, the Club der Ehemaligen, and the Wikimedia foundation.

Thank you!

Table of Contents

Abstract

In our daily lives we are faced with thousands of decisions: from complex 'should I cross while it's on a red light?', to abstract 'do I spell color with o or ou?', to sensory dominated questions like 'did my phone just vibrate?'. To navigate all of these different types of decisions, the brain has to incorporate a plethora of information from sensory and memory systems, requiring many neuronal populations from distinct cortical areas to work together. Neuroscientists posit that cortical oscillations play an important part in this process. I investigated the role of such cortical rhythms for the short retention of information in working memory and decision making with three experimental studies.

In all experiments, participants were asked to compare two sequentially presented stimuli. To solve this task, the first stimulus has to be kept in memory for a short while and is then compared to the second. While participants held the first stimulus in memory, magneto- and electroencephalographic recordings revealed a parametric modulation of parietal and prefrontal beta oscillations with the to-be-remembered stimulus feature. At the same time, we observed a previously unknown prefrontal gamma power decrease that was negatively correlated with the beta band effects. Therefore we suspect that there is a fronto-parietal network that communicates in these two frequency bands during working memory. In addition, we found decision-related activity in premotor beta power that encoded participants' choices 0.7 seconds before they enacted their responses. Moreover, we also found a well-known parietal signal, which tracked the evolution of the decision over time. Interestingly, this signal was modulated by the difficulty of the decisions, indicating that present theories about perceptual decision making need to be extended.

Zusammenfassung

Der Mensch trifft täglich tausende Entscheidungen, von komplexen („Gehe ich über die rote Ampel?“), über abstrakte („Buchstabiere ich Foto mit F oder Ph?“), zu sensorisch geprägten („Hat mein Telefon gerade vibriert?“). Das Gehirn muss dabei flexibel auf eine Vielzahl von sensorischen Reizen und Entscheidungstypen reagieren. Um dies zu ermöglichen, arbeiten viele Neurone in ganz unterschiedlichen kortikalen Arealen zusammen. Neurowissenschaftler vermuten, dass kortikale Oszillationen dabei eine zentrale Rolle spielen. Sie reflektieren das Zusammenwirken vieler Neurone und werden zur Kommunikation neuronaler Populationen genutzt. In der vorliegenden Arbeit wurde die Rolle einzelner Rhythmen für das kurzfristige Speichern von Informationen im Arbeitsgedächtnis, sowie das Treffen von Entscheidungen untersucht.

Dieser Dissertation liegen drei Studien zugrunde, im Rahmen derer Versuchspersonen zwei nacheinander dargebotene Stimuli vergleichen sollten. Um diese Aufgabe zu bewältigen, muss der erste Stimulus kurz im Gedächtnis behalten werden. Dann kommt es zur eigentlichen Entscheidung, dem Abgleich der beiden Stimuli. Bei diesem Versuch konnten wir mit Hilfe von Magneto- und Elektroenzephalographie Oszillationen messen, die sich mit den Stimuluseigenschaften veränderten. Arbeitsgedächtnisprozesse waren dabei mit Beta-Oszillationen assoziiert. Insbesondere zeigten sich parietale und präfrontale Beta-Oszillationen, die mit Gamma-Oszillationen im präfrontalen Kortex zusammenspielten. Daher vermuten wir, dass ein fronto-parietales Netzwerk für das Behalten von Stimulus-Information von Bedeutung ist und diskutieren im Folgenden zugrundeliegende Mechanismen. Außerdem konnten wir während des Treffens von Entscheidungen prämotorische Beta-Oszillationen messen, die 0,7 Sekunden vor der Antwort der Versuchsteilnehmer die Entscheidung reflektierten. Darüber hinaus zeigten sich auch bekannte parietale Signale, die den Prozess der Entscheidungsfindung abbildeten. Interessanterweise waren diese Signale vom Schwierigkeitsgrad der Aufgabe abhängig. Dies spricht dafür, dass aktuelle Theorien zu neuronalen Grundlagen der Entscheidungsfindung ergänzt werden müssen.

Abbreviations

BA	Brodmann area
BOLD	blood-oxygen-level dependent
CPP	centro-parietal positivity
DDM	drift-diffusion model
EEG	electroencephalography
ERP	event related potential
$f1/f2$	vibrotactile stimulus 1 / 2
FEF	frontal eye fields
fMRI	functional magnetic resonance imaging
IFG	inferior frontal gyrus
IPL	intraparietal lobule
IPS	intraparietal sulcus
LIP	lateral intraparietal area
MI	primary motor cortex
MVPA	multivariate pattern analysis
MEG	magnetoencephalography
PFC	prefrontal cortex
PMC	premotor cortex
PPC	posterior parietal cortex
RDM	random-dot motion
RF	receptive field
SI	primary somatosensory cortex
SII	secondary somatosensory cortex
$S1/S2$	RDM stimulus 1 / 2
SC	superior colliculus
SDT	signal detection theory
SFC	sequential frequency comparison
SSEP/F	steady-state evoked potential/field
TMS	transcranial magnetic stimulation
WM	working memory

List of Original Articles

This dissertation is based on the following peer-reviewed articles:

von Lautz AH, Herding J, Ludwig S, Nierhaus T, Maess B, Villringer A and Blankenburg F (2017): Gamma and Beta Oscillations in Human MEG Encode the Contents of Vibrotactile Working Memory. Front. Hum. Neurosci. 11:576. doi: 10.3389/fnhum.2017.00576

Herding J, Ludwig S, **von Lautz AH**, Spitzer B and Blankenburg F (under review): Centro-parietal EEG potentials index subjective evidence and difficulty during perceptual decision making. Neuroimage

von Lautz AH, Herding J and Blankenburg F (under review): Neuronal Signatures of a Random-Dot Motion Comparison task. Neuroimage

1 Introduction

In this particularly hot summer it is not beyond imagination that you choose to buy a watermelon from a small stand on the way home. Of course, you wish to buy not any watermelon, but a ripe and juicy one. According to humourist literature ("fixating the melon's secret", Kishon & Labatzke, 1975) the procedure of selecting a ripe and juicy melon consists of looking, feeling, smelling, and listening for a hollow sound and then comparing these features to another watermelon. Moreover, if the quality of tested watermelons doesn't suit you, you go to the next stand and try the ones there. This example encompasses several features of typical decision-making tasks used in neuroscience. To find just the right watermelon you need to *perceive* the colour, texture, smell, and sound. Then, you must keep this information for a short while in *memory* before testing the subsequent watermelon. Finally, you are tasked with judging which one was better: *making a decision*. Neuroscientists use such tasks in simple form to have control about the mental steps necessary to correctly solve this problem. For example, they would typically let participants only see the melons and let them decide between two, a challenge called 'sequential comparison task'. Or an experimenter would give participants the job of testing watermelons from multiple stands and deciding whether they were of good or poor quality. In this case, a person would need to *sequentially sample* watermelons up until she is confident that the particular stand sells good- or poor-quality fruit. In contrast with the study of psychophysics, which tests only the behaviour of participants, neuroscientists typically also record signals from the brain during such tasks and try to determine the neural basis of each mental step (e.g., *perceiving, memory, making a decision*).

In the present thesis, I will introduce how neuroscientists study such decisions in humans and other species. I will describe major lines of research investigating the neural substrates of the outlined mental steps using two well-studied experimental paradigms that fit to the aforementioned watermelon selection: sequential comparison and sequential sampling tasks. Then I will present my contribution to this field of research in the form of three

studies that provide new insights into human working memory and decision making with magneto- and electroencephalography (M/EEG). Subsequently, I will link my findings to the larger context of current research and point to future avenues.

1.1 Researching perceptual decision making

The study of human decisions has a long history reaching back to ancient Greece (Aristotle, 1987; Epicurus, 1940). Whereas Greek philosophers argued for a nonmaterial soul determining all behaviour, the Enlightenment challenged this view and in particular Descartes (1649) advocated a dualist approach, where simple motor behaviours could be explained by actions of the material body (Descartes & Hall, 1664; Descartes & Monnoyer, 1988). In the 19th century Gustav Fechner went one step further and used empirical methods (Bacon, 1620) to unite behavioural measures with subjective, individual perception (Fechner, 1860). Similar to my introductory task with watermelons, Fechner tasked volunteers to lift two weights in succession and questioned them which was heavier, a sequential comparison task. This simple task provides a powerful tool to study human behaviour, because it allows to control an objective stimulus variable – the weight – and observe subjective perceptual differences between stimuli. Using this approach, Fechner was able to describe a logarithmic mapping between the physical magnitude of a stimulus and the extend of sensation it produces, the Weber-Fechner law that gave first insights into possible constraints of how information is processed by humans. Psychophysics, as Fechner called his mathematical descriptions of human psychology, has been aided in the study of the human brain by the invention of signal detection theory (SDT). Originally used to classify the detection of weak signals, the SDT proposes that an observer can respond to a stimulus in four ways: detect (hit), not detect (miss), detect the absence (correct reject), erroneously detect (false alarm). The advantage over conventional methods of only analysing hits and misses is that the SDT assumes an internal measurement of the stimulus feature that is proportional to the actual feature but includes noise. Therefore, also correct rejections and false alarms provide evidence for the internal measurement. The decision process for a

given stimulus can be modelled as taking a sample of two overlapping noisy (gaussian) distributions and applying a simple criterion. Most notably for the present thesis, we can take multiple samples from a stimulus over time and get ever-improving estimates of whether the stimulus belongs in one or the other part of the two overlapping distributions. Conceptually, this can be seen as accumulating evidence before applying a criterion. In the context of decision making studies, the internal measurement that we take for a stimulus is often referred to as a decision variable (DV). This DV has been linked closely to neuroscience, because an area involved in decision making should exhibit neural activity that correlates with the DV throughout an experimental task (Gold & Shadlen, 2007; Tanner & Swets, 1954). Experiments therefore are usually optimized to separate the mental steps involved in the decision processes in time or include only one stimulus feature that has to be detected by accumulating evidence. In the following, I will introduce results from two of the most common experiments operationalized to investigate the neural activity underlying decision making.

1.2 Sequential comparison tasks

Sequential comparison tasks, as Fechner used, are still an important tool to study psychophysics and have had a great impact onto neuroscience when used in conjunction with measurements of neural responses from the brain of primates and rodents. Mountcastle, Talbot, Sakata, and Hyvärinen (1969) were first to train monkeys in a vibrotactile version of this task, termed sequential frequency comparison (SFC) task, and recorded neural data (Mountcastle, Steinmetz, & Romo, 1990; Mountcastle, Talbot, Dar-Smith, & Kornhuber, 1967). In this setup (figure 1.1), a subject is presented with two vibrotactile frequencies in the flutter range (5-50 Hz), namely frequency 1 ($f1$) and frequency 2 ($f2$). The task is to decide whether the second ($f2$) frequency is higher or lower than the first ($f1$). To solve this challenge the subject must sequentially go through cognitive processes that are classically split into four parts. First, $f1$ is perceived. Second, $f1$ is being kept in memory, while the subject waits for the subsequent stimulus. Third, $f1$ is compared with

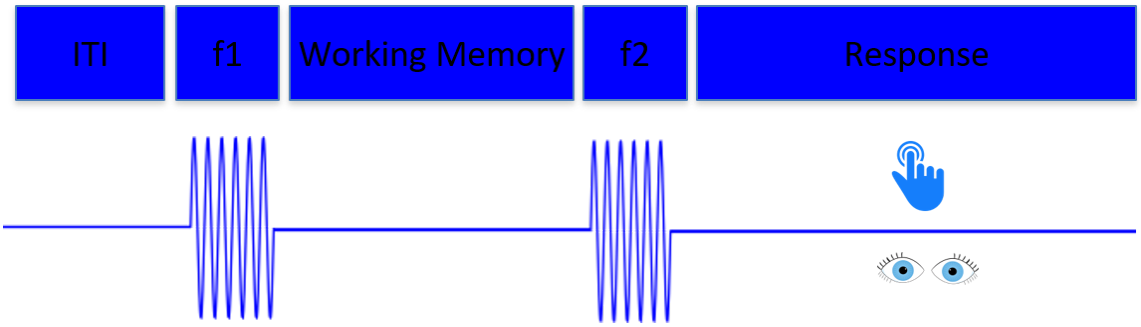

Figure 1.1: Sequential frequency comparison (SFC) task. Two vibrotactile frequencies are presented to the index finger in succession, $f1$ and $f2$. The task is to decide whether $f2$ is larger than $f1$ or vice-versa. Between $f1$ and $f2$ is a working memory interval in which the frequency of the first stimulus has to be retained. After perception of $f2$, responses are made, typically via button press or saccade.

the perception of $f2$, thereby forming a decision. Fourth, the subject reports the choice, usually by pressing a button or enacting a saccade to a choice-specific visual target.

1.2.1 Sequential comparison tasks: perception

Perception of the first stimulus drives quickly adapting (QA) neurons in Brodmann areas 1 and 3b of the contralateral primary somatosensory cortex (SI). These neurons receive afferent signals from mechanoreceptors in the skin, which are routed via the Thalamus and are closely interconnected (Merzenich & Harrington, 1969; Mountcastle et al., 1967; Talbot & Mountcastle, 1968). The majority of monkey SI neurons align their spiking activity to the periodicity of the stimulus, which can also be observed in human M/EEG as steady-state evoked potentials/fields (SSEP/F) (Mountcastle et al., 1990; Nangini, Ross, Tam, & Graham, 2006; Tobimatsu, Zhang, & Kato, 1999). Moreover, a portion of S1 neurons increase their firing rate monotonically with increasing vibrotactile frequency (Hernández et al., 2010; Hernández, Zainos, & Romo, 2000; Lemus, Hernández, Luna, Zainos, & Romo, 2010; Luna, Hernández, Brody, & Romo, 2005; Salinas, Hernández, Zainos, & Romo, 2000). Notably, only those QA neurons that modulate their firing rates by the vibrotactile frequency showed differential patterns in error trials, indicating that the brain uses these neurons to inform behaviour (Salinas et al., 2000). Therefore, it is well-established that the firing rates and the rhythmic SSEF/Ps observed with M/EEG represent the encoding of

sensory evidence on which later decisions are based. Interestingly, the firing rate predicts the monkeys' behaviour better than the periodicity of the neural responses and while periodicity is high in SI, it is almost absent in SII, speaking against a communication mechanism through periodic firing as would be predicted from SSEF/Ps (Hernández et al., 2000; Luna et al., 2005; Salinas et al., 2000). An alternative possibility is that QA neurons encode stimuli by the number of discrete bursts of spikes instead of single spikes. Such a coding scheme has been observed in visual tasks and has been suggested to efficiently encode stimulus features (Kepecs & Lisman, 2003; Kepecs, Wang, & Lisman, 2002; Krahe & Gabbiani, 2004; Reinagel, Godwin, Sherman, & Koch, 1999; Romo & de Lafuente, 2013). Notably, because other relevant monkey work has focused on bursts (e.g., Lundqvist et al., 2016), the stimulation times extend beyond the time of a burst in these vibrotactile studies (always 500ms) and therefore a code based on spikes is indistinguishable to one based upon bursts (Romo & de Lafuente, 2013). However, it remains unclear if bursting covaries with behavioural performance on a trial-by-trial level as has been observed for spikes (Luna et al., 2005). Regardless whether bursting or spiking underlies an encoding by rate, such a code could be positively or negatively correlated in upstream areas, as is observed throughout the sensorimotor hierarchy in this task including SII, prefrontal and motor cortices (Hernández et al., 2010; Salinas et al., 2000).

1.2.2 Sequential comparison tasks: working memory

Such a dual rate code, with populations either increasing or decreasing with stimulus frequencies, was also observed in the absence of stimulation: during the short retention interval between $f1$ and $f2$. In particular, Romo, Brody, Hernández, and Lemus (1999) recorded from the inferior convexity of the prefrontal cortex and identified neurons whose firing rate changed monotonically with the vibrotactile frequency held in working memory (WM). Visual tasks have long associated sustained prefrontal firing with WM (Funahashi, Bruce, & Goldman-Rakic, 1989; Fuster & Alexander, 1971; Goldman-Rakic, 1995), however, this study demonstrates that the contents of WM can directly map onto firing rate changes in single neurons. Further analyses indicate that the representation of stimulus information

by population dynamics of prefrontal neurons degrades after stimulus presentation, but re-emerges with different tunings towards the end of the working memory delay (Barak, Tsodyks, & Romo, 2010). This is particularly interesting, because it challenges the view that WM is encoded in sustained firing throughout delay periods, with biophysically plausible alternatives both in rhythmicity (Fiebig & Lansner, 2017; Lundqvist, Herman, Warden, Brincat, & Miller, 2018; Lundqvist et al., 2016) and synaptic changes (Mongillo, Barak, & Tsodyks, 2008; Stokes, 2015). This current high-level debate (for either side, see: Constantinidis et al., 2018; Lundqvist, Herman, & Miller, 2018) is so interesting for vibrotactile SFC studies, because firing rates directly represent the contents of WM, not overall changes. Recent evidence, however, suggests that both single neurons and populations may be responsible for WM in this task. Haegens, Vergara, Rossi-Pool, Lemus, and Romo (2017) recorded local field potentials (LFPs), which reflect local neuronal ensembles, and single neurons from monkey premotor cortex during a multimodal version of the SFC task. They found a modulation of LFP beta oscillations reflecting the stimulus features during WM. In addition, premotor spike-field coherence with the beta band was also related to the stimulus features, indicating a tuning of firing rate to this rhythm. These findings suggest that both population-related beta modulations and the closely affiliated spike activity encode the contents of WM.

This close coupling of beta oscillations with spiking activity underlying tactile WM has also been suspected from a series of EEG studies. Spitzer, Wacker, and Blankenburg (2010) gave human volunteers a similar SFC task and found a parametric modulation of the beta band in the right inferior frontal gyrus (IFG), suggesting that both monkey and human prefrontal cortices (PFC) exhibit content-specific activity during WM. In a follow-up study, Spitzer and Blankenburg (2011) demonstrated that this prefrontal activity was independent of encoding processes, by retro-cueing to one of two presented vibrotactile stimuli. Furthermore, Spitzer and Blankenburg (2012) hypothesized that this parametric encoding of abstract magnitudes was supramodal. In addition to the tactile task, they implemented a sequential visual flicker and a sequential acoustic flutter comparison task. Across all these modalities, prefrontal beta power monotonically encoded the frequency

information of the stimulus. However, this parametric code consists of a monotonic increase in beta power with the vibrotactile stimulus held in working memory and did not exhibit the negative component of a dual code as had been observed in monkey PFC (Romo et al., 1999). Because the precise link between the large-scale signals recorded with EEG and single neuron firing rates are poorly understood, it remains unclear whether the difference in power reflects a population imbalance of the dual code observed in monkeys, where about 60% of modulated neurons reflected a monotonic increase (Romo et al., 1999; Spitzer et al., 2010). This is of particular note, because working memory has been associated with sustained firing rates in the PFC (Funahashi et al., 1989; Fuster & Alexander, 1971; Goldman-Rakic, 1995; Pasternak & Greenlee, 2005) and gamma, not beta, appears to be closely related to neural firing rates even when recorded with surface EEG (Whittingstall & Logothetis, 2009). However, increases in gamma activity during working memory do not necessarily reflect sustained firing rates, but a more dynamic system of neural firing patterns (Cromer, Roy, & Miller, 2010; Durstewitz & Seamans, 2006; Shafi et al., 2007; Stokes et al., 2013). Indeed, recent monkey recordings revealed a pattern of brief gamma bursts accompanying encoding and re-activation of stimulus information while beta bursts reflected a default state of maintenance that was interrupted by gamma (Lundqvist et al., 2016). Notably, it is quite possible that such short gamma bursts have been averaged out of datasets by summation over multiple trials to increase the signal to noise ratio in previous human recordings (Stokes & Spaak, 2016). Furthermore, during EEG recordings the skull acts as a low-pass filter (Pfurtscheller & Cooper, 1975), making it difficult to pick up on gamma oscillations. The only MEG study investigating gamma in an SFC task, found overall gamma increases in SI, SII and frontal cortices during working memory, but did not investigate the parametric encoding of stimulus features (Haegens, Osipova, Oostenveld, & Jensen, 2010). Therefore, it remains an open question how the parametric beta band modulations observed by Spitzer and colleagues are associated with dynamic changes in gamma frequencies.

1.2.3 Sequential comparison tasks: decision making

The next part of the SFC task, comparing $f1$ and $f2$ to form a decision is associated with neural firing in premotor cortices (PMC) that are modulated by subtracting $f1$ from $f2$ (Hernández et al., 2010; Hernández, Zainos, & Romo, 2002; Jun et al., 2010; Romo, Hernández, & Zainos, 2004), which has also been observed in SII (Romo, Hernández, Zainos, Lemus, & Brody, 2002). Notably, the decisions were indicated by button press and therefore likely associated with PMC rather than with FEF when responses are indicated with saccades (see also Gold & Shadlen, 2007). Underlining this function, the PMC firing rates were modulated reversely during incorrect trials, indicating that they followed the monkey's choice rather than the physical attributes of the stimuli (Hernández et al., 2002; Romo et al., 2004). Most interestingly, because the retention of vibrotactile stimuli was associated with beta power in humans (Spitzer et al., 2010), Haegens, Nacher, Luna, Romo, and Jensen (2011) recorded local field potentials (LFPs) from monkey PMC and found that beta band power reflected the difference between $f2$ and $f1$. Importantly, when monkeys were instructed to respond independent of the task, neural firing and beta LFPs were not modulated by the decision process in PMC (see also Haegens et al., 2017). These findings in monkeys correspond well to recent EEG studies extending a role of the beta band for decision making to humans during this task (Herding, Ludwig, & Blankenburg, 2017; Herding, Spitzer, & Blankenburg, 2016). Agreeing with Haegens et al. (2011), Herding et al. (2016) demonstrated that beta band power in premotor areas was modulated by participants' choices, always with the decision outcome $f2 > f1$ resulting in a larger beta response than the outcome $f2 < f1$. These same findings were replicated for saccade responses, and in line with an intentional framework for decision making (Shadlen, Kiani, Hanks, & Churchland, 2008), the beta modulation was source localized to the FEF instead of PMC (Herding et al., 2017). Moreover, these studies used Bayesian modelling of participants' behaviour to estimate the subjective contribution of beta to choices, revealing both a clear pattern of beta invariant to the response mapping (index/middle finger) and a scaling by choice even when trials were incorrect. Yet, it remains unclear whether this choice-related beta band effect in the EEG extends beyond somatosensory processing,

which has been associated closely with this frequency band (Pfurtscheller, 1981).

Building upon this finding of choice-related beta modulation, Ludwig, Herding, and Blankenburg (2018) added a response delay to this task, in which the response mapping was not provided. With this slight change in setup, they found an almost identical beta band effect in the posterior parietal cortex (PPC), but not in premotor areas. This indicates that premotor areas are only directly involved in the decision process when the decision outcome is known. The PPC on the other hand appears to fulfil an effector-unspecific role and might have a more general role in the decision process. This is particularly interesting, because another parietal signal, the classic P300 (Chapman & Bragdon, 1964; Sutton, Braren, Zubin, & John, 1965), has long been associated with decision making (Donchin & Cohen, 1967; Rohrbaugh, Donchin, & Eriksen, 1974). More so, the P300, recently also termed centro-parietal positivity (CPP - more on it later), has been theorized not to reflect a unitary neural event after stimulus onset, but a dynamically changing neural signature of making a decision over time (Twomey, Murphy, Kelly, & O'Connell, 2015). Thus, the question remains how the choice related beta band effect in SFC tasks relates to decision signals in other paradigms, specifically the CPP and beta-gamma modulations observed with MEG in accumulation of evidence tasks (Donner, Siegel, Fries, & Engel, 2009; Donner et al., 2007; Kelly & O'Connell, 2013, 2015; O'Connell, Dockree, & Kelly, 2012; Philiastides, Heekeren, & Sajda, 2014; Twomey, Kelly, & O'Connell, 2016; Twomey et al., 2015)

1.3 Accumulation of evidence tasks

The other line of research I want to introduce builds also on Fechner's work on psychophysics, and in particular is the result of his legacy in mathematical psychology that drove ever-improving accounts of choice behaviour throughout the 20th century. This led to the development of signal detection theory, which as previously mentioned, has the advantage of taking into account noise behaviour and the structure of incorrect trials (Tanner & Swets, 1954). Neuroscientific experiments have used this theory to model perceptual

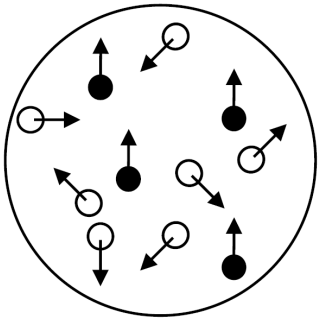

Figure 1.2: Example of random-dot motion kinematogram. The white dots represent the dots moving randomly, the black ones the coherently moving dots. The task is usually to detect coherent motion, varying the number of coherently moving dots determines the difficulty and time needed to perform the judgement.

decision making as a process of sequential sampling that results in an accumulation of evidence for a decision. Underlying this model is the idea that a decision variable (DV) represents the set of all evidence for a decision and for binary choices modern models posit a single mechanism that accumulates evidence over time for one choice over another (Shadlen & Kiani, 2013). For example, in our introductory example when we strive to find a good watermelon stand, we would sample melons from one stand sequentially, until we are sure the stand sells fruit of high or low quality. Every time we try a fruit, we would get a piece of evidence in favour of one possible choice, which over time accumulates to inform a decision – typically modelled as crossing an absolute bound. The neuroscientific hypothesis is that one decision variable tracks the current state of such evidence accumulation and that we can observe such a variable in the brain.

To track this neural correlate of perceptual decision making, neuroscientists have used predominantly one decision making task: the random-dot motion (RDM) direction discrimination. In the RDM task (figure 1.2) participants are shown dots on a monitor that move around. A portion of these dots move coherently in the same direction and the challenge is to detect this movement. Because the number of dots moving coherently is typically low and movement can only be spotted through a change over time, the perceptual challenge is usually difficult, and it can take between a few hundred milliseconds to seconds to detect the motion. Moreover, because the dots typically move randomly, it is possible to perceive a wrong direction.

This task is particularly powerful for psychophysics, because it requires no distinct working memory process and it lends itself well to be modelled as an accumulation-to-bound process (O'Connell, Shadlen, Wong-Lin, & Kelly, 2018). In such models it is assumed that subjects continuously sample from the dot-motion stimulus, perceive the motion direction of individual dots and accumulate evidence for one direction over time. When participants have a level of confidence in the direction, the decision bound is crossed and the decision communicated. This is usually done in monkey experiments by eye movements. The model can be further simplified by having the subjects decide between two opposite directions that are known in advance, thus becoming a binary accumulation process. Notably, because choices are typically indicated by performing a saccade to one of two targets associated with the choices, the decision process can be treated as a process of movement selection. Therefore, beyond motion sensitive neurons in MT/V5, recordings are primarily carried out in those areas associated with motor preparation and eye-movement execution, resulting in neural correlates of a decision variable in the superior colliculus (SC), frontal eye fields (FEF), lateral intraparietal area (LIP) and the dorsolateral prefrontal cortex (DLPFC) (for review see Gold & Shadlen, 2007).

1.3.1 Accumulation of evidence tasks with nonhuman primates

Employing the RDM task while recording from macaques, Britten, Shadlen, Newsome, and Movshon (1992) were able to link a small set of middle temporal visual area (MT/V5) neurons to concurrent choice behaviour. Even when the coherence was at 0% and all dots were moving randomly, MT firing rates predicted choices significantly (Britten, Newsome, Shadlen, Celebrini, & Movshon, 1996). Motion sensitive neurons in area MT are well-known to respond strongly to visual stimuli moving in a particular direction, exhibiting tuning to stimuli moving through their receptive fields (Baker, Petersen, Newsome, & Allman, 1981; Van Essen, Maunsell, & Bixby, 1981; Zeki, 1974, 1980). Using this knowledge of systematic motion direction organization in MT, microstimulation has been used to successively activate motion direction specific systems, thereby demonstrating a causal relationship of MT neurons for task performance (Ditterich, Mazurek, & Shadlen, 2003;

Salzman, Britten, & Newsome, 1990; Salzman, Murasugi, Britten, & Newsome, 1992). Most interestingly, when using a version of the RDM task with the opportunity to respond as soon as possible, MT microstimulation influences both choice and RTs in the stimulated neurons' preferred motion direction. In turn, when MT neurons are deactivated, the decision making process is impaired, likely because the sensory encoding is interrupted (Katz, Yates, Pillow, & Huk, 2016). On a functional level these findings indicate that MT processes the motion information and thus provides the sensory evidence on which decisions are formed.

To find out the neural substrates of a decision variable, a large body of monkey recordings targeted the FEF, because it is well-connected to visual areas, and known to encode the saccade processing required to respond in the RDM paradigm (Felleman & Van Essen, 1991; Hanes & Schall, 1996; Schall, Hanes, Thompson, & King, 1995; Schall & Morel, 1995; Thompson, Hanes, Bichot, & Schall, 1996; Van Essen, Anderson, & Felleman, 1992). Moreover, suprathreshold electrical stimulation evokes saccades while subthreshold stimulation elicits changes to saccade selection and spatial attention (Burman & Bruce, 1997; Moore & Armstrong, 2003; Moore & Fallah, 2001; Robinson & Fuchs, 1969). Gold and Shadlen (2000) interrupted motion viewing during the evidence accumulation process while monkeys viewed the RDM stimuli. Then they immediately applied a short electrical current to the FEF, which resulted in a saccade whose direction and amplitude was influenced by the current state of the decision process, reflecting the evolution of a decision variable (Gold & Shadlen, 2000; Gold, Shadlen, & Munoz, 2003). However, while the FEF is clearly involved in the decision process, it appears that only a small part of FEF neurons track the DV, while others encode stimulus properties during and after the decision, possibly to evaluate the outcome (Ding & Gold, 2012). Together, these studies indicate that the FEF is related to action-performance in RDM tasks with saccade responses, but also encodes stimulus and outcome related information.

Besides the more perceptual aspects of MT and the action-related activity in FEF, the lateral intraparietal area (LIP) has been extensively studied in RT-dependent versions of the RDM task. LIP has been focused on, because anatomically it receives inputs from

MT and outputs to the FEF (Andersen, Brotchie, & Mazzoni, 1992; Blatt, Andersen, & Stoner, 1990; Lewis & Van Essen, 2000). In particular, the LIP is tightly coupled to areas involved in eye movement control (Andersen, Asanuma, Essick, & Siegel, 1990). LIP neurons fire when a saccade is planned into their receptive fields (Andersen, Essick, & Siegel, 1987) and its neurons fire persistently when an animal withholds a saccade to a target (Barash, Bracewell, Fogassi, Gnadt, & Andersen, 1991; Gnadt & Andersen, 1988). Thus, LIP function appeared to be between perceptual processing and eye-movement execution, responsible for sensorimotor integration mediated by cognitive control (for review, Andersen & Buneo, 2002). Therefore, it was unsurprising when Shadlen and Newsome (1996, 2001) demonstrated that activity in LIP neurons, whose receptive fields were aligned with visual targets in the RDM task, increased before saccades to these targets were executed. Surprisingly however, single neuron activity was modulated by the presentation of dot-motion and correlated with RDM coherency. That is, activity reflected the difficulty of individual RDM patches by faster increases of firing rates in easy trials, indicating that LIP neurons tracked the evolution of the decision process. Most interestingly, LIP firing rates accumulated to a fixed threshold at the time of response independent of trial difficulty, fitting to drift-diffusion models of decision processing (Roitman & Shadlen, 2002a; Shadlen & Newsome, 1996, 2001). Contrary to MT however, LIP microstimulation appears to only slightly affect choice and RT (Hanks, Ditterich, & Shadlen, 2006). Moreover, when short motion pertubations were added to the RDM kinematogram, RT and choices were modulated by these over a sustained period of time (Huk, 2005). Together, these findings indicate that LIP neurons reflect the integration of decision information over time and microstimulaton pertubations drive the encoded decision variable with respect to a decision bound.

Most relevant to the present thesis (task design study 1 & 3), when responses could not be immediately taken and monkeys had to map targets to a spatially undetermined color-code, LIP neurons still represented the DV even though no specific saccade planning was possible (Bennur & Gold, 2011). This indicates that LIP function includes tracking the evolving DV independent of a specific motor response. However, a recent study

using causal de-activation of LIP neurons during decision formation suggests that LIP neurons may not be critical for computing perceptual decisions, and may only reflect secondary processes that correlate with the actual computation (Katz et al., 2016). This is particularly interesting, because concurrent recordings from six regions involved in decision making including MT, FEF and LIP suggest that information is not confined to specific cortical regions but shared among relevant brain areas and transmitted via bursts (Siegel, Buschman, & Miller, 2015). This observation ties in well with earlier studies suggesting that decision information is present even in areas functionally specific to early visual processing and may be communicated there via feedback from downstream cortices (Donner, Sagi, Bonneh, & Heeger, 2008; Nienborg & Cumming, 2009; Siegel, Engel, & Donner, 2011). If information is shared along the whole perception-action loop in a network between distributed regions, studying the whole system instead of isolated areas might be necessary, as is done in human neuroimaging.

1.3.2 Accumulation of evidence tasks using M/EEG in humans

Studies of perceptual decision making with nonhuman primates have discovered that many different areas throughout the cortical hierarchy are involved and share information across large distances. Yet, we know little about how these areas dynamically interact to form decisions, because studies recording from single cells are always limited to small populations and few cortical areas. In contrast, studies using neuroimaging with human subjects can trace neuronal dynamics across the whole head and concurrently throughout cortices. In addition, human subjects can be asked directly on what their perceptions and decisions were, e.g. how confidently they made a choice, and are recorded in much larger number, leading to better inferences about common mechanisms. Notably however, little is known about how many of the rhythms measured with M/EEG correspond to single-cell recordings and how they compare to signals detected in fMRI BOLD contrasts (Buzsáki & Wang, 2012; Jann, Kottlow, Dierks, Boesch, & Koenig, 2010; Keller et al., 2013; Lee et al., 2014; Logothetis, Pauls, Augath, Trinath, & Oeltermann, 2001; Scheeringa et al., 2011; Whittingstall & Logothetis, 2009).

Coherent oscillations between cortical areas may dynamically regulate the information flow across sets of neuronal populations (Engel, Fries, & Singer, 2001; Fries, 2015; Salinas & Sejnowski, 2001; Sejnowski, 2006; Varela, Lachaux, Rodriguez, & Martinerie, 2001) and MEG is well-suited to study such cortical dynamics (Siegel et al., 2011). Using MEG to discover the role of cortical oscillations for perceptual decision making, Donner et al. (2007) asked human volunteers to detect RDM motion (rather than choosing between directions) and found that beta power was elevated throughout the dorsal visual pathway including MT, intraparietal sulcus (IPS) and dlPFC for correct vs. incorrect trials. Interestingly, this activity predicted the accuracy and not the content of the upcoming choice, suggesting that beta reflected the computation of decisions rather than the content (see also Siegel et al., 2011). In another experiment, volunteers were shown an RDM patch at different coherence levels and had to indicate the motion direction (Siegel, Donner, Oostenveld, Fries, & Engel, 2007). After a typical event-related field, they observed a parametric scaling of occipital gamma power with the stimulus coherence and the opposite, but less robust, pattern in alpha and beta bands. Because the visual areas partial to this effect are known to be involved in motion processing, such as MT, this suggests that gamma reflects processing of the evidence on which decisions are based.

To investigate the action component of such perceptual choices, in another experiment Donner et al. (2009) presented RDM stimuli for a fixed time and before responses were given with either hand, a short delay was enforced onto the participants. Gamma band activity increased over the contralateral (pre-) motor cortex, and low frequency alpha and beta oscillations decreased with respect to the ipsilateral hemisphere. Notably, this pattern built up during stimulus viewing, likely reflecting the accumulation of evidence for a decision that would be source localized to FEF when responding with saccades instead (Herding et al., 2017). The lateralization of beta-band activity over central electrodes in particular appears to reflect an emerging motor plan that is directly associated with participants' choices. Building upon this finding, de Lange, Rahnev, Donner, and Lau (2013) demonstrated that pre-stimulus variance of lateralized power in the beta band predicted choices and that the accumulation of beta lateralization was modulated by

motion coherence. In sum, these MEG studies demonstrate signals corresponding to the sensory processing in MT and the action-related activity in FEF as observed in nonhuman primates and suggest an active role of beta and gamma oscillations in encoding the stimulus content. However, monkey studies have found extensive correlates of neuronal activity in the posterior parietal cortex with the evolution of a decision variable, which could not be identified with MEG. This is particularly curious, because recent EEG studies have observed consistent evidence of a centro-parietal potential (CPP or P300) that may be a candidate signal for such a parietal mechanism (Kelly & O'Connell, 2015).

The CPP has been identified as a rhythm matching the evolution of a decision variable during perceptual decision making tasks (Kelly & O'Connell, 2013, 2015; Philiastides et al., 2014; Twomey et al., 2015). One strategy to find this signal in RDM tasks has been to eliminate the typically observed ERPs resulting from stimulus onsets by presenting a field of randomly moving dots before coherent motion onset, thereby allowing for a seamless transition (Kelly & O'Connell, 2013). Moreover, responses are often made by button press using either left or right hands, to enable observation of lateralized beta power (as in de Lange et al., 2013; Donner et al., 2009). Using this setup, Kelly and O'Connell (2013) recorded EEG while humans performed the RDM task. They found that the CPP exhibited an accumulation-to-bound with respect to the decision of up- vs downward motion. In addition, the rate of CPP build-up was modulated by the sensory evidence strength, exhibiting a defining property of theoretical accounts of a decision variable. Even though effector specific activity in form of the lateralized readiness potential (Eimer, 1998; Smulders & Miller, 2012) did also show a ramping up, this activity was driven by the abstract, centroparietal signal. Moreover, in a previous study with a change detection task, hand movement specific motor signals, such as the previously observed beta lateralization, also exhibited a pattern of build-up to a threshold just before responses were executed, however, were abolished when manual responses were not carried out (O'Connell et al., 2012). This indicates that the CPP appears one directional in this process and only represents the accumulation-to-bound in a positive manner. This means that it doesn't represent different choices – a signed value - but the absolute value of the DV. The effector-

specific beta activity on the other hand includes information about choices, because they have to be enacted on. Such an interpretation of the CPP is in line with observations in LIP neurons and theoretical accounts that posit the supramodal accumulation of evidence for distinct alternatives in the same cortical areas that race each other (Brown & Heathcote, 2008; Roitman & Shadlen, 2002b; Usher & McClelland, 2001). Moreover, recent evidence suggests that neural correlates of a DV are independent of motor plans in LIP (Bennur & Gold, 2011) and corresponding human area IPS includes distinct systems implementing motor and perceptual decisions, suggesting functional heterogeneity (Filimon, Philiastides, Nelson, Kloosterman, & Heekeren, 2013). Therefore, it remains unclear what exactly is encoded by the centroparietal signals observed with EEG from this area and what precise cognitive function underlies the ramping up of activity.

If the CPP is the same signal as the P300, as recently suggested (Twomey et al., 2015), then a large body of evidence has indicated a relationship with a plethora of alternative cognitive processes (Nieuwenhuis, 2011; Nieuwenhuis, Aston-Jones, & Cohen, 2005). One measure in particular appears to fit well to recent observations of the CPP: confidence (Hillyard, Squires, Bauer, & Lindsay, 1971; Squires, Hillyard, & Lindsay, 1973). Because the CPP is not selective in its accumulation for one choice over another, it may only reflect the absolute value of a DV. Such a signal is closely related to confidence, which can be viewed as the distance between the DV and the closest decision bound (Urai & Pfeffer, 2014). A confidence signal would therefore not be selective for choices; however, it would still be affected by them. If participants commit an error, the DV should reach the same threshold as in a correct trial, while confidence should be lower (Shadlen & Kiani, 2013). Most interestingly, Philiastides et al. (2014) used a face-house discrimination task in which participants also had to sequentially sample and integrate information over time. They found that a CPP gradually built-up over time with the amount of evidence for either choice, as predicted from drift-diffusion models (DDM) and corresponding to RDM tasks. However, the signal did not reach a fixed threshold, but was still modulated by the amount of evidence for a choice. Because a simple DDM could not account for this, the authors demonstrated that adding a proxy for confidence on each trial could. This indicates that

at the time of response, the CPP includes information about choice confidence. However, participants weren't specifically asked how confident they were in their decisions, and it remains unclear whether this part of the CPP can be related directly to confidence judgements, as has been done in fMRI (e.g., Hebart, Schriever, Donner, & Haynes, 2016).

1.3.3 Accumulation of evidence tasks using fMRI in humans

Functional magnetic resonance imaging (fMRI) has indeed provided another avenue of human neuroimaging research to investigate perceptual decision making and confidence with high spatial acuity. Heekeren, Marrett, Bandettini, and Ungerleider (2004) gave participants a similar face-house discrimination task as described in the previous section (Philiastides et al., 2014) and used the spatial specificity of face processing in the fusiform face area (FFA) and house processing in the parahippocampal place area (PPA) to investigate relative blood-oxygen-level dependent (BOLD) increases. BOLD is known to increase in the FFA and PPA when faces and houses are perceived, respectively and can be related to single neuronal codes for either stimulus (Epstein & Kanwisher, 1998; Haxby, Hoffman, & Gobbini, 2000; Ishai, Ungerleider, Martin, Schouten, & Haxby, 1999; Kanwisher, McDermott, & Chun, 1997; Logothetis et al., 2001; Logothetis & Wandell, 2004; McCarthy, Puce, Gore, & Allison, 1997). A region responsible for decision making should covary with either FFA or PPA activity depending on whether faces or houses were perceived (Heekeren et al., 2004). Because the BOLD response is sluggish, it can only pick up on the overall activity during a trial and a modulation by evidence in either area is likely difficult to detect. However, the authors postulated that a candidate decision making area should show a pattern of easy trials associated with higher BOLD responses than hard trials, because in easy trials BOLD responses should reach a high level faster. They found that the left dorsolateral PFC (dlPFC) showed such an activity pattern and in a follow-up demonstrated that this was independent of the response modality (Heekeren, Marrett, Ruff, Bandettini, & Ungerleider, 2006). In addition, the role of the dlPFC appears to be one of integrating evidence, modeled as the drift in DDM, because when repetitive transcranial magnetic stimulation (TMS) was applied to this area to interrupt the decision process,

accuracy and response times were stymied in line with an interpretation as decreasing drift rate (Philiastides, Auksztulewicz, Heekeren, & Blankenburg, 2011). Notably in the context of the present thesis, this prefrontal activity appears to be co-activated with the IPS and FEF, suggesting a frontoparietal network involved in encoding of stimulus information and decision making (Heekeren et al., 2006; Ho, Brown, & Serences, 2009; Kayser, Buchsbaum, Erickson, & D'Esposito, 2010; Liu & Pleskac, 2011). In particular, Liu and Pleskac (2011) designed an RDM task where they gave information about the response modality, either button press or saccade, before or after the stimulus presentation (see design of study 1 of this thesis). Because participants could answer as fast as they wanted, with no forced delay as in Heekeren et al. (2004), the BOLD responses were increased for more difficult trials (Hanks & Summerfield, 2017), indicating that participants accumulated evidence for a longer time. Besides frontal areas and the anterior insula, the modulation was present in saccade-related areas FEF and IPS. Crucially, the foreknowledge and response modality did not have an effect on this activity pattern, suggesting no effector specificity of the neural system underlying evidence accumulation. These findings fit well with recent observations in monkey LIP, indicating that information about RDM direction was present before monkeys knew where the saccade target was going to be (Bennur & Gold, 2011).

Together, human neuroimaging provides a complimentary view to monkey recordings and provides evidence for the involvement of prefrontal and parietal areas in perceptual decision making[1]. Most notably, the dlPFC appears to fulfil the role of a domain general evidence accumulator, not evident from monkey single-cell recordings. Apart from these prefrontal findings, human fMRI and M/EEG studies show a remarkable similarity with monkey recordings in the areas involved in perceptual decision making. Especially the pattern of parietal signals tracking the evidence accumulation of noisy input and (pre-) motor areas exhibiting variability with the execution of choices is consistent across species and methods. Moreover, it appears that the information about the current state of decision making, a DV, is available to many areas and not restricted to a central decision maker.

[1] In addition, fMRI has revealed a role for the anterior insula during evidence accumulation (Ho et al., 2009; Liu and Pleskac, 2011). Because the insula is related to many different cognitive functions and because the present studies haven't found signals corresponding to such activity, I have left this introduction for another place (Menon and Uddin, 2010).

This is particularly important, as neural oscillations studied with M/EEG often reflect the dynamics of a cortical representation. More so, the dynamics of a general decision making mechanism are likely to be similar across cognitive tasks, such as the RDM and the SFC task, even if sensory modality or stimuli involve distinct cortical areas.

1.3.4 Common neural codes across perceptual decision making tasks

Evidence of common neural codes was found in studies using the RDM stimulus in a sequential comparison setup. Zaksas and Pasternak (2006) recorded from areas MT and PFC, while monkeys performed a delayed match-to-sample task on the motion direction of two sequentially presented RDM stimuli. During perception of the first stimulus, MT and PFC neurons were direction selective, but selectivity in PFC emerged 40ms after MT. During the delay period, neurons in both areas were attuned to direction, but through transient, not sustained firing. Similarly, the decision information was present in both MT and PFC, but the PFC was modulated 100 ms later and predictive of the upcoming choice. This indicates that PFC neurons encode task-relevant features about visual motion and represent the decisions that are based on comparisons taking place in MT. In addition, Hussar and Pasternak (2012) recorded from two distinct principal types of PFC neurons, pyramidal and interneurons, during the same task. They found that while both were involved in perception, mostly pyramidal cells carried information throughout the delay period, in a transient, dynamic code. Furthermore, the cell type determined whether the neuron was attuned to matching versus non-matching RDM directions. This suggests that the PFC employs a dual code for decision making in which different cell types have distinct contributions. To investigate the network states involved in this visual comparison task, Wimmer, Ramon, Pasternak, and Compte (2016) analysed LFPs from the lateral PFC from monkeys comparing either the motion directions or speeds of two RDM patches. During perception, theta and gamma power was increased, while beta decreased. In the subsequent delay, beta power encoded the relevant RDM feature, agreeing with findings in human neuroimaging (Spitzer & Blankenburg, 2012; Spitzer et al., 2010). Broadband LFP activity reflected the difference between S2 and S1 and was split into an early signed

modulation (S2-S1) and a later absolute choice-related component that reflected the buildup of the perceptual decision. Albeit in different areas, these results appear remarkably similar to findings of decision beta in SFC tasks on the one hand (Haegens et al., 2011; Herding et al., 2016), and the CPP (Kelly & O'Connell, 2013) on the other. However, until the studies included in the present thesis, there have not been any human neuroimaging approaches investigating these common cortical dynamics.

1.4 Objectives of this dissertation

Throughout the research for this dissertation, my primary aim has been to find the neural substrates underlying working memory and decision making with the intention to understand these cognitive functions better. Neural oscillations have been associated with these specific mental tasks, however, several important questions on the role of beta and gamma oscillations, in particular, remain unanswered. I addressed these gaps in our knowledge in three studies using a sequential comparison task with tactile (study 1+2) and visual stimuli (study 3). Moreover, I bridged the gap of perceptual decision making research using the predominant random-dot motion stimuli in a new comparison task setup (study 3). In conjunction with neural oscillations, I investigated broadband centro-parietal signals, and related them to motor beta, trial difficulty and confidence (study 2+3). Finally, this thesis accumulates the information from these three very related studies and outlines common themes surrounding the beta and gamma band as well as possible common ground with the CPP.

Summary of Original Research Articles

2

2.1 Study 1: Gamma and Beta Oscillations in Human MEG Encode the Contents of Vibrotactile Working Memory

From single-cell recordings in monkeys to large-scale human EEG, the parametric encoding of vibrotactile frequency during working memory is well-established (Romo et al., 1999; Spitzer et al., 2010). As reviewed in the introduction, a number of recent EEG studies have identified cortical oscillations in the beta band to represent the frequency information during a short delay in a vibrotactile sequential frequency comparison task. However, visual and auditory working memory studies have found a crucial role of gamma oscillations for working memory, not observed in previous vibrotactile EEG studies (Roux & Uhlhaas, 2014). In addition, the only MEG study investigating tactile working memory found a modulation of SI and - most interestingly - of SII during stimulus retention, but didn't investigate a parametric modulation in prefrontal areas (Haegens et al., 2010). While the authors did find an overall increase in frontal gamma during WM, this was limited to contrasting periods of working memory with a prestimulus baseline and was not content specific. Therefore, our first goal was to investigate whether frontal gamma encodes stimulus features during WM. In addition to this aim, a line of monkey and human neuroimaging studies has identified the intraparietal sulcus (IPS) as a hub for numerosity processing, a mental task very similar to the vibrotactile features in our design (Nieder, 2016). However, studies using EEG have not been able to localize IPS activity reflecting the vibrotactile frequency held in WM as is known from fMRI (Wu et al., 2018). Therefore, we aimed at detecting both high frequency oscillations in the gamma band and stimulus information from the IPS for the first time.

We recorded 306-channel whole-head magnetoencephalography while participants performed a version of the vibrotactile frequency comparison task. Notably, our original task design intended to also investigate how beta-gamma codes of decision making were

influenced by foreknowledge of the response modality, and therefore the task included responses with button press and saccades. However, due to technical problems, we had to discard the analysis of decision making related activity.

Our main analysis probed with a zero-mean contrast of the four different vibrotactile frequencies held in working memory at 15, 19, 23 and 27 Hz, whether there were channels, frequencies or time points in which a parametric code of vibrotactile frequencies was present. With a nonparametric cluster-based permutation test we identified three areas that showed such a pattern, all around the center of the WM interval. First, replicating previous EEG findings, beta power in the right IFG at around 30-35 Hz. Second, low beta power (10-20Hz) in bilateral parietal channels which was source localized to the IPS. Third, matching the beta effect in source location in the right IFG, gamma power (74-90 Hz) was negatively modulated by the vibrotactile frequency, thus showing the opposite pattern of the beta band effects. Notably, we did not replicate effects of overall broadband gamma power increases in SI, SII and frontal cortices as had been observed in a similar vibrotactile task (Haegens et al., 2010), while replicating the patterns typically observed in vibrotactile SFC tasks with M/EEG (Bauer, 2006; Spitzer et al., 2010).

These results indicate that there is a frontoparietal network underlying the retention of vibrotactile stimuli with an extended role of the beta band that may interact with gamma to enable working memory. We demonstrate for the first time with MEG that the IPS is also involved in this process and that the gamma band, which is associated more directly with neuronal firing than beta, might drive the prefrontal processing (Lundqvist et al., 2016; Whittingstall & Logothetis, 2009).

2.2 Study 2: Centro-parietal EEG Potentials Index Subjective Evidence and Difficulty

Recent studies indicate that the CPP in human EEG tracks the integration of noisy sensory input over time. It remains unclear however, whether the comparison of two short

vibrotactile frequencies elicits a similar response, as this percept does not include the accumulation of noisy evidence over an extended period. Moreover, it remains unknown whether the premotor beta band that scales with subjects' upcoming choices is related to the CPP. This is particularly interesting, because the CPP reflects the absolute, unsigned strength of accumulated evidence ($|S2 - S1|$), while choice dependent beta is a signed value ($S2 - S1$) reflecting the direction of the decision (e.g., Siegel et al., 2011; Urai & Pfeffer, 2014).

In this study, we used EEG data from six variants of the SFC task (n=116) and applied a model based on Bayesian inference to the behavioural data to estimate the subjectively perceived frequency differences (SPFDs). We found that parietal ERPs reflected the SPFCs shortly after the second stimulus offset (168-709ms) in a signed fashion, thus indicating the direction of choice. Crucially, this early parietal signal was correlated with choice-related beta power on a single trial level. While not implying causation, this can be viewed as first evidence for a previously unknown EEG signature that indexes the updating of subjective evidence in relation to the ensuing choice. The timing of these two signals as well as their source locations in parietal and premotor cortex further underline the possibility that the early ERPs serve to communicate the evidence for one motor plan or its alternative and the premotor beta band reflects the choice planning based upon this evidence.

In addition to this early parietal modulation by signed difference, we observed later parietal ERPs (273-953ms after stimulus offset) that correlated with the absolute strength of evidence. Interestingly, this later modulation was source localized not only to parietal areas, but also included the bilateral IFG, which relates it to the parametric encoding of the vibrotactile frequencies during WM. Similar to study 3 we also did not observe an absolute threshold of CPP accumulation, but rather a scaling of the late ERPs by subjective task difficulty. Further analysis revealed that this effect complied with the definition of statistical decision confidence in all aspects (Hangya, Sanders, & Kepecs, 2016; Sanders, Hangya, & Kepecs, 2016).

In summary, these findings indicate that early centroparietal ERPs reflect the evidence on which decisions are based, while later modulations might refer to the strength of evidence

informing a decision, which is closely related to measures of confidence.

2.3 Study 3: Neuronal Signatures of a Random-Dot Motion Comparison Task

Both the vibrotactile frequency comparison task and the random-dot motion task have been studied extensively in humans and monkeys, as I introduced earlier. However, there is remarkably little research aiming at finding common codes across these perceptual decision making tasks. So far, no human neuroimaging study has investigated the RDM task with vibrotactile stimuli nor studied the sequential comparison of random-dot motion stimuli. This is particularly curious, because pupillometry in humans and electrophysiological recordings in monkeys using a combination of these classical tasks have produced high-impact studies that gave novel insights into the encoding of decision information (Urai, Braun, & Donner, 2017; Wimmer et al., 2016). Here, we recorded EEG while human volunteers were tasked to compare the coherence of two sequentially presented random-dot motion stimuli ($S1$, $S2$) and responded by button press. If findings from SFC studies indeed transfer to the visual domain, we should observe a parametric beta band code in PFC as well as a modulation of premotor beta by choice. Moreover, RDM stimuli should elicit typical visual effects as well as a correlate of the accumulation of evidence in the form of a CPP. Crucially, the decision variable in this task reflects the comparison of the first with the second stimulus, thus we should not observe a CPP during perception of $S1$. Moreover, the CPP should scale with the difference between the two, not the coherence of $S2$.

We asked 28 subjects to perform this task and used their behavioral data to model the subjectively perceived coherence difference (SPCD) for each subject and trial. Using variational Bayes, our model accounted for the time-order effect/error (Hellström, 1985), a bias typically observed in sequential comparisons. In analogy to study 1, our WM analysis was a parametric contrast of the four $S1$ coherence levels. To look into the decision making

interval, we performed a $2x2$ GLM of choice ($S2 > S1$ vs $S2 < S1$) and performance (correct vs incorrect). Moreover, we investigated the CPP and contrasted it by subjects' choices and each trial's SPCD in three levels of 'easy', 'medium' and 'hard'.

In our WM analysis we found a significant cluster of prefrontal channels that were modulated by the level of $S1$ coherence retained throughout the inter-stimulus-interval. In agreement with previous EEG studies using vibrotactile stimuli (Spitzer & Blankenburg, 2012; Spitzer et al., 2010), this effect source localized to the right IFG, suggesting that the working memory related beta is supramodal and can be observed with stimuli not relying on frequency magnitudes. We also found a negative modulation of gamma, replicating findings from study 1. However, this effect was mainly driven by the lowest coherence stimuli and will require further investigation. Curiously, we also found a negative modulation of low beta band activity by the $S1$ coherence level in centroparietal channels, source localizing to bilateral MI and precuneus.

The analysis of decision-related activity found a modulation of premotor beta band activity 700ms before responses were made that was elevated for choices of $S2 > S1$ in comparison to those of $S2 < S1$. This is in line with recent vibrotactile SFC studies in humans, corresponding in time, frequency and location (Herding et al., 2016) and also agrees with monkey LFPs (Haegens et al., 2011; Haegens et al., 2017). There was no effect when splitting trials into 3 levels by SPCD (easy, medium, hard), thus reflecting the choices in a binary code. The CPP was modulated both in response to the perception of $S2$ and with respect to responses. $S2$-locked activity accrued during the stimulus presentation and stayed on a fixed level afterwards. Crucially, the amplitude of this level was modulated by the trials' difficulty ($S2 - S1'$) and not by the coherence of $S2$. Furthermore, the $S2$-locked CPP was modulated by choice and reached a higher amplitude for choices $S2 < S1$ than $S2 > S1$, the opposite of the beta band effect. Response-locked CPP showed a pattern of signal accumulation to a peak at the time of response. Notably, this peak was both influenced by choice and the difficulty of trials. At the time of response the CPP did not reach a fixed threshold, like in simple boundary-crossing models, but was scaled by the SPCD, with difficult trials exhibiting smaller amplitudes and incorrect trials demonstrating

even smaller amplitudes. This effect was only evident in the last 300ms before responding and in particular, seemed to be driven by a lower starting point to the accumulation rather than variance during the accumulation.

Our findings indicate an extended role of the beta band for both working memory and decision making in comparison tasks, regardless of sensory modality. Beta has been suggested to reflect the "status quo" of information (Engel & Fries, 2010). In our studies however, it appears to reflect more than that. It is modulated by the abstract magnitudes in comparison tasks (vibrotactile frequency or RDM coherence) and therefore reflects the WM content, as well as the content of decision making, already very early, 700ms before responding. In conjunction with fast, transient gamma it might therefore reflect the re-activation of content (Spitzer & Haegens, 2017) and/or the maintenance state (also of choice) that is interrupted by gamma (Lundqvist, Herman, & Miller, 2018).

The CPP was strongly modulated by trial difficulty at the time of response, suggesting it reflects a cognitive process that is not wholly explained by crossing a bound in a simple drift-diffusion model. More complex models based on sequential Bayesian updating or with collapsing bounds may be necessary to keep the drift-diffusion view in place. Moreover, it is possible that the CPP reflects an accumulation to an absolute bound, but the signal we observed included other parietal signals encoding the decision confidence. Finally, the CPP was also modulated by participants' choices, indicating a relationship with premotor beta that is yet to be investigated.

In sum, this study was able to bridge gap between decision making paradigms and sensory domains, indicating a common role for beta band driven content encoding and the CPP as an evidence accumulation mechanism that has ties to confidence.

3 General Discussion

In the research summarized in the previous section, we gained new insights into the role of neural oscillations ascribed to cognitive functions, especially working memory modulated beta and gamma, decision-related beta power and the supramodal nature of the CPP for tracking decisions.

In the first study, we were able to uncover previously hypothesized but never demonstrated modulations of prefrontal gamma and parietal beta power by vibrotactile frequencies held in working memory. Most interestingly, the parietal beta modulations could be source localized to the IPS, an area known to be involved in numerosity processing. These results indicate that a frontoparietal network underlies working memory that employs beta and gamma oscillations in a mechanistic fashion.

The second study encompassed six EEG experiments, whose analysis consistently showed a CPP that accumulated during decision making. With respect to the second stimulus, we observed a scaling of the CPP, first by the subsequent choice and later by trial difficulty, which we relate to confidence. In addition, we found a correlation between choice-related beta and the CPP, suggesting common codes during decision processing. Our findings point to a role of the CPP that goes beyond signaling the status of a DV and insinuate that such a role is related to the decision outcome.

In the most recent experiment, we showed that the functional roles attributed to beta oscillations in the tactile task hold up in a visual variant, indicating a general, supramodal mechanism. Similarly, we demonstrated that non-lateralized choice-dependent beta can also account for decisions when using RDM stimuli. In addition, both stimulus- and response-locked CPPs reflected the tracking of a decision variable during a comparison task that was informed by working memory. This is of particular note, because there was no relationship of the CPP during RDM perception, suggesting independence from sensory processes. Finally, the CPP scaled with subjectively perceived difficulty at the time of response, which further indicates that the CPP incorporates confidence signals.

3.1 Unifying accounts of prefrontal beta band oscillations during working memory

All experiments reviewed here replicated the finding that beta band power from IFG is parametrically modulated by abstract quantitative information (vibrotactile frequency or RDM coherence) held in working memory during a short interval between two stimuli. Spitzer et al. (2010) had identified this effect at 20-25 Hz with EEG during a similar vibrotactile SFC task. Interestingly, when we used a visual variant of the task, but the same EEG equipment as these authors, the effect was surprisingly similar at 18-26 Hz, however, was found significantly higher (30-35 Hz) in MEG recordings on almost the same vibrotactile task. Because in EEG the skull acts as a low-pass filter (Pfurtscheller & Cooper, 1975) and the observed effect may be an epiphenomenon of averaging further temporally smeared beta bursts, it is quite possible that the prefrontal oscillations even extend into the gamma range. Recent monkey recordings appear to concur with a representation in higher beta oscillations, with a medial premotor beta peak above 25 Hz (Haegens et al., 2017). This may particularly important, as lower beta modulations (13-20 Hz) occur jointly with alpha (Hanslmayr, Spitzer, & Bäuml, 2009) and decrease in task-relevant areas while higher beta-band rhythms (20-35) mirror gamma and increase with engagement (Tallon-Baudry, Bertrand, Peronnet, & Pernier, 1998). It may therefore be necessary, in the future, to separate lower beta activity more clearly from higher beta oscillations to avoid grouping them in one beta band.

Our findings in the prefrontal cortex were clearly in the upper beta band and appeared to be related to active processing rather than inhibitory in nature. Enhanced beta has been hypothesized to signal the "status quo" of maintaining the current sensorimotor or cognitive state (Engel & Fries, 2010). However, our findings go beyond overall changes. We provide evidence that beta oscillations hold information about the content (vibrotactile frequency or RDM coherence) of working memory on a given trial, joining a growing body of evidence for such a role (Spitzer & Blankenburg, 2011; Spitzer et al., 2010; Wimmer et al., 2016). This type of feature specific activity has also been found in neuronal spiking and high frequency LFPs (Nieder & Miller, 2003; Pesaran, Pezaris, Sahani, Mitra, & Andersen,

2002; Romo et al., 1999) and has been studied extensively with fMRI (Christophel, Hebart, & Haynes, 2012; Christophel, Klink, Spitzer, Roelfsema, & Haynes, 2017; Uluc, Schmidt, Wu, & Blankenburg, 2018; Wu et al., 2018). Yet, it remains unclear how neural activity measured as spike firing rates and BOLD signals relate to the previously observed EEG beta band oscillations. In particular, it is unknown, whether beta activity correlates positively or negatively with these activity measurements (Spitzer & Haegens, 2017). Upper beta band oscillations are likely to correspond closer to those in gamma, who have been associated with higher spike rates and increases in BOLD, while low beta may be associated negatively with activity, corresponding to alpha (Hanslmayr et al., 2011; Michels et al., 2010). However, it is also possible that beta is neither associated with activity increases nor decreases, as observed in some studies (Rule, Vargas-Irwin, Donoghue, & Truccolo, 2017; Whittingstall & Logothetis, 2009). Therefore our findings with MEG are of particular note, because we demonstrated that both high prefrontal and low parietal beta were associated with the abstract magnitudes held in working memory in the same fashion. We did not, however, observe overall changes, further underlining that beta fulfills a content-specific role. I therefore suspect that the functional role of beta is not directly related to overall spiking/BOLD activity increases as has been observed in gamma, but reflects the updating of content (Spitzer & Haegens, 2017).

3.2 Diverging findings with MEG and EEG

One major difference between our MEG recordings and previous EEG studies was that we observed parametric changes in gamma spectral power by the to-be-maintained frequency $f1$. One explanation why parametric WM in high frequency gamma oscillations was not detected in the large amount of previous vibrotactile EEG studies (Herding et al., 2016; Spitzer & Blankenburg, 2011, 2012; Spitzer, Fleck, & Blankenburg, 2014; Spitzer et al., 2010) is the previously mentioned nature of the human skull to act as a low-pass filter (Pfurtscheller & Cooper, 1975). Specifically, EEG and MEG can exhibit distinct frequency versus power relationships in high frequencies, because the capacitive properties of the

extracellular medium, i.e. skin and scalp muscle artefacts, distort the EEG, but not the MEG signal (Buzsáki & Wang, 2012; Dehghani, Bédard, Cash, Halgren, & Destexhe, 2010; Demanuele, James, & Sonuga-Barke, 2007). In addition, we used a multitaper approach based on Slepian sequences with a fixed window of 200 ms in the MEG study compared to a window of 400 ms in previous EEG recordings. This shorter time window results in less smoothing in the time domain, which gives rougher estimates, but may have provided us with the possibility to detect more short-lived effects. Because of these differences, we also used the shorter window for exploratory analysis in more recent experiments, for example study 3, resulting in the same negative gamma modulation by the abstract quantity held in working memory as observed with MEG. For prospective WM studies or an eventual meta-analysis of the present findings I therefore also recommend trying out a short window for multitaper analysis of higher frequencies.

In addition to gamma, the MEG recordings differed from EEG recordings in one more area: the IPS. We found that low beta band power (10-20) from this area was parametrically modulated by the abstract quantity retained in WM. There are two methodological reasons that could account for why we detected this modulation with MEG and not EEG (cf. Spitzer et al., 2014). One, MEG has a higher signal-to-noise ratio for shallow sources (Goldenholz et al., 2009). Two, MEG is more sensitive to sulcal than gyral sources, because it is blind to radial dipoles, biasing source analysis in favor of sulcal sources (Ahlfors, Han, Belliveau, & Hämäläinen, 2010). However, while unexpected from the previous EEG literature, the involvement of the IPS in quantity processing was not wholly surprising. Concurrent to our research, fMRI studies found a role of the IPS for vibrotactile, visual, and auditory frequency maintenance (Uluc et al., 2018; Wu et al., 2018). Moreover, similar to the abstract stimuli we employ, tasks using concrete numbers have found a direct link between multivariate BOLD-responses in the IPS and quantity (Eger et al., 2009). This finding builds upon a body of work with nonhuman primates that has revealed a crucial involvement of intraparietal regions for the encoding of quantitative features that are ordered along a continuum (Jacob, Vallentin, & Nieder, 2012; Nieder, 2016), including supramodal frequency (Vergara, Rivera, Rossi-Pool, & Romo, 2016). Furthermore, the IPS has been

well-established as a hub for working memory in junction with the prefrontal cortex in studies on capacity limits and appears to be essential for short term object retention (Todd & Marois, 2004, 2005; Vogel & Machizawa, 2004; Xu & Chun, 2006). Therefore, a role of the IPS in conjunction with the PFC has been well-established, yet it remains unclear what role beta band oscillations at low frequencies contribute to working memory in this area. In particular, the low beta we observed with MEG includes frequencies associated with the mu rhythm (Chatrian, Petersen, & Lazarte, 1959; Gastaut & Bert, 1954), whose functional role has been viewed as alpha-like suppression for somatosensation[1]. Contrary to this interpretation, we did not observe overall ERD/ERS, but a parametric modulation of lower beta/mu power by the content held in working memory. It is therefore unlikely that the observed effect reflects a generic inhibition or gating mechanism. One possibility is that the inhibition is content specific, explicitly because another stimulus is being presented subsequently that is sure to be different in vibrotactile frequency. Thus, the stimulus frequency held in working memory could be inhibited. However, the parametric modulation of IPS did not extend to the time of f2 stimulation, rendering this interpretation unlikely. Similarly, the mu rhythm is associated with attention (Anderson & Ding, 2011) and it is possible that participants paid more attention to higher frequencies. This is unlikely for two reasons. First, we did not observe behavioral effects in this direction, and second, prefrontal gamma band and occipital alpha would be expected to be similarly modulated, which we also did not observe (in this direction). Therefore, a role of the IPS for numerosity processing and working memory is well-established and it appears that our observations are difficult to reconcile with the inhibitory nature of low frequencies. I speculate that our observations reflect an active maintenance mechanism, possibly interacting with prefrontal gamma.

[1] Note that there is a different view on mu as a correlate of the mirror neuron system: (Naeem, Prasad, Watson, and Kelso, 2012; Pineda, 2005)

3.3 A frontoparietal beta-gamma code

One idea could be that the IPS maintains the information and is top-down controlled by prefrontal areas in a periodic replay based upon interactions of beta and gamma. This idea is analogous to computational modeling of neuronal firing patterns in animals proposing that working memory arises from periodically reactivating the content held in working memory, guided by gamma and theta oscillations (Fuentemilla, Penny, Cashdollar, Bunzeck, & Düzel, 2010; Jensen & Lisman, 2005; Lisman, 1999; Lisman & Idiart, 1995). This concept likely extends beyond the theta-related hippocampus to other areas and frequency bands (Lundqvist et al., 2016; Mongillo et al., 2008) and could be modulated on short time scales by attention (Awh, Jonides, & Reuter-Lorenz, 1998). Moreover, there is evidence of PFC-PPC coupling in the beta and delta bands, with delta reflecting task-irrelevant stimulus dimensions and beta only those immediately relevant (Antzoulatos & Miller, 2016). Yet so far, a gamma-beta relationship has only been shown within the prefrontal cortex (Lundqvist et al., 2016) and not across frontoparietal areas. However, this same idea may serve to explain the pattern of concurrent high beta band increases and gamma decreases with the abstract quantity held in working memory I observed both with MEG and EEG in separate tactile and visual studies. Lundqvist et al. (2016) observed brief gamma (45-100 Hz) and beta (20-35 Hz) bursts during single cell and LFP recordings of monkeys performing a working memory task. The gamma bursts increased during encoding and recall, while the beta bursts reflected a default network state that was interrupted by gamma. My findings could be an epiphenomenon of such a coding scheme, but reflected in mean power differences due to averaging over trials smoothing out individual bursts. Further analysis using SFC tasks in humans should concentrate on understanding the single trial dynamics. Because signal to noise ratios in M/EEG can be low, this has proven difficult in the past. One avenue may lie in observing the cross-frequency coupling, both in power changes and rhythmicity (Fransen, van Ede, & Maris, 2015). Another promising method to investigate the network configuration of oscillations may lie in the extraction of frequency-specific timecourses with high temporal resolution (Vidaurre et al., 2018; Vidaurre et al., 2016). However, perhaps more importantly,

mechanistic accounts of PPC-PFC function will have to evaluate whether gamma from superficial cortical layers and beta from deep layers also enact a similar relationship in other cortical areas (Christophel et al., 2017; Miller, Lundqvist, & Bastos, 2018).

Under close examination this idea of a dynamic frontoparietal beta-gamma code speaks against working memory as a function grounded in sustained prefrontal firing rates (Funahashi et al., 1989; Fuster & Alexander, 1971; Goldman-Rakic, 1995; Pasternak & Greenlee, 2005). Studies demonstrating continuous delay activity have relied heavily on trial and spike averaging, convoluting more complex single trial dynamics (Rainer & Miller, 2002; Shafi et al., 2007). Indeed, similar to the previously mentioned beta-gamma patterns (Lundqvist et al., 2016), most neurons are variable in their spiking behavior in both timing and duration throughout retention intervals and show dynamic coding schemes transitioning between coding states (Cromer et al., 2010; Durstewitz & Seamans, 2006; Spaak, Watanabe, Funahashi, & Stokes, 2017; Stokes et al., 2013). Moreover, recent neuroimaging studies suggest that working memory can be 'activity silent' when stimuli are unattended or irrelevant for current task demands (Lewis-Peacock, Drysdale, Oberauer, & Postle, 2012; Stokes, 2015; Wolff, Ding, Myers, & Stokes, 2015; Wolff, Jochim, Akyürek, & Stokes, 2017). While the role of such silent states is currently under high-level debate (Christophel, Iamshchinina, Yan, Allefeld, & Haynes, 2018), evidence converges on the idea that working memory does not rely on sustained prefrontal firing as a solitary mechanism (Lundqvist, Herman, & Miller, 2018; Spaak et al., 2017). My data agrees with this notion. First, contrary to Haegens et al. (2010) we did not observe an overall increase of gamma power during working memory as would be expected from sustained firing, while EEG findings for alpha and beta were replicated. Second, irrespective of whether gamma power changes reflected bursting, the observed changes in gamma were in a finite time window and not sustained throughout the whole interval. Third, while single-trial dynamics remain unclear, the pattern of gamma decrease with concurrent beta increase in PFC and PPC hint at a relationship between these frequency bands for working memory. The key to a unifying explanation for these effects may be provided by a very recent monkey study: Lundqvist, Herman, and Miller (2018) found that gamma increased, and beta

decreased shortly before items in working memory had to be used for decision making, while gamma decreased and beta increased when stimuli were not needed anymore. The authors interpret this as beta oscillations regulating control over gamma and working memory, a view summarily fitting to our results and recent investigations into the role of beta "beyond the status quo" (Haegens et al., 2017; Ludwig et al., 2018; Lundqvist, Herman, & Miller, 2018; Spitzer & Haegens, 2017). In this view, beta oscillations provide a mechanism to guide neural ensembles for the (re-)activation of maintained information. This builds on the observation that beta facilitates top-down driven communication across long distances and cortical areas (Antzoulatos & Miller, 2016; Arnal & Giraud, 2012; Bastos et al., 2015; Engel & Fries, 2010; Michalareas et al., 2016; Sejnowski, 2006; Siegel, Donner, & Engel, 2012; Varela et al., 2001; Wang, 2010), but beyond static maintenance can be characterized as a dynamic mechanism that can facilitate content-specific encoding and read-out by "waking up" in the form of short temporal bursts (Fries, 2015; Jones, 2016; Lundqvist, Herman, & Miller, 2018; Spitzer & Haegens, 2017). The question remains however, whether beta facilitates information "wake up" over long range connections, e.g. from sensory areas or if it is a mechanism of central processing in the prefrontal cortex. This is particularly interesting, because during visual and tactile tasks I have found consistent parametric modulations of beta oscillations in the PFC while none from sensory areas.

3.4 Distributed codes or central working memory?

While we observed working memory related activity consistently only in the prefrontal cortex, recent accounts also focus on a role for parietal and sensory cortices (Bettencourt & Xu, 2015; Christophel et al., 2017; Sreenivasan, Curtis, & D'Esposito, 2014; Xu & Jeong, 2015). In particular, studies using MVPA on fMRI recordings during the maintenance of precise visual details could reliably decode stimulus content from sensory cortices, yet failed in frontal areas (Christophel et al., 2012; Emrich, Riggall, LaRocque, & Postle, 2013; Riggall & Postle, 2012). When operationalizing the retention of vibrotactile frequencies

however, fMRI has revealed multivariate parametric codes in prefrontal and sensory areas (Schmidt, Wu, & Blankenburg, 2017; Wu et al., 2018). Thus, multiple avenues of research into working memory have found very distinct regions to be involved - how can these findings be consolidated? One idea is that the locus of working memory follows the processing in terms of the cortical hierarchy (Eriksson, Vogel, Lansner, Bergström, & Nyberg, 2015; Fuster & Bressler, 2012; Zimmer, 2008). Moreover, Christophel et al. (2017) postulate that for one, all cortical regions can maintain information over a short period of time. And for two, that the nature of the task dictates the relevant region in the cortical hierarchy depending on low level sensory features and the level of abstraction of the to-be-remembered stimulus. With such an interpretation of previous results, the areas involved in working memory can range from the prefrontal cortex for abstract, complex stimuli to low-level features in primary sensory cortices. Contrary to early MVPA fMRI studies tasking volunteers to remember low-level sensory details, we used abstract magnitude information, either in the form of vibrotactile flutters or the perceived coherence of a random dot kinematogram. Therefore, it is expected from this account that the representation in our studies materializes in areas such as the PFC and higher-order parietal regions, which process abstract, supramodal information. Furthermore, this idea may serve to explain the beta band modulation in motor areas before pressing a button we observed in terms of active perceptual memory. In this case, the motor-specific areas would also maintain information over a short period of time relevant to their place in the cortical hierarchy: the motor code for a subsequent button press.

3.5 Beta band during decision making

Beyond a role for working memory, we found an involvement of premotor beta band activity during decision making in a visual task and used previous findings of decision-related beta in tactile tasks to establish an association with concurrent centroparietal signals. Unfortunately, due to technical difficulties with both the vibrotactile stimulation device and the eye-tracking system, an analysis of our MEG data set in relation to decision making

was unsuccessful (cf. Chandler, Hayes, Townsend, & Thwaites, 2015). This is particularly lamentably, because Donner et al. (2007) used MEG in a RDM task and found that beta band activity predicted the accuracy and not the content of upcoming perceptual reports, for which we found no evidence with EEG.

The modulation of upper beta band power by subjects' choices we observed in sequential comparison tasks is in accord with choice signals in monkey LFPs (Haegens et al., 2011) in frequency, timing and cross-species location. Moreover, the increase in beta power for choices $S2 > S1$ vs. $S2 < S1$ follows the same direction common to all previous studies (Haegens et al., 2011; Herding et al., 2017; Herding et al., 2016; Ludwig et al., 2018). Remarkably, when comparing patterns of visual (study 3, figure 4) and tactile studies (Herding et al., 2016, figure 4) the time-frequency maps and topographies appear incredibly similar even though stimulus processing relied on distinct sensory modalities and the tasks had divergent timings.

This similarity between tactile and visual decision making indicates that the underlying process is supramodal and might indeed depend on the motor output rather than the sensory domain as predicted from the intentional framework of decision making (Shadlen et al., 2008). Further evidence stems from data used in study 2, experiments 1 and 2. Published also as Herding et al. (2016, 2017), this data demonstrates that depending on the response modality, the choice-selective beta band modulation can be source localized either to the premotor cortex for button press or the FEF for saccade responses. While these tasks used essentially the same sequential frequency comparison, we can now add that also in the comparison of sequentially sampled RDM stimuli the decision-related beta band modulation can be observed. This is particularly interesting, because during motor processing the beta frequency band does not solely represent motor preparation, as historically thought (Pfurtscheller, 1981). Indeed, when participants responded with either their left or right hand, lateralized beta band power over contralateral MI scaled with the process of accumulating evidence for a decision, tracking the evolving decision variable (Donner et al., 2009; O'Connell et al., 2012). In our recordings with button-press responses, we used the right index and middle fingers, which in addition were counterbalanced

across volunteers, eliminating the possibility that contralateral sensorimotor beta band modulations accounted for choice-dependent beta exclusively. Moreover, because in study 3 we used a visual task and found almost identical results, we can separate such decision-beta from the beta oscillations observed during somatosensory perception. If this modulation is indeed independent from perception and is related to the choice information, then we should only be able to find it if a response mapping is provided. Therefore, in study 2, experiments 3+4, also published as Ludwig et al. (2018), participants were only provided with the response mapping after a short delay and had to transform the decision information onto a colour code. Interestingly, in those trials where responses could not be immediately transformed into motor commands the beta band was also similarly modulated, but in posterior parietal cortex, not premotor areas. Taken together with our visual and tactile experiments employing direct mappings, this implies that the way we respond determines where in the sensorimotor hierarchy the decision is processed and supports an intentional framework (Shadlen et al., 2008). Furthermore, our findings indicate that the beta band reflects the categorical, abstract content of a decision, even in the absence of a motor plan. This is particularly interesting, because also broadband centroparietal signals (CPP) have been theorized to reflect the closely related process of accumulating evidence.

3.6 Common ground for CPP and decision beta

Both the premotor beta oscillations and the CPP we observed are candidate signals to reflect large-scale neural ensembles expressing the repeated sequential sampling and integration in sensorimotor neurons observed in studies with nonhuman primates (Gold & Shadlen, 2007; Hanks & Summerfield, 2017; Kelly & O'Connell, 2015; Spitzer & Haegens, 2017). In particular, they correspond well to studies focusing on the role of the PPC for decision formation. As introduced earlier, the LIP is closely connected to the accumulation of motion information from direction-selective neurons in MT, but also with frontal areas such as the FEF (Ding & Gold, 2012). Notably, the LIP and FEF can both exhibit ramping

up of neural activity and can reach a fixed level prior to saccade responses (Ding & Gold, 2010, 2012; Hanes & Schall, 1996; Roitman & Shadlen, 2002b). While the function of single neurons in these areas has been studied extensively, the precise role of the large-scale signals recorded with EEG, decision beta and CPP, remains uncertain.

The closest link between monkey and our human studies might be found between my third study and Wimmer et al. (2016). They recorded LFPs from monkey lateral prefrontal cortex during a sequential comparison task of the speed and direction of two RDM patches. During stimulus perception beta power was reduced, but theta and gamma increased. Throughout the working memory interval beta power encoded the task-relevant $S1$ feature, matching our findings in visual and tactile recordings. After $S2$ onset broadband LFP activity tracked the difference between $S1$ and $S2$ with an early sensory-related component reflecting the stimulus difference and a later component associated with the behavioural decision build-up. This is remarkably similar to our findings concerning the CPP, but in a wholly different area. However, the lPFC is very well-connected with the PPC (Cole, Pathak, & Schneider, 2010) and my own findings add to a well-established relationship between these areas (Cole et al., 2013; Cole & Schneider, 2007; Duncan, 2010; Muhle-Karbe, Duncan, De Baene, Mitchell, & Brass, 2017; Nieder, 2016). These results, in conjunction with ours, indicate that during cognitive tasks a network of prefrontal and parietal areas transition dynamically between neural coding states in a variety of frequency bands rather than one type of oscillation or broadband signal underlying perceptual decision making.

The coupling between CPP and choice-related beta in our findings, however, indicates that broadband signals and the beta band fulfil very related roles. I speculate that the CPP reflects the absolute value of a DV - maybe confidence - in an accumulation-to-bound manner, while the choice-related beta band serves to communicate the result of this process, continuously over time as is crucial for response preparation. This serves to explain, why choice-related beta appears so early in all our recordings (studies 2 & 3), about 150 ms after onset of the second stimulus, and disappears long before motor action is taken. This observation indicates that choice-related beta is strongest, when the CPP accumulates the most and the most updating of information is necessary (Twomey et al., 2015). Moreover,

this explains also why premotor beta band modulations could only be observed when the response modality was clear (Ludwig et al., 2018): the information was retained in the PPC till responses could be made. If the choice-related beta was exclusively related to response preparation, we would have observed such a modulation before subjects responded, regardless. However, further research into the beta band – CPP relationship will be necessary, to which I want to point in the next section.

3.7 Future Avenues

The present studies call for follow-up experiments. First, similar to our task design in study 1 (see attached study: von Lautz et al., 2017), it may be interesting to know where choice-beta will originate if there is a delay before responding and the response modality (button press / saccade) is either known or unknown on a trial-by-trial basis. I would hypothesize that in trials with unknown response modality beta band modulations source localize to the PPC, while in trials where subjects know how to answer, this effect originates from premotor areas or FEF.

Second, we observed a scaling of the CPP with subjectively perceived stimulus differences and related these changes to statistical decision confidence. A crucial next step will be to record actual ratings of confidence on single trials to uncover how confidence interacts with the accumulation of evidence tracked by the CPP. In particular, it remains unclear whether at the time of response a fixed threshold bound is reached or if the signal is modulated by confidence (Gherman & Philiastides, 2015; Kelly & O'Connell, 2013, 2015; Philiastides et al., 2014; Twomey et al., 2016). For example, our recordings in study 3 demonstrate that the CPP builds-up as expected from an accumulation process, but is scaled by trial difficulty at the time of response. A drift-diffusion model with non-collapsing bounds would have predicted that a fixed threshold of CPP amplitude is reached independent of trial difficulty as observed in similar recordings (Kelly & O'Connell, 2013). For future mechanistic explanations and the large body of modelling work on such decision processes

we should identify if confidence signals, e.g. from the ventral striatum as observed with fMRI (Hebart et al., 2016), are either mixed with or alternatively directly influence the CPP.

Third, it will be important to investigate gamma oscillations in this task more thoroughly, because – as previously discussed – the beta band is theorized to reflect the re-activation of content (Spitzer & Haegens, 2017) and might reflect a maintenance state that is interrupted by short gamma bursts (Lundqvist, Herman, & Miller, 2018; Lundqvist et al., 2016). Because re-activation of content may only be necessary across timespans above one second, it will be important to investigate gamma during a longer WM interval. Moreover, gamma has not been investigated during decision making in the SFC task and a possible relationship with the CPP should be investigated. MEG however, appears unsuited to detect a centro-parietal field[2], and previous MEG studies were not able to find such a parietal signal (e.g., Donner et al., 2009). One avenue would be to record concurrent M/EEG and use both signals to detect high-frequency gamma and the CPP. In addition, recent developments based on the Hidden Markov Model have been used to identify fast transient states in M/EEG data (Vidaurre et al., 2018; Vidaurre et al., 2016), and could be a promising method to characterize such a mechanism.

3.8 General Summary

As climate change leads to ever higher temperatures (Parmesan & Yohe, 2003), buying good quality watermelons will become more important. So, what can we say about the neural basis of finding the right melon? First, when we feel the watermelon, the power of neural oscillations in the alpha band increase over task-irrelevant visual areas. Concurrently, low beta (mu) oscillations increase over the ipsilateral hemisphere of the hand doing the feeling, while decreasing over the contralateral. Then, while we keep how the watermelon felt in memory before selecting another to test, beta band power increases with this abstract

[2]It would be called 'field', and not 'potential' because flux is measured in terms of space

quantity, while gamma decreases. Finally, before we point to the watermelon we want to buy, broadband centroparietal signals characterize the process of accumulating evidence for one melon or the other while beta band activity from premotor areas reflects our choice. These large-scale neural oscillations reflect the dynamic, fast-paced changes in single neurons and neuronal populations that unite their rhythms, making them detectable with neuroimaging methods from outside the human skull. This suggests that the brain uses neural oscillations to communicate information between different areas and that the more we understand about these rhythms the better we can understand the language the brain uses.

Bibliography

Ahlfors, S. P., Han, J., Belliveau, J. W., & Hämäläinen, M. S. (2010). Sensitivity of MEG and EEG to source orientation. *Brain Topography*. doi:10.1007/s10548-010-0154-x

Andersen, R. A., Asanuma, C., Essick, G., & Siegel, R. M. (1990). Corticocortical connections of anatomically and physiologically defined subdivisions within the inferior parietal lobule. *Journal of Comparative Neurology*. doi:10.1002/cne.902960106

Andersen, R. A., Brotchie, P. R., & Mazzoni, P. (1992). Evidence for the lateral intraparietal area as the parietal eye field. *Current Opinion in Neurobiology*. doi:10.1016/0959-4388(92)90143-9

Andersen, R. A., & Buneo, C. A. (2002). Intentional Maps in Posterior Parietal Cortex. *Annual Review of Neuroscience*. doi:10.1146/annurev.neuro.25.112701.142922

Andersen, R. A., Essick, G. K., & Siegel, R. M. (1987). Neurons of area 7 activated by both visual stimuli and oculomotor behavior. *Experimental Brain Research*. doi:10.1007/BF00248552. arXiv: 1206.5768

Anderson, K. L., & Ding, M. (2011). Attentional modulation of the somatosensory mu rhythm. *Neuroscience*. doi:10.1016/j.neuroscience.2011.02.004

Antzoulatos, E. G., & Miller, E. K. (2016). Synchronous beta rhythms of frontoparietal networks support only behaviorally relevant representations. *eLife*. doi:10.7554/eLife.17822

Aristotle. (1987). De Anima. In *A New Aristotle Reader*.

Arnal, L. H., & Giraud, A. L. (2012). Cortical oscillations and sensory predictions. doi:10.1016/j.tics.2012.05.003

Awh, E., Jonides, J., & Reuter-Lorenz, P. a. (1998). Rehearsal in spatial working memory. *Journal of experimental psychology. Human perception and performance*. doi:10.1037/0096-1523.24.3.780

Bacon, F. (1620). Novum Organum. In *The Oxford Francis Bacon, Vol. 11: The Instauratio magna Part II: Novum organum and Associated Texts*. doi:10.1093/oseo/instance.00007242. arXiv: arXiv:1011.1669v3

Baker, J. F., Petersen, S. E., Newsome, W. T., & Allman, J. M. (1981). Visual response properties of neurons in four extrastriate visual areas of the owl monkey (Aotus trivirgatus): a quantitative comparison of medial, dorsomedial, dorsolateral, and middle temporal areas. *Journal of neurophysiology*. doi:10.1152/jn.1981.45.3.397

Barak, O., Tsodyks, M., & Romo, R. (2010). Neuronal population coding of parametric working memory. *J Neurosci*. doi:10.1523/JNEUROSCI.1875-10.2010

Barash, S., Bracewell, R. M., Fogassi, L., Gnadt, J. W., & Andersen, R. A. (1991). Saccade-related activity in the lateral intraparietal area. I. Temporal properties; comparison with area 7a. *Journal of Neurophysiology*. doi:10.1080/15533174.2013.843552

Bastos, A. M., Vezoli, J., Bosman, C. A., Schoffelen, J. M., Oostenveld, R., Dowdall, J. R., … Fries, P. (2015). Visual areas exert feedforward and feedback influences through distinct frequency channels. *Neuron*. doi:10.1016/j.neuron.2014.12.018

Bauer, M. (2006). Tactile Spatial Attention Enhances Gamma-Band Activity in Somatosensory Cortex and Reduces Low-Frequency Activity in Parieto-Occipital Areas. *Journal of Neuroscience*. doi:10.1523/JNEUROSCI.5228-04.2006

Bennur, S., & Gold, J. I. (2011). Distinct Representations of a Perceptual Decision and the Associated Oculomotor Plan in the Monkey Lateral Intraparietal Area. *Journal of Neuroscience*. doi:10.1523/JNEUROSCI.4417-10.2011. arXiv: NIHMS150003

Bettencourt, K. C., & Xu, Y. (2015). Decoding the content of visual short-term memory under distraction in occipital and parietal areas. *Nature Neuroscience*. doi:10.1038/nn.4174. arXiv: 15334406

Blatt, G. J., Andersen, R. A., & Stoner, G. R. (1990). Visual receptive field organization and cortico-cortical connections of the lateral intraparietal area (area LIP) in the macaque. *Journal of Comparative Neurology*. doi:10.1002/cne.902990404

Britten, K., Newsome, W. T., Shadlen, M. N., Celebrini, S., & Movshon, J. A. (1996). A relationship between behavioral choice and the visual responses of neurons in macaque MT. *Visual Neuroscience*. doi:10.1017/S095252380000715X

Britten, K., Shadlen, M. N., Newsome, W. T., & Movshon, J. (1992). The analysis of visual motion: a comparison of neuronal and psychophysical performance. *The Journal of Neuroscience*. doi:10.1523/JNEUROSCI.12-12-04745.1992. arXiv: arXiv:1011.1669v3

Brown, S. D., & Heathcote, A. (2008). The simplest complete model of choice response time: Linear ballistic accumulation. *Cognitive Psychology*. doi:10.1016/j.cogpsych.2007.12.002. arXiv: arXiv:1011.1669v3

Burman, D. D., & Bruce, C. J. (1997). Suppression of task-related saccades by electrical stimulation in the primate's frontal eye field. *J Neurophysiol*. doi:0022-3077/97

Buzsáki, G., & Wang, X.-J. (2012). Mechanisms of Gamma Oscillations. *Annual Review of Neuroscience*. doi:10.1146/annurev-neuro-062111-150444. arXiv: NIHMS150003

Chandler, G., Hayes, D., Townsend, M., & Thwaites, A. (2015). *Technical Report : Testing and operating the QuaeroSys Piezostimulator* (tech. rep. No. June). doi:https://doi.org/10.17863/CAM.12955

Chapman, R. M., & Bragdon, H. R. (1964). Evoked responses to numerical and non-numerical visual stimuli while problem solving. *Nature*. doi:10.1038/2031155a0

Chatrian, G. E., Petersen, M. C., & Lazarte, J. A. (1959). The blocking of the rolandic wicket rhythm and some central changes related to movement. *Electroencephalography and Clinical Neurophysiology*. doi:10.1016/0013-4694(59)90048-3

Christophel, T. B., Hebart, M. N., & Haynes, J. D. (2012). Decoding the Contents of Visual Short-Term Memory from Human Visual and Parietal Cortex. *Journal of Neuroscience*. doi:10.1523/JNEUROSCI.0184-12.2012

Christophel, T. B., Iamshchinina, P., Yan, C., Allefeld, C., & Haynes, J. D. (2018). Cortical specialization for attended versus unattended working memory. *Nature Neuroscience*. doi:10.1038/s41593-018-0094-4

Christophel, T. B., Klink, P. C., Spitzer, B., Roelfsema, P. R., & Haynes, J. D. (2017). The Distributed Nature of Working Memory. doi:10.1016/j.tics.2016.12.007

Cole, M. W., Pathak, S., & Schneider, W. (2010). Identifying the brain's most globally connected regions. *NeuroImage*. doi:10.1016/j.neuroimage.2009.11.001

Cole, M. W., Reynolds, J. R., Power, J. D., Repovs, G., Anticevic, A., & Braver, T. S. (2013). Multi-task connectivity reveals flexible hubs for adaptive task control. *Nature Neuroscience*. doi:10.1038/nn.3470

Cole, M. W., & Schneider, W. (2007). The cognitive control network: Integrated cortical regions with dissociable functions. *NeuroImage*. doi:10.1016/j.neuroimage.2007.03.071

Constantinidis, C., Funahashi, S., Lee, D., Murray, J. D., Qi, X.-L., Wang, M., & Arnsten, A. F. (2018). Persistent Spiking Activity Underlies Working Memory. *The Journal of Neuroscience*. doi:10.1523/JNEUROSCI.2486-17.2018

Cromer, J. A., Roy, J. E., & Miller, E. K. (2010). Representation of Multiple, Independent Categories in the Primate Prefrontal Cortex. *Neuron*. doi:10.1016/j.neuron.2010.05.005. arXiv: NIHMS150003

de Lange, F. P., Rahnev, D. A., Donner, T. H., & Lau, H. (2013). Prestimulus Oscillatory Activity over Motor Cortex Reflects Perceptual Expectations. *Journal of Neuroscience*. doi:10.1523/JNEUROSCI.1094-12.2013. arXiv: NIHMS150003

Dehghani, N., Bédard, C., Cash, S. S., Halgren, E., & Destexhe, A. (2010). Comparative power spectral analysis of simultaneous elecroencephalographic and magnetoencephalographic recordings in humans suggests non-resistive extracellular media. *Journal of Computational Neuroscience*. doi:10.1007/s10827-010-0263-2. arXiv: 1003.5538

Demanuele, C., James, C. J., & Sonuga-Barke, E. J. S. (2007). Distinguishing low frequency oscillations within the 1/f spectral behaviour of electromagnetic brain signals. *Behavioral and Brain Functions*. doi:10.1186/1744-9081-3-62

Descartes, R. (1649). *Passions De L'Ame: the Passions of the Soul Hacket (From French)*. Indianapolis,IN.

Descartes, R., & Hall, T. S. (1664). Treatise of Man. In *Great Minds Series (2003)*. doi:10.4997/JRCPE.2009.418

Descartes, R., & Monnoyer, J.-M. (1988). *Les passions de l'âme*.

Ding, L., & Gold, J. I. (2010). Caudate Encodes Multiple Computations for Perceptual Decisions. *Journal of Neuroscience*. doi:10.1523/JNEUROSCI.2894-10.2010

Ding, L., & Gold, J. I. (2012). Neural correlates of perceptual decision making before, during, and after decision commitment in monkey frontal eye field. *Cerebral Cortex*. doi:10.1093/cercor/bhr178

Ditterich, J., Mazurek, M. E., & Shadlen, M. N. (2003). Microstimulation of visual cortex affects the speed of perceptual decisions. *Nature Neuroscience*. doi:10.1038/nn1094

Donchin, E., & Cohen, L. (1967). Averaged evoked potentials and intramodality selective attention. *Electroencephalography and Clinical Neurophysiology*. doi:10.1016/0013-4694(67)90061-2

Donner, T. H., Sagi, D., Bonneh, Y. S., & Heeger, D. J. (2008). Opposite Neural Signatures of Motion-Induced Blindness in Human Dorsal and Ventral Visual Cortex. *Journal of Neuroscience*. doi:10.1523/JNEUROSCI.2371-08.2008

Donner, T. H., Siegel, M., Fries, P., & Engel, A. K. (2009). Buildup of Choice-Predictive Activity in Human Motor Cortex during Perceptual Decision Making. *Current Biology*. doi:10.1016/j.cub.2009.07.066

Donner, T. H., Siegel, M., Oostenveld, R., Fries, P., Bauer, M., & Engel, A. K. (2007). Population activity in the human dorsal pathway predicts the accuracy of visual motion detection. *Journal of neurophysiology*. doi:10.1152/jn.01141.2006

Duncan, J. (2010). The multiple-demand (MD) system of the primate brain: mental programs for intelligent behaviour. doi:10.1016/j.tics.2010.01.004

Durstewitz, D., & Seamans, J. K. (2006). Beyond bistability: Biophysics and temporal dynamics of working memory. *Neuroscience*. doi:10.1016/j.neuroscience.2005.06.094

Eger, E., Michel, V., Thirion, B., Amadon, A., Dehaene, S., & Kleinschmidt, A. (2009). Deciphering cortical number coding from human brain activity patterns. *Current biology : CB*. doi:10.1016/j.cub.2009.08.047

Eimer, M. (1998). The lateralized readiness potential as an on-line measure of central response activation processes. *Behavior Research Methods, Instruments, and Computers*. doi:10.3758/BF03209424

Emrich, S. M., Riggall, A. C., LaRocque, J. J., & Postle, B. R. (2013). Distributed Patterns of Activity in Sensory Cortex Reflect the Precision of Multiple Items Maintained in Visual Short-Term Memory. *Journal of Neuroscience*. doi:10.1523/JNEUROSCI.5732-12.2013

Engel, A. K., & Fries, P. (2010). Beta-band oscillations-signalling the status quo? doi:10.1016/j.conb.2010.02.015

Engel, A. K., Fries, P., & Singer, W. (2001). Dynamic predictions: Oscillations and synchrony in top–down processing. *Nature Reviews Neuroscience*. doi:10.1038/35094565. arXiv: NIHMS150003

Epicurus. (1940). Letter to Menoeceus. In *The Stoic and Epicurean philosophers: The complete extant writings of Epicurus, Epictetus, Lucretius and Marcus Aurelius*.

Epstein, R., & Kanwisher, N. (1998). A cortical representation the local visual environment. *Nature*. doi:10.1038/33402

Eriksson, J., Vogel, E. K., Lansner, A., Bergström, F., & Nyberg, L. (2015). Neurocognitive Architecture of Working Memory. doi:10.1016/j.neuron.2015.09.020. arXiv: arXiv: 1408.1149

Fechner, G. (1860). Elemente der Psychophysik. *Elemente dur psychophysik*. doi:10.1212/01.CON.0000410032.34477.56

Felleman, D. J., & Van Essen, D. C. (1991). Distributed hierarchical processing in the primate cerebral cortex. *Cerebral Cortex*. doi:10.1093/cercor/1.1.1

Fiebig, F., & Lansner, A. (2017). A Spiking Working Memory Model Based on Hebbian Short-Term Potentiation. *The Journal of Neuroscience*. doi:10.1523/JNEUROSCI.1989-16.2017

Filimon, F., Philiastides, M. G., Nelson, J. D., Kloosterman, N. A., & Heekeren, H. R. (2013). How Embodied Is Perceptual Decision Making? Evidence for Separate Processing of Perceptual and Motor Decisions. *Journal of Neuroscience*. doi:10.1523/JNEUROSCI.2334-12.2013

Fransen, A. M., van Ede, F., & Maris, E. (2015). Identifying neuronal oscillations using rhythmicity. *NeuroImage*. doi:10.1016/j.neuroimage.2015.06.003

Fries, P. (2015). Rhythms for Cognition: Communication through Coherence. doi:10.1016/j.neuron.2015.09.034. arXiv: 15334406

Fuentemilla, L., Penny, W. D., Cashdollar, N., Bunzeck, N., & Düzel, E. (2010). Theta-Coupled Periodic Replay in Working Memory. *Current Biology*. doi:10.1016/j.cub.2010.01.057

Funahashi, S., Bruce, C. J., & Goldman-Rakic, P. S. (1989). Mnemonic coding of visual space in the monkey's dorsolateral prefrontal cortex. *Journal of Neurophysiology*. doi:10.1152/jn.1989.61.2.331

Fuster, J. M., & Alexander, G. E. (1971). Neuron Activity Related to Short-Term Memory. *Science*. doi:10.1126/science.173.3997.652

Fuster, J. M., & Bressler, S. L. (2012). Cognit activation: A mechanism enabling temporal integration in working memory. doi:10.1016/j.tics.2012.03.005. arXiv: NIHMS150003

Gastaut, H. J., & Bert, J. (1954). EEG changes during cinematographic presentation. *EEG Clinical Neurophysiology*. doi:10.1016/0013-4694(54)90058-9

Gherman, S., & Philiastides, M. G. (2015). Neural representations of confidence emerge from the process of decision formation during perceptual choices. *NeuroImage*. doi:10.1016/j.neuroimage.2014.11.036

Gnadt, J. W., & Andersen, R. A. (1988). Memory related motor planning activity in posterior parietal cortex of macaque. *Experimental Brain Research. Experimentelle Hirnforschung. Expérimentation Cérébrale*. doi:10.1007/BF00271862

Gold, J. I., & Shadlen, M. N. (2000). Representation of a perceptual decision in developing oculomotor commands. *Nature*. doi:10.1038/35006062

Gold, J. I., & Shadlen, M. N. (2007). The neural basis of decision making. *Annu. Rev. Neurosci.* doi:10.1146/annurev.neuro.29.051605.113038. arXiv: NIHMS150003

Gold, J. I., Shadlen, M. N., & Munoz, D. (2003). The influence of behavioral context on the representation of a perceptual decision in developing oculomotor commands. *The Journal of neuroscience : the official journal of the Society for Neuroscience*. doi:10.1523/jneurosci.0577-07.2007

Goldenholz, D. M., Ahlfors, S. P., Hämäläinen, M., Sharon, D., Ishitobi, M., Vaina, L. M., & Stufflebeam, S. M. (2009). Mapping the signal-to-noise-ratios of cortical sources in magnetoencephalography and electroencephalography. *Human Brain Mapping*. doi:10.1002/hbm.20571

Goldman-Rakic, P. S. (1995). Cellular basis of working memory. doi:10.1016/0896-6273(95)90304-6

Haegens, S., Nacher, V., Luna, R., Romo, R., & Jensen, O. (2011). -Oscillations in the monkey sensorimotor network influence discrimination performance by rhythmical inhibition of neuronal spiking. *Proceedings of the National Academy of Sciences*. doi:10.1073/pnas.1117190108

Haegens, S., Osipova, D., Oostenveld, R., & Jensen, O. (2010). Somatosensory working memory performance in humans depends on both engagement and disengagement of regions in a distributed network. *Human Brain Mapping*. doi:10.1002/hbm.20842

Haegens, S., Vergara, J., Rossi-Pool, R., Lemus, L., & Romo, R. (2017). Beta oscillations reflect supramodal information during perceptual judgment. *Proceedings of the National Academy of Sciences*. doi:10.1073/pnas.1714633115

Hanes, D. P., & Schall, J. D. (1996). Neural control of voluntary movement initiation. *Science*. doi:10.1126/science.274.5286.427

Hangya, B., Sanders, J. I., & Kepecs, A. (2016). A Mathematical framework for statistical decision confidence. doi:10.1162/NECO_a_00864. arXiv: 1309.2848v1

Hanks, T. D., Ditterich, J., & Shadlen, M. N. (2006). Microstimulation of macaque area LIP affects decision-making in a motion discrimination task. *Nature Neuroscience*. doi:10.1038/nn1683

Hanks, T. D., & Summerfield, C. (2017). Perceptual Decision Making in Rodents, Monkeys, and Humans. doi:10.1016/j.neuron.2016.12.003. arXiv: 073734

Hanslmayr, S., Volberg, G., Wimber, M., Raabe, M., Greenlee, M. W., & Bauml, K.-H. T. (2011). The Relationship between Brain Oscillations and BOLD Signal during Memory Formation: A Combined EEG-fMRI Study. *Journal of Neuroscience*. doi:10.1523/JNEUROSCI.3140-11.2011

Hanslmayr, S., Spitzer, B., & Bäuml, K. H. (2009). Brain oscillations dissociate between semantic and nonsemantic encoding of episodic memories. *Cerebral Cortex*. doi:10.1093/cercor/bhn197

Haxby, J. V., Hoffman, E. A., & Gobbini, M. I. (2000). The distributed human neural system for face perception. doi:10.1016/S1364-6613(00)01482-0

Hebart, M. N., Schriever, Y., Donner, T. H., & Haynes, J. D. (2016). The Relationship between Perceptual Decision Variables and Confidence in the Human Brain. *Cerebral Cortex*. doi:10.1093/cercor/bhu181

Heekeren, H. R., Marrett, S., Bandettini, P. A., & Ungerleider, L. G. (2004). A general mechanism for perceptual decision-making in the human brain. *Nature*. doi:10.1038/nature02966

Heekeren, H. R., Marrett, S., Ruff, D. A., Bandettini, P. A., & Ungerleider, L. G. (2006). Involvement of human left dorsolateral prefrontal cortex in perceptual decision making is independent of response modality. *Proceedings of the National Academy of Sciences*. doi:10.1073/pnas.0603949103

Hellström, Å. (1985). The Time-Order Error and Its Relatives. Mirrors of Cognitive Processes in Comparing. doi:10.1037/0033-2909.97.1.35

Herding, J., Ludwig, S., & Blankenburg, F. (2017). Response-Modality-Specific Encoding of Human Choices in Upper Beta Band Oscillations during Vibrotactile Comparisons. *Frontiers in Human Neuroscience*. doi:10.3389/fnhum.2017.00118

Herding, J., Spitzer, B., & Blankenburg, F. (2016). Upper beta band oscillations in human premotor cortex encode subjective choices in a vibrotactile comparison task. *Journal of Cognitive Neuroscience*. doi:10.1162/jocn_a_00932. arXiv: 1511.04103

Hernández, A., Nácher, V., Luna, R., Zainos, A., Lemus, L., Alvarez, M., … Romo, R. (2010). Decoding a perceptual decision process across cortex. *Neuron*. doi:10.1016/j.neuron.2010.03.031

Hernández, A., Zainos, A., & Romo, R. (2000). Neuronal correlates of sensory discrimination in the somatosensory cortex. *Proceedings of the National Academy of Sciences*. doi:10.1073/pnas.120018597

Hernández, A., Zainos, A., & Romo, R. (2002). Temporal evolution of a decision-making process in medial premotor cortex. *Neuron*. doi:10.1016/S0896-6273(02)00613-X

Hillyard, S. A., Squires, K. C., Bauer, J. W., & Lindsay, P. H. (1971). Evoked potential correlates of auditory signal detection. *Science*. doi:10.1126/science.172.3990.1357

Ho, T. C., Brown, S., & Serences, J. T. (2009). Domain General Mechanisms of Perceptual Decision Making in Human Cortex. *Journal of Neuroscience*. doi:10.1523/JNEUROSCI.5984-08.2009. arXiv: NIHMS150003

Huk, A. C. (2005). Neural Activity in Macaque Parietal Cortex Reflects Temporal Integration of Visual Motion Signals during Perceptual Decision Making. *Journal of Neuroscience*. doi:10.1523/JNEUROSCI.4684-04.2005

Hussar, C. R., & Pasternak, T. (2012). Memory-Guided Sensory Comparisons in the Prefrontal Cortex: Contribution of Putative Pyramidal Cells and Interneurons. *Journal of Neuroscience*. doi:10.1523/JNEUROSCI.5135-11.2012

Ishai, A., Ungerleider, L. G., Martin, A., Schouten, J. L., & Haxby, J. V. (1999). Distributed representation of objects in the human ventral visual pathway. *Proceedings of the National Academy of Sciences*. doi:10.1073/pnas.96.16.9379

Jacob, S. N., Vallentin, D., & Nieder, A. (2012). Relating magnitudes: The brain's code for proportions. doi:10.1016/j.tics.2012.02.002

Jann, K., Kottlow, M., Dierks, T., Boesch, C., & Koenig, T. (2010). Topographic electrophysiological signatures of fMRI resting state networks. *PLoS ONE*. doi:10.1371/journal.pone.0012945

Jensen, O., & Lisman, J. E. (2005). Hippocampal sequence-encoding driven by a cortical multi-item working memory buffer. doi:10.1016/j.tins.2004.12.001

Jones, S. R. (2016). When brain rhythms aren't 'rhythmic': implication for their mechanisms and meaning. doi:10.1016/j.conb.2016.06.010

Jun, J. K., Miller, P., Hernández, A., Zainos, A., Lemus, L., Brody, C. D., & Romo, R. (2010). Heterogenous Population Coding of a Short-Term Memory and Decision Task. *Journal of Neuroscience*. doi:10.1523/JNEUROSCI.2062-09.2010. arXiv: NIHMS150003

Kanwisher, N., McDermott, J., & Chun, M. M. (1997). The fusiform face area: a module in human extrastriate cortex specialized for face perception. *The Journal of ...* doi:10.1098/Rstb.2006.1934. arXiv: 0208024 [gr-qc]

Katz, L. N., Yates, J. L., Pillow, J. W., & Huk, A. C. (2016). Dissociated functional significance of decision-related activity in the primate dorsal stream. *Nature*. doi:10.1038/nature18617. arXiv: 15334406

Kayser, A. S., Buchsbaum, B. R., Erickson, D. T., & D'Esposito, M. (2010). The Functional Anatomy of a Perceptual Decision in the Human Brain. *Journal of Neurophysiology*. doi:10.1152/jn.00364.2009

Keller, C. J., Bickel, S., Honey, C. J., Groppe, D. M., Entz, L., Craddock, R. C., … Mehta, A. D. (2013). Neurophysiological Investigation of Spontaneous Correlated and Anticorrelated Fluctuations of the BOLD Signal. *Journal of Neuroscience*. doi:10.1523/JNEUROSCI.4837-12.2013. arXiv: NIHMS150003

Kelly, S. P., & O'Connell, R. G. (2013). Internal and external influences on the rate of sensory evidence accumulation in the human brain. *J Neurosci*. doi:10.1523/JNEUROSCI.3355-13.2013

Kelly, S. P., & O'Connell, R. G. (2015). The neural processes underlying perceptual decision making in humans: Recent progress and future directions. doi:10.1016/j.jphysparis.2014.08.003

Kepecs, A., & Lisman, J. E. (2003). Information encoding and computation with spikes and bursts. In *Network: Computation in Neural Systems*. doi:10.1088/0954-898X/14/1/306

Kepecs, A., Wang, X.-J., & Lisman, J. E. (2002). Bursting neurons signal input slope. *The Journal of Neuroscience*. doi:22/20/9053[pii]

Kishon, E., & Labatzke, P. (1975). *Das Geheimnis der Melone* (2.Ed.). Bonn: schumm.

Krahe, R., & Gabbiani, F. (2004). Burst firing in sensory systems. doi:10.1038/nrn1296

Lee, H. S., Ghetti, A., Pinto-Duarte, A., Wang, X., Dziewczapolski, G., Galimi, F., … Heinemann, S. F. (2014). Astrocytes contribute to gamma oscillations and recognition memory. *Proceedings of the National Academy of Sciences*. doi:10.1073/pnas.1410893111

Lemus, L., Hernández, A., Luna, R., Zainos, A., & Romo, R. (2010). Do sensory cortices process more than one sensory modality during perceptual judgments? *Neuron*. doi:10.1016/j.neuron.2010.06.015. arXiv: NIHMS150003

Lewis-Peacock, J. A., Drysdale, A. T., Oberauer, K., & Postle, B. R. (2012). Neural evidence for a distinction between short-term memory and the focus of attention. *Journal of Cognitive Neuroscience*. doi:10.1162/jocn_a_00140. arXiv: 1511.04103

Lewis, J. W., & Van Essen, D. C. (2000). Corticocortical connections of visual, sensorimotor, and multimodal processing areas in the parietal lobe of the macaque monkey. *Journal*

of Comparative Neurology. doi:10.1002/1096-9861(20001204)428:1⟨112::AID-CNE8⟩3.0.CO;2-9

Lisman, J. E. (1999). Relating hippocampal circuitry to function: Recall of memory sequences by reciprocal dentate-CA3 interactions. doi:10.1016/S0896-6273(00)81085-5

Lisman, J. E., & Idiart, M. A. (1995). Storage of 7 ± 2 short-term memories in oscillatory subcycles. *Science*. doi:10.1126/science.7878473

Liu, T., & Pleskac, T. J. (2011). Neural correlates of evidence accumulation in a perceptual decision task. *Journal of Neurophysiology*. doi:10.1152/jn.00413.2011

Logothetis, N. K., Pauls, J., Augath, M., Trinath, T., & Oeltermann, A. (2001). Neurophysiological investigation of the basis of the fMRI signal. *Nature*. doi:10.1038/35084005. arXiv: 0001

Logothetis, N. K., & Wandell, B. A. (2004). Interpreting the BOLD Signal. *Annual Review of Physiology*. doi:10.1146/annurev.physiol.66.082602.092845

Ludwig, S., Herding, J., & Blankenburg, F. (2018). Oscillatory EEG signatures of postponed somatosensory decisions. *Human Brain Mapping*. doi:10.1002/hbm.24198

Luna, R., Hernández, A., Brody, C. D., & Romo, R. (2005). Neural codes for perceptual discrimination in primary somatosensory cortex. *Nature Neuroscience*. doi:10.1038/nn1513

Lundqvist, M., Herman, P., & Miller, E. K. (2018). Working Memory: Delay Activity, Yes! Persistent Activity? Maybe Not. *The Journal of Neuroscience*. doi:10.1523/JNEUROSCI.2485-17.2018

Lundqvist, M., Herman, P., Warden, M. R., Brincat, S. L., & Miller, E. K. (2018). Gamma and beta bursts during working memory readout suggest roles in its volitional control. *Nature Communications*. doi:10.1038/s41467-017-02791-8. arXiv: 122598

Lundqvist, M., Rose, J., Herman, P., Brincat, S. L. L., Buschman, T. J. J., & Miller, E. K. (2016). Gamma and Beta Bursts Underlie Working Memory. *Neuron*. doi:10.1016/j.neuron.2016.02.028. arXiv: 15334406

McCarthy, G., Puce, A., Gore, J. C., & Allison, T. (1997). Face-specific processing in the human fusiform gyrus. *Journal of Cognitive Neuroscience*. doi:10.1162/jocn.1997.9.5.605

Menon, V., & Uddin, L. Q. (2010). Saliency, switching, attention and control: a network model of insula function. doi:10.1007/s00429-010-0262-0. arXiv: arXiv:1011.1669v3

Merzenich, M. M., & Harrington, T. (1969). The sense of flutter-vibration evoked by stimulation of the hairy skin of primates: Comparison of human sensory capacity with the responses of mechanoreceptive afferents innervating the hairy skin of monkeys. *Experimental Brain Research*. doi:10.1007/BF00234457

Michalareas, G., Vezoli, J., van Pelt, S., Schoffelen, J. M., Kennedy, H., & Fries, P. (2016). Alpha-Beta and Gamma Rhythms Subserve Feedback and Feedforward Influences among Human Visual Cortical Areas. *Neuron*. doi:10.1016/j.neuron.2015.12.018. arXiv: 15334406

Michels, L., Bucher, K., Lüchinger, R., Klaver, P., Martin, E., Jeanmonod, D., & Brandeis, D. (2010). Simultaneous EEG-fMRI during a working memory task: Modulations in low and high frequency bands. *PLoS ONE*. doi:10.1371/journal.pone.0010298

Miller, E. K., Lundqvist, M., & Bastos, A. M. (2018). Working Memory 2.0. *Neuron*, 463–475. doi:10.1016/j.neuron.2018.09.023

Mongillo, G., Barak, O., & Tsodyks, M. (2008). SynaptiC Theory of Working Memory. *Science*. doi:10.1126/science.1150769. arXiv: 0402594v3 [arXiv:cond-mat]

Moore, T., & Armstrong, K. M. (2003). Selective gating of visual signals by microstimulation of frontal cortex. *Nature*. doi:10.1038/nature01341

Moore, T., & Fallah, M. (2001). Control of eye movements and spatial attention. *Proceedings of the National Academy of Sciences*. doi:10.1073/pnas.98.3.1273

Mountcastle, V. B., Steinmetz, M., & Romo, R. (1990). Frequency discrimination in the sense of flutter: psychophysical measurements correlated with postcentral events in behaving monkeys. *The Journal of neuroscience : the official journal of the Society for Neuroscience*. doi:10.1523/JNEUROSCI.10-09-03032.1990. arXiv: /dx.doi.org/10.1108/BIJ-10-2012-0068 [http:]

Mountcastle, V. B., Talbot, W. H., Sakata, H., & Hyvärinen, J. (1969). Cortical neuronal mechanisms in flutter-vibration studied in unanesthetized monkeys. Neuronal periodicity and frequency discrimination. *Journal of Neurophysiology*. doi:10.1152/jn.1969.32.3.452

Mountcastle, V. B., Talbot, W. H., Dar-Smith, I., & Kornhuber, H. H. (1967). Neural basis of the sense of flutter-vibration. *Science*. doi:10.1126/science.155.3762.597

Muhle-Karbe, P. S., Duncan, J., De Baene, W., Mitchell, D. J., & Brass, M. (2017). Neural Coding for Instruction-Based Task Sets in Human Frontoparietal and Visual Cortex. *Cerebral cortex (New York, N.Y. : 1991)*. doi:10.1093/cercor/bhw032

Naeem, M., Prasad, G., Watson, D. R., & Kelso, J. A. (2012). Electrophysiological signatures of intentional social coordination in the 10-12Hz range. *NeuroImage*. doi:10.1016/j.neuroimage.2011.08.010

Nangini, C., Ross, B., Tam, F., & Graham, S. J. (2006). Magnetoencephalographic study of vibrotactile evoked transient and steady-state responses in human somatosensory cortex. *NeuroImage*. doi:10.1016/j.neuroimage.2006.05.045

Nieder, A. (2016). The neuronal code for number. doi:10.1038/nrn.2016.40

Nieder, A., & Miller, E. K. (2003). Coding of cognitive magnitude: Compressed scaling of numerical information in the primate prefrontal cortex. *Neuron*. doi:10.1016/S0896-6273(02)01144-3. arXiv: arXiv:0804.1718v1

Nienborg, H., & Cumming, B. G. (2009). Decision-related activity in sensory neurons reflects more than a neurons causal effect. *Nature*. doi:10.1038/nature07821. arXiv: NIHMS150003

Nieuwenhuis, S. (2011). Learning, the P3, and the locus coeruleus-norepinephrine system. *Neural basis of motivational and cognitive control*. doi:10.7551/mitpress/9780262016438.003.0012

Nieuwenhuis, S., Aston-Jones, G., & Cohen, J. D. (2005). Decision making, the P3, and the locus coeruleus-norepinephrine system. doi:10.1037/0033-2909.131.4.510. arXiv: 1507.01561

O'Connell, R. G., Dockree, P. M., & Kelly, S. P. (2012). A supramodal accumulation-to-bound signal that determines perceptual decisions in humans. *Nature Neuroscience*. doi:10.1038/nn.3248

O'Connell, R. G., Shadlen, M. N., Wong-Lin, K. F., & Kelly, S. P. (2018). Bridging Neural and Computational Viewpoints on Perceptual Decision-Making. doi:10.1016/j.tins.2018.06.005

Parmesan, C., & Yohe, G. (2003). A globally coherent fingerprint of climate change impacts across natural systems. *Nature*. doi:10.1038/nature01286

Pasternak, T., & Greenlee, M. W. (2005). Working memory in primate sensory systems. doi:10.1038/nrn1603

Pesaran, B., Pezaris, J. S., Sahani, M., Mitra, P. P., & Andersen, R. A. (2002). Temporal structure in neuronal activity during working memory in macaque parietal cortex. *Nature Neuroscience*. doi:10.1038/nn890. arXiv: 0309034 [q-bio]

Pfurtscheller, G. (1981). Central beta rhythm during sensorimotor activities in man. *Electroencephalography and Clinical Neurophysiology*. doi:10.1016/0013-4694(81)90139-5

Pfurtscheller, G., & Cooper, R. (1975). Frequency dependence of the transmission of the EEG from cortex to scalp. *Electroencephalography and Clinical Neurophysiology*. doi:10.1016/0013-4694(75)90215-1

Philiastides, M. G., Auksztulewicz, R., Heekeren, H. R., & Blankenburg, F. (2011). Causal role of dorsolateral prefrontal cortex in human perceptual decision making. *Current Biology*. doi:10.1016/j.cub.2011.04.034

Philiastides, M. G., Heekeren, H. R., & Sajda, P. (2014). Human Scalp Potentials Reflect a Mixture of Decision-Related Signals during Perceptual Choices. *Journal of Neuroscience*. doi:10.1523/JNEUROSCI.3012-14.2014

Pineda, J. A. (2005). The functional significance of mu rhythms: Translating "seeing" and "hearing" into "doing". doi:10.1016/j.brainresrev.2005.04.005. arXiv: j.cogbrainres.2005.08.014. [10.1016]

Rainer, G., & Miller, E. K. (2002). Timecourse of object-related neural activity in the primate prefrontal cortex during a short-term memory task. *The European journal of neuroscience*. doi:10.1046/j.1460-9568.2002.01958.x

Reinagel, P., Godwin, D., Sherman, S. M., & Koch, C. (1999). Encoding of Visual Information by LGN Bursts. *Journal of Neurophysiology*. doi:10.1152/jn.1999.81.5.2558

Riggall, A. C., & Postle, B. R. (2012). The Relationship between Working Memory Storage and Elevated Activity as Measured with Functional Magnetic Resonance Imaging. *The Journal of neuroscience : the official journal of the Society for Neuroscience*. doi:10.1523/JNEUROSCI.1892-12.2012

Robinson, D. A., & Fuchs, A. F. (1969). Eye movements evoked by stimulation of frontal eye fields. *Journal of Neurophysiology*. doi:10.1109/77.783791

Rohrbaugh, J. W., Donchin, E., & Eriksen, C. W. (1974). Decision making and the P300 component of the cortical evoked response. *Perception & Psychophysics*. doi:10.3758/BF03213960

Roitman, J. D., & Shadlen, M. N. (2002a). Response of neurons in the lateral intraparietal area during a combined visual discrimination reaction time task. *The Journal of neuroscience : the official journal of the Society for Neuroscience*. doi:10.1016/S0377-2217(02)00363-6. arXiv: NIHMS150003

Roitman, J. D., & Shadlen, M. N. (2002b). Response of neurons in the lateral intraparietal area during a combined visual discrimination reaction time task. *Journal of Neuroscience*. doi:10.1016/S0377-2217(02)00363-6. arXiv: NIHMS150003

Romo, R., Brody, C. D., Hernández, A., & Lemus, L. (1999). Neuronal correlates of parametric working memory in the prefrontal cortex. *Nature*. doi:10.1038/20939

Romo, R., & de Lafuente, V. (2013). Conversion of sensory signals into perceptual decisions. doi:10.1016/j.pneurobio.2012.03.007

Romo, R., Hernández, A., & Zainos, A. (2004). Neuronal Correlates of a Perceptual Decision in Ventral Premotor Cortex. *Neuron*. doi:10.1016/S0896-6273(03)00817-1

Romo, R., Hernández, A., Zainos, A., Lemus, L., & Brody, C. D. (2002). Neuronal correlates of decision-making in secondary somatosensory cortex. *Nature Neuroscience*. doi:10.1038/nn950

Roux, F., & Uhlhaas, P. J. (2014). Working memory and neural oscillations: Alpha-gamma versus theta-gamma codes for distinct WM information? doi:10.1016/j.tics.2013.10.010

Rule, M. E., Vargas-Irwin, C. E., Donoghue, J. P., & Truccolo, W. (2017). Dissociation between sustained single-neuron spiking and transient β-LFP oscillations in primate motor cortex. *Journal of Neurophysiology*. doi:10.1152/jn.00651.2016

Salinas, E., Hernández, A., Zainos, A., & Romo, R. (2000). Periodicity and firing rate as candidate neural codes for the frequency of vibrotactile stimuli. *The Journal of neuroscience : the official journal of the Society for Neuroscience*. doi:20/14/5503[pii]

Salinas, E., & Sejnowski, T. J. (2001). Correlated neuronal activity and the flow of neural information. doi:10.1038/35086012. arXiv: NIHMS150003

Salzman, C., Britten, K., & Newsome, W. T. (1990). Cortical microstimulation influences perceptual judgements of motion direction. *Nature*. doi:10.1038/346174a0. arXiv: 0801.3609

Salzman, C., Murasugi, C., Britten, K., & Newsome, W. T. (1992). Microstimulation in visual area MT: effects on direction discrimination performance. *The Journal of Neuroscience*. doi:10.1523/JNEUROSCI.12-06-02331.1992

Sanders, J. I., Hangya, B., & Kepecs, A. (2016). Signatures of a Statistical Computation in the Human Sense of Confidence. *Neuron*. doi:10.1016/j.neuron.2016.03.025

Schall, J. D., Hanes, D. P., Thompson, K. G., & King, D. J. (1995). Saccade target selection in frontal eye field of macaque. I. Visual and premovement activation. *J Neurosci*. doi:10.1523/jneurosci.4906-08.2009

Schall, J. D., & Morel, A. (1995). Topography of visual cortex connections with frontal eye field in macaque: convergence and segregation of processing streams. *The Journal of Neuroscience*.

Scheeringa, R., Fries, P., Petersson, K. M., Oostenveld, R., Grothe, I., Norris, D. G., … Bastiaansen, M. C. (2011). Neuronal Dynamics Underlying High- and Low-Frequency EEG Oscillations Contribute Independently to the Human BOLD Signal. *Neuron*. doi:10.1016/j.neuron.2010.11.044

Schmidt, T. T., Wu, Y.-h., & Blankenburg, F. (2017). Content-Specific Codes of Parametric Vibrotactile Working Memory in Humans. *The Journal of Neuroscience*. doi:10.1523/JNEUROSCI.1167-17.2017

Sejnowski, T. J. (2006). Network Oscillations: Emerging Computational Principles. *Journal of Neuroscience*. doi:10.1523/JNEUROSCI.3737-05d.2006

Shadlen, M. N., & Kiani, R. (2013). Decision making as a window on cognition. doi:10.1016/j.neuron.2013.10.047. arXiv: NIHMS150003

Shadlen, M. N., Kiani, R., Hanks, T. D., & Churchland, A. K. (2008). Neurobiology of decision making: An intentional framework. In *Better Than Conscious? Decision Making, the*

Human Mind, and Implications For Institutions. doi:10.7551/mitpress/9780262195805.003.0004

Shadlen, M. N., & Newsome, W. T. (1996). Motion perception: seeing and deciding. *Proceedings of the National Academy of Sciences*. doi:10.1073/pnas.93.2.628

Shadlen, M. N., & Newsome, W. T. (2001). Neural Basis of a Perceptual Decision in the Parietal Cortex (Area LIP) of the Rhesus Monkey. *Journal of Neurophysiology*. doi:10.1152/jn.2001.86.4.1916

Shafi, M., Zhou, Y., Quintana, J., Chow, C., Fuster, J. M., & Bodner, M. (2007). Variability in neuronal activity in primate cortex during working memory tasks. *Neuroscience*. doi:10.1016/j.neuroscience.2006.12.072

Siegel, M., Buschman, T. J., & Miller, E. K. (2015). Cortical information flow during flexible sensorimotor decisions. *Science*. doi:10.1126/science.aab0551. arXiv: arXiv:1011.1669v3

Siegel, M., Donner, T. H., & Engel, A. K. (2012). Spectral fingerprints of large-scale neuronal interactions. doi:10.1038/nrn3137

Siegel, M., Donner, T. H., Oostenveld, R., Fries, P., & Engel, A. K. (2007). High-frequency activity in human visual cortex is modulated by visual motion strength. *Cerebral Cortex*. doi:10.1093/cercor/bhk025

Siegel, M., Engel, A. K., & Donner, T. H. (2011). Cortical Network Dynamics of Perceptual Decision-Making in the Human Brain. *Frontiers in Human Neuroscience*. doi:10.3389/fnhum.2011.00021

Smulders, F. T., & Miller, J. O. (2012). The Lateralized Readiness Potential. In *The Oxford Handbook of Event-Related Potential Components*. doi:10.1093/oxfordhb/9780195374148.013.0115

Spaak, E., Watanabe, K., Funahashi, S., & Stokes, M. G. (2017). Stable and Dynamic Coding for Working Memory in Primate Prefrontal Cortex. *The Journal of Neuroscience*. doi:10.1523/JNEUROSCI.3364-16.2017

Spitzer, B., & Blankenburg, F. (2011). Stimulus-dependent EEG activity reflects internal updating of tactile working memory in humans. *Proceedings of the National Academy of Sciences*. doi:10.1073/pnas.1104189108

Spitzer, B., & Blankenburg, F. (2012). Supramodal parametric working memory processing in humans. *The Journal of neuroscience : the official journal of the Society for Neuroscience*. doi:10.1523/JNEUROSCI.5280-11.2012

Spitzer, B., Fleck, S., & Blankenburg, F. (2014). Parametric Alpha- and Beta-Band Signatures of Supramodal Numerosity Information in Human Working Memory. *Journal of Neuroscience*. doi:10.1523/JNEUROSCI.4580-13.2014

Spitzer, B., & Haegens, S. (2017). Beyond the Status Quo: A Role for Beta Oscillations in Endogenous Content (Re-) Activation. *eneuro*. doi:10.1523/ENEURO.0170-17.2017

Spitzer, B., Wacker, E., & Blankenburg, F. (2010). Oscillatory Correlates of Vibrotactile Frequency Processing in Human Working Memory. *Journal of Neuroscience*. doi:10.1523/JNEUROSCI.6041-09.2010

Squires, K. C., Hillyard, S. A., & Lindsay, P. H. (1973). Vertex potentials evoked during auditory signal detection: Relation to decision criteria. *Perception & Psychophysics*. doi:10.3758/BF03212388

Sreenivasan, K. K., Curtis, C. E., & D'Esposito, M. (2014). Revisiting the role of persistent neural activity during working memory. doi:10.1016/j.tics.2013.12.001. arXiv: NIHMS150003

Stokes, M. G. (2015). 'Activity-silent' working memory in prefrontal cortex: A dynamic coding framework. doi:10.1016/j.tics.2015.05.004

Stokes, M. G., Kusunoki, M., Sigala, N., Nili, H., Gaffan, D., & Duncan, J. (2013). Dynamic coding for cognitive control in prefrontal cortex. *Neuron*. doi:10.1016/j.neuron.2013.01.039

Stokes, M. G., & Spaak, E. (2016). The Importance of Single-Trial Analyses in Cognitive Neuroscience. doi:10.1016/j.tics.2016.05.008

Sutton, S., Braren, M., Zubin, J., & John, E. R. (1965). Evoked-potential correlates of stimulus uncertainty. *Science*. doi:10.1126/science.150.3700.1187

Talbot, W. H., & Mountcastle, V. B. (1968). The Sense of Flutter-Vibration : the Human the Monkey of Mechanoreceptive Comparison of Capacity With Response Patterns Aff erents From. *Journal of Neurophysiology*. doi:10.1167/15.1.8

Tallon-Baudry, C., Bertrand, O., Peronnet, F., & Pernier, J. (1998). Induced gamma-band activity during the delay of a visual short-term memory task in humans. *The Journal of neuroscience : the official journal of the Society for Neuroscience*. doi:20026318

Tanner, W. P., & Swets, J. A. (1954). A decision-making theory of visual detection. *Psychological Review*. doi:10.1037/h0058700

Thompson, K. G., Hanes, D. P., Bichot, N. P., & Schall, J. D. (1996). Perceptual and motor processing stages identified in the activity of macaque frontal eye field neurons during visual search. *J Neurophysiol*. doi:10.1152/jn.1996.76.6.4040

Tobimatsu, S., Zhang, Y., & Kato, M. (1999). Steady-state vibration somatosensory evoked potentials: Physiological characteristics and tuning function. *Clinical Neurophysiology*. doi:10.1016/S1388-2457(99)00146-7

Todd, J. J., & Marois, R. (2004). Capacity limit of visual short-term memory in human posterior parietal cortex. *Nature*. doi:10.1038/nature02466

Todd, J. J., & Marois, R. (2005). Posterior parietal cortex activity predicts individual differences in visual short-term memory capacity. *Cognitive, affective & behavioral neuroscience*. doi:10.3758/CABN.5.2.144

Twomey, D. M., Kelly, S. P., & O'Connell, R. G. (2016). Abstract and Effector-Selective Decision Signals Exhibit Qualitatively Distinct Dynamics before Delayed Perceptual Reports. *Journal of Neuroscience*. doi:10.1523/JNEUROSCI.4162-15.2016

Twomey, D. M., Murphy, P. R., Kelly, S. P., & O'Connell, R. G. (2015). The classic P300 encodes a build-to-threshold decision variable. *European Journal of Neuroscience*. doi:10.1111/ejn.12936

Uluc, I., Schmidt, T. T., Wu, Y.-h., & Blankenburg, F. (2018). Content-specific codes of parametric auditory working memory in humans. *NeuroImage*. doi:10.1016/j.neuroimage.2018.08.024

Urai, A. E., Braun, A., & Donner, T. H. (2017). Pupil-linked arousal is driven by decision uncertainty and alters serial choice bias. *Nature Communications*. doi:10.1038/ncomms14637. arXiv: arXiv:1011.1669v3

Urai, A. E., & Pfeffer, T. (2014). An Action-Independent Signature of Perceptual Choice in the Human Brain. *Journal of Neuroscience*. doi:10.1523/JNEUROSCI.0477-14.2014

Usher, M., & McClelland, J. L. (2001). The time course of perceptual choice: The leaky, competing accumulator model. *Psychological Review*. doi:10.1037/0033-295X.108.3.550

Van Essen, D. C., Anderson, C. H., & Felleman, D. J. (1992). Information processing in the primate visual system: An integrated systems perspective. doi:10.1126/science.1734518

Van Essen, D. C., Maunsell, J. H., & Bixby, J. L. (1981). The middle temporal visual area in the macaque: Myeloarchitecture, connections, functional properties and topographic organization. *Journal of Comparative Neurology*. doi:10.1002/cne.901990302

Varela, F., Lachaux, J. P., Rodriguez, E., & Martinerie, J. (2001). The brainweb: Phase synchronization and large-scale integration. *Nature Reviews Neuroscience*. doi:10.1038/35067550

Vergara, J., Rivera, N., Rossi-Pool, R., & Romo, R. (2016). A Neural Parametric Code for Storing Information of More than One Sensory Modality in Working Memory. *Neuron*. doi:10.1016/j.neuron.2015.11.026

Vidaurre, D., Hunt, L. T., Quinn, A. J., Hunt, B. A., Brookes, M. J., Nobre, A. C., & Woolrich, M. W. (2018). Spontaneous cortical activity transiently organises into frequency specific phase-coupling networks. *Nature Communications*. doi:10.1038/s41467-018-05316-z

Vidaurre, D., Quinn, A. J., Baker, A. P., Dupret, D., Tejero-Cantero, A., & Woolrich, M. W. (2016). Spectrally resolved fast transient brain states in electrophysiological data. *NeuroImage*. doi:10.1016/j.neuroimage.2015.11.047. arXiv: arXiv:1011.1669v3

Vogel, E. K., & Machizawa, M. G. (2004). Neural activity predicts individual differences in visual working memory capacity. *Nature*. doi:10.1038/nature02447

von Lautz, A. H., Herding, J., Ludwig, S., Nierhaus, T., Maess, B., Villringer, A., & Blankenburg, F. (2017). Gamma and Beta Oscillations in Human MEG Encode the Contents of Vibrotactile Working Memory. *Frontiers in Human Neuroscience*. doi:10.3389/fnhum.2017.00576

Wang, X.-J. (2010). Neurophysiological and Computational Principles of Cortical Rhythms in Cognition. *Physiological Reviews*. doi:10.1152/physrev.00035.2008. arXiv: NIHMS150003

Whittingstall, K., & Logothetis, N. K. (2009). Frequency-Band Coupling in Surface EEG Reflects Spiking Activity in Monkey Visual Cortex. *Neuron*. doi:10.1016/j.neuron.2009.08.016

Wimmer, K., Ramon, M., Pasternak, T., & Compte, A. (2016). Transitions between Multiband Oscillatory Patterns Characterize Memory-Guided Perceptual Decisions in Prefrontal Circuits. *Journal of Neuroscience*. doi:10.1523/JNEUROSCI.3678-15.2016

Wolff, M. J., Ding, J., Myers, N. E., & Stokes, M. G. (2015). Revealing hidden states in visual working memory using electroencephalography. *Frontiers in Systems Neuroscience*. doi:10.3389/fnsys.2015.00123

Wolff, M. J., Jochim, J., Akyürek, E. G., & Stokes, M. G. (2017). Dynamic hidden states underlying working-memory-guided behavior. *Nature Neuroscience*. doi:10.1038/nn.4546

Wu, Y.-h., Uluc, I., Schmidt, T. T., Tertel, K., Kirilina, E., & Blankenburg, F. (2018). Overlapping frontoparietal networks for tactile and visual parametric working memory representations. *NeuroImage*. doi:10.1016/j.neuroimage.2017.10.059

Xu, Y., & Chun, M. M. (2006). Dissociable neural mechanisms supporting visual short-term memory for objects. *Nature*. doi:10.1038/nature04262

Xu, Y., & Jeong, S. K. (2015). The Contribution of Human Superior Memory and Perception. *Mechanisms of sensory working memory: attention and performance XXV*, 33–42.

Zaksas, D., & Pasternak, T. (2006). Directional Signals in the Prefrontal Cortex and in Area MT during a Working Memory for Visual Motion Task. *Journal of Neuroscience*. doi:10.1523/JNEUROSCI.3420-06.2006

Zeki, S. M. (1974). Functional organization of a visual area in the posterior bank of the superior temporal sulcus of the rhesus monkey. *The Journal of Physiology*. doi:10.1113/jphysiol.1974.sp010452. arXiv: NIHMS150003

Zeki, S. M. (1980). The response properties of cells in the middle temporal area (area MT) of owl monkey visual cortex. *Proceedings of the Royal Society of London - Biological Sciences*. doi:10.1098/rspb.1980.0022

Zimmer, H. D. (2008). Visual and spatial working memory: From boxes to networks. doi:10.1016/j.neubiorev.2008.05.016

Original Studies

4

frontiers in Human Neuroscience

ORIGINAL RESEARCH
published: 04 December 2017
doi: 10.3389/fnhum.2017.00576

Gamma and Beta Oscillations in Human MEG Encode the Contents of Vibrotactile Working Memory

Alexander H. von Lautz[1,2], Jan Herding[1,2], Simon Ludwig[1], Till Nierhaus[1,3], Burkhard Maess[3], Arno Villringer[3] and Felix Blankenburg[1,2]*

[1] Neurocomputation and Neuroimaging Unit, Department of Education and Psychology, Freie Universität Berlin, Berlin, Germany, [2] Bernstein Center for Computational Neuroscience Berlin, Berlin, Germany, [3] Max Planck Institute for Human Cognitive and Brain Sciences, Leipzig, Germany

Ample evidence suggests that oscillations in the beta band represent quantitative information about somatosensory features during stimulus retention. Visual and auditory working memory (WM) research, on the other hand, has indicated a predominant role of gamma oscillations for active WM processing. Here we reconciled these findings by recording whole-head magnetoencephalography during a vibrotactile frequency comparison task. A Braille stimulator presented healthy subjects with a vibration to the left fingertip that was retained in WM for comparison with a second stimulus presented after a short delay. During this retention interval spectral power in the beta band from the right intraparietal sulcus and inferior frontal gyrus (IFG) monotonically increased with the to-be-remembered vibrotactile frequency. In contrast, induced gamma power showed the inverse of this pattern and decreased with higher stimulus frequency in the right IFG. Together, these results expand the previously established role of beta oscillations for somatosensory WM to the gamma band and give further evidence that quantitative information may be processed in a fronto-parietal network.

Keywords: working memory, MEG, somatosensory, gamma, beta, oscillations

OPEN ACCESS

Edited by:
Vladimir Litvak,
UCL Institute of Neurology,
United Kingdom

Reviewed by:
Peter Uhlhaas,
University of Glasgow,
United Kingdom
Chia-Hsiung Cheng,
Chang Gung University, Taiwan
Haiteng Jiang,
University of Minnesota, United States

****Correspondence:***
Alexander H. von Lautz
alexander.von-lautz@bccn-berlin.de

Received: *16 August 2017*
Accepted: *16 November 2017*
Published: *04 December 2017*

Citation:
von Lautz AH, Herding J, Ludwig S, Nierhaus T, Maess B, Villringer A and Blankenburg F (2017) Gamma and Beta Oscillations in Human MEG Encode the Contents of Vibrotactile Working Memory. Front. Hum. Neurosci. 11:576. doi: 10.3389/fnhum.2017.00576

INTRODUCTION

The ability to maintain behaviorally important sensory information over short periods of time is a key component of working memory (WM). The neural basis of this cognitive function has been attributed to the lateral prefrontal cortex (PFC), whose neural firing rates are modulated during stimulus retention (for review, see D'Esposito, 2007). Research in the somatosensory domain provides evidence that single neurons in the PFC can encode WM content by monotonically increasing and decreasing their firing rate (Romo et al., 1999; Brody et al., 2003). In these studies responses of neurons from the right inferior convexity of the PFC were recorded in behaving monkeys trained to decide whether the second (f2) of two sequentially presented frequencies was higher or lower than the first (f1). Hence, this task requires remembering f1 throughout a short retention interval between both stimuli. Firing rates observed during this retention interval changed as a function of f1 and were directly related to behavior, in line with an interpretation as a neural substrate of parametric WM (for review, see Romo and de Lafuente, 2013).

Complementing these findings from non-human primates, human electroencephalography (EEG) recordings during the same task have revealed a parametric increase of oscillatory

power in the beta band (15–35 Hz) as a function of f1 (Spitzer et al., 2010; Spitzer and Blankenburg, 2012). The source of this modulation was consistently found in the right inferior frontal gyrus (IFG) of the PFC. Expanding on these findings, Spitzer and Blankenburg (2012) and Spitzer et al. (2014) demonstrated this effect across sensory modalities and stimulus features, indicating a generalized role of prefrontal beta oscillations for maintaining quantitative information.

Magnetoencephalography (MEG) studies on the other hand have identified modulations of high frequency gamma oscillations (>40 Hz) accompanying somatosensory WM (Bauer et al., 2006; Haegens et al., 2010). In a vibrotactile delayed match-to-sample task, Haegens et al. (2010) demonstrated that relative to a pre-stimulus baseline, gamma power increased during the WM interval in the secondary somatosensory (SII) and frontal cortices. Furthermore, the frontal power increase correlated positively with behavioral performance, suggesting a functional role for gamma oscillations around 65–80 Hz. These results corroborate findings from other sensory domains (for reviews, see Benchenane et al., 2011; Roux and Uhlhaas, 2014; Lara and Wallis, 2015) and intracranial recordings in monkeys (Pesaran et al., 2002). Specifically, MEG studies in humans have shown that visual and auditory WM is accompanied by sustained gamma band activity in modality specific sensory areas (Lutzenberger et al., 2002; Kaiser et al., 2003; Jokisch and Jensen, 2007).

However, the available evidence for an involvement of high frequency oscillations in somatosensory WM is limited to contrasting periods of high vs. low WM load. Indeed, while investigations into the functional role of the beta-band demonstrated a parametric mapping of stimulus identity to oscillatory power, the role of gamma in maintaining stimulus features remains unclear.

In the present study, we investigated the role of cortical oscillations for the parametric encoding of human somatosensory WM. Subjects performed a vibrotactile frequency comparison task with stimuli consisting of different frequencies delivered to the left index finger. The neural substrates of performing this task were measured non-invasively with whole-head MEG, allowing for the tracking of fast oscillatory changes in high frequencies. We hypothesized that in addition to the well-established modulation of frontal beta band power by f1, oscillations in the gamma band would also be modulated by the to-be-maintained stimulus frequency.

MATERIALS AND METHODS

Participants

Twenty-three healthy volunteers (12 females, 23–37 years of age, median: 28) participated in the study and underwent a 30-min behavioral training session to learn the task one week before the MEG recording. All participants reported being right-handed, according to the Edinburgh Handedness Inventory (Oldfield, 1971), having no history of neurological illness and normal or corrected-to-normal vision. Volunteers provided written informed consent as approved by the local ethics committee of the Freie Universität Berlin in accordance with the Human Subjects Guidelines of the Declaration of Helsinki.

Experimental Paradigm

Participants were asked to decide whether the second of two sequentially presented vibrotactile frequencies was higher or lower than the first, either by making a saccade to a visual target or by selecting the target via button press (**Figure 1**). Each trial started with a fixation cross being presented at the center of a screen in front of the participant for a variable duration (750–1250 ms) at a viewing distance of 90 cm. The response type (saccade or button press) for a given trial was indicated subsequently by a square or diamond presented at the location of the fixation cross for 250 ms (first response cue, RC1; **Figure 1**). Alternatively, in 50% of trials, a circle appeared at this time, indicating that the response mapping would only be disclosed via a second response cue just before participants were allowed to respond (RC2; **Figure 1**). Then, the two vibrotactile flutter stimuli (with frequencies 11–31 Hz) were briefly presented to the left index finger (250 ms each), separated by 1000 ms. The frequency of the first stimulus (f1) was varied between 15 and 27 Hz in steps of 4 Hz while the frequency of the second stimulus (f2) was either 2 or 4 Hz higher or lower than f1. The f2 presentation was followed by a delay of 1000 ms, after which the second response cue was presented for 250 ms (RC2; **Figure 1**). If the first response cue had already provided the response mapping (i.e., RC1 = diamond or square), a circle was presented. In case the first response cue was uninformative (i.e., RC1 = circle), the second response cue revealed whether participants should respond via button press or saccade (i.e., RC2 = diamond or square). Following this, two colored target dots were presented at the left and right side of the screen with eccentricity of 12° visual angle ('go'-cue). One dot was blue, and the other one yellow, with the specific spatial configuration being counterbalanced across trials (i.e., blue dot was equally likely on either side). Each participant applied one of two possible color mappings (i.e., if f2 > f1, choose blue; if f2 < f1, choose yellow, or vice versa) that were counterbalanced across participants, and selected one of the colored dots according to their decision as soon as the target dots appeared (i.e., either by button press or saccade, depending on the cued response modality).

Partipants completed six blocks with 128 trials each. Within each block, half the trials were answered by button press, the other half by saccades (64/64). Similarly counterbalanced was the position of the informative response cue, with half the response types indicated before and the other half after stimulus presentation (64/64). The total of 768 trials per participant resulted in a scanning time of about 75 min.

Stimuli

All stimuli were created using a PC running the MATLAB-based Psychophysics toolbox (Brainard, 1997). Vibrotactile stimulation was delivered by a piezoelectric Braille stimulation device (QuaeroSys, Schotten, Germany) to the left index finger. The 16 pins of the 4 × 4 Braille display were driven

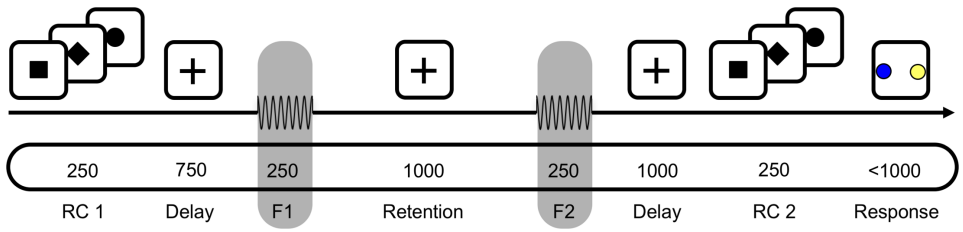

FIGURE 1 | A schematic of the task for one example trial. First, a response cue (RC1) was presented for 250 ms to indicate whether to answer by saccade or button press. In half the trials a circle appeared instead, which indicated that the response modality would be indicated just before responding. After a 750 ms delay, the base frequency f1 was presented for 250 ms, followed by a 1000 ms retention interval. After presentation of the comparison frequency f2, the decision was delayed for 1000 ms until a second response cue (RC2) was shown for 250 ms. Participants responded by selecting one of the two colored targets, e.g., blue for f2 > f1, by saccade or button press. In the schematic, the top section depicts visual input; the middle the tactile; and the bottom the timing (in ms) of input.

by a constant 121 Hz carrier signal whose amplitude was modulated by sinusoids with frequencies between 11 and 31 Hz, resulting in a percept of vibrotactile flutter at the modulation frequency (Tobimatsu et al., 1999). The stimuli were loaded into the buffer of the Braille stimulation device 1 s before the presentation of f1, as the communication of PC and Braille stimulator created noticeable artifacts. To mask the noise of the Braille display, white noise was replayed at 66 dB from electromechanical transducers and transmitted via sound conducting tubes to the ears inside the MEG helmet.

Data Acquisition

Participants were positioned upright in the MEG system with their arms placed comfortably on a table in front of them. They were instructed to keep fixation on the presentation screen and not to move during the experiment. Magnetoencephalography was recorded using a whole-head MEG Vectorview NM2169N (Elekta Neuromag Oy, Helsinki, Finland) with a total of 306 MEG channels (102 magnetometers, 204 planar gradiometers). A band-pass filter of 0.03–500 Hz was applied during acquisition at 1500 samples/second and five head position indicator (HPI) coils attached to the scalp, three on the forehead and one on each mastoid, tracked the head movements continuously. Three fiducials (nasion, left and right preauricular points) as well as over 500 scalp points were measured with a Polhemus FASTRAK 3D digitizer to obtain the head shape of each participant. We did not employ electrooculography, because initial tests revealed that electrodes placed on the head increased artifacts from the QuaeroSys stimulation device (cf. Chandler et al., 2015).

Participants' responses were tracked via a NNL-Response Grip from Nordic Neuro Lab (BNC – serial port) and an iView X MEG eye-tracking system (SensoMotoric Instruments GmbH, Berlin, Germany) sampled at 50 Hz. Saccades to the left or to the right further than nine degrees off-center were interpreted as a response to the according side. Trials in which participants showed lateral eye movements before the colored targets appeared and those in which the wrong response modality was used were excluded from further analysis. Before each block started, the eye-tracker was calibrated and validated with a standard five-point procedure.

Data Processing

All MEG data were preprocessed using the Oxford Centre for Human Brain Activity software library (OSL)[1] drawing on the Fieldtrip toolbox[2] (Oostenveld et al., 2011) and SPM12 (Wellcome Department of Cognitive Neurology, London, United Kingdom[3]).

As a first preprocessing step, we identified noisy channels and periods of strong artifacts by visually inspecting the continuous recordings. Then, using the MaxMove software (Elekta Neuromag), noise sources outside the skull were removed by applying signal-space separation with its temporal extension. Head movement compensation based on continuous tracking of the HPI coils was used and each individual's data transformed to the co-ordinate frame of their third scanning block. Subsequently the continuous data were bandpass filtered at 0.1–165 Hz, down-sampled to 512 samples per second and cut into epochs with respect to f1 onset in a time window of −1000 to +1500 ms. After visual inspection of individual trials to identify extreme muscle artifacts, squid jumps and signal drop out, an independent component analysis (ICA), as implemented in the EEGLAB toolbox (Delorme and Makeig, 2004), was calculated to identify blink, saccade and heart beat components, which were excluded in the remixing of the data. We conservatively rejected only those components that showed a very typical artifactual nature. In a final visual inspection, trials with persisting artifacts were manually removed.

To obtain a time-frequency (TF) representation of spectral power we used a sliding window Fourier transform at steps of 20 ms and applied a Hann taper with seven cycles length for frequencies 5–40 Hz. For higher frequencies, we used a multitaper Fourier transform with a fixed sliding window of 200 ms and ±10 Hz smoothing.

Evoked power was calculated for each f1-f2 stimulus pair by computing the TF representation of the according event related

[1]http://ohba-analysis.github.io/
[2]http://www.fieldtriptoolbox.org
[3]www.fil.ion.ucl.ac.uk/spm/

fields (ERFs). ERFs were obtained by averaging all baseline-corrected trials (with respect to 650–150 ms prior to f1) for each stimulus pair in the time domain. Induced power was calculated by subtracting the ERFs of each stimulus pair from according single trials before transforming the single-trial data into the TF domain. The resulting single-trial TF representations were averaged for each condition (i.e., per stimulus pairs) to yield estimates of average induced power per condition. Finally, we applied a frequency-specific baseline correction by subtracting the average power in each frequency band 650–150 ms before f1 onset from the whole trial. For further analyses and display purposes, we combined the set of two orthogonal gradiometers at each location, resulting in 102 rectified planar gradiometers.

Statistical Analysis

Time-frequency maps were convolved with a 3 Hz × 300 ms Gaussian smoothing kernel (Kilner et al., 2005) to reduce variability between trials. To investigate parametric coding of f1 frequency during the retention interval, we implemented a general linear model (GLM) with a one-factorial repeated measures design for individual trials with the four f1 conditions as factor levels (i.e., f1 = 15, 19, 23, or 27 Hz). The accordingly estimated parameter maps (beta images) were weighted with a zero-mean contrast vector of [−0.75, −0.25, 0.25, 0.75]. The resulting contrast images depict the parametric difference across the four conditions in each TF bin.

These images from all individuals were statistically validated via a cluster-based permutation test procedure over all subjects (Maris and Oostenveld, 2007). This test controls the false-alarm rate by using a cluster statistic that is evaluated under a permutation distribution of summary statistics of the observed data, which we established with 5000 randomly sign-flipped permutations. A cluster was defined as a group of adjacent time-frequency bins whose cluster-defining threshold surmounted $p_{\text{threshold}} < 0.05$. Clusters exceeding the family-wise error (FWE) corrected threshold of $p_{\text{FWE}} < 0.05$ (corrected for time, frequency, and channels) were considered to be statistically significant. Cluster-based inference, which serves to reject the null hypothesis of the whole time-frequency-channel window, was supplemented by conventional linear trend analysis over time, pooled over the channels and frequency bands in which a significant effect had been observed. The aforementioned analysis steps were also applied to equal-sized subsets of correct and incorrect trials. For each cluster, the statistical comparisons were then based upon those channels and frequencies exhibiting a significant effect in the main parametric contrast of induced power. This cluster analysis was supplemented by conventional *t*-tests between correct and incorrect trials on all timepoints where significant clusters had been identified and were subjected to Bonferroni–Holm correction.

To maximize the power of these parametric contrasts, we pooled trials over both response modalities (i.e., saccades and button presses) and response cues (i.e., before and after stimulus presentation). To ensure that there were no differences between the underlying subgroups for the parametric WM effects, we applied the same procedure for these separate conditions. Moreover, to verify that response times (RTs) – as a measure of WM load – did not have an influence on the parametric coding of vibrotactile frequencies, we contrasted the four estimated parameter maps from the GLM inversion (i.e., one beta image for each base frequency) by the according individual mean RTs, instead of the actual f1 frequencies as in the main analysis. Both control analyses did not reveal any significant clusters during the WM period of this task.

Source Reconstruction

The 3-D sources of the observed effects at the sensor level were reconstructed using T1-weighted structural magnetic resonance (MR) images. The images were acquired with a Siemens 3.0 Tesla TIM Trio or Verio scanner, either using a T1-weighted MPRAGE sequence (TR = 2300 ms, TE = 2.96 ms, flip angle = 9°, FOV = 256 mm × 240 mm × 176 mm, voxel size = 1.0 mm isotropic) or a T1-weighted MP2RAGE sequence (TR = 5000 ms, TE = 2.92 ms, TI1 = 700 ms, TI2 = 2500 ms, flip angle 1 = 4°, flip angle 2 = 5°, matrix size = 240 × 256 × 176, voxel size = 1.0 mm isotropic). The individual structural MR images were used to create cortical meshes of 8196 vertices by warping meshes from a brain template to the inverse spatial normalization of individual brains. The MEG recording sites were co-registered with the MRI using three fiducials: the nasion as well as the left and right pre-auricular points. The forward model (i.e., leadfield matrix) was estimated as a realistic single shell (Nolte, 2003).

The inversion of the forward model was based on the preprocessed MEG data in the time domain, prior to TF transformation. Before model inversion, the time domain signal was bandpass-filtered and epoched to representative time-frequency windows that reflected the features of the sensor space analysis; namely the significant times and frequencies of the cluster-based permutation test for the localization of the WM effect, and the time of f1 presentation in combination with according frequency bands (i.e., frequency of f1 ±1 Hz) for the localization of somatosensory steady-state evoked fields (SSEFs). The forward model was inverted using multiple sparse priors (MSP; Friston et al., 2008) under group constraints (Litvak and Friston, 2008) as implemented in SPM12 for each condition separately. For each participant, the results of model inversion were summarized by 3-D images reflecting the spectral source amplitude averaged over the corresponding TF windows of interest. These matched the significant clusters of the sensor level analysis for the WM effect, and were according to time and frequency of f1 presentation for the localization of SSEFs. For the source reconstruction of the WM effect, the summary images were contrasted in analogy to the sensor space analysis, namely by a parametric contrast corresponding to the four different f1 values (i.e., f1 = 15, 19, 23, 27 with contrast vector = [−0.75, −0.25, 0.25, 0.75]). For the source reconstruction of SSEFs, the 3-D summary images of spectral source power during f1 presentation (at corresponding frequencies) were weighted by the individual amplitudes of SSEFs as observed at the sensor level. Since somatosensory SSEFs (i.e., somatosensory steady-state evoked potentials recorded with EEG) are known to show a bell-shaped amplitude profile over stimulus frequencies in

the flutter range when recorded at the scalp (e.g., Snyder, 1992; Tobimatsu et al., 1999), this specific amplitude profile was also used to identify the most likely cortical sources of SSEFs. On the group level, individual source estimates were contrasted using conventional *t*-tests. Sources that exceeded a statistical threshold of $p < 0.01$ ($p < 0.001$ for SSEFs; both uncorrected) were displayed to indicate the most likely sources underlying the effects observed at the sensor level. References to anatomical landmarks were established with the SPM anatomy toolbox (Eickhoff et al., 2005) and are expressed in the Montreal Neurological Institute and Hospital (MNI) coordinate system.

RESULTS

Behavior

Participants correctly discriminated on average 69% ($SD = 7\%$, **Table 1**) of all presented stimulus pairs and each participant's correct responses exceeded the guess rate of 50%. A within-subjects ANOVA with the factors 'base stimulus frequencies' in Hz (15, 19, 23, 27) and 'difficulty' (±4 Hz vs. ±2 Hz) was performed on percentages of correct responses (PCR), logit-transformed to account for the non-normality of the residuals. This analysis revealed no effect of base stimulus frequency (i.e., f1) on the percentage of correct responses [$F(3,66) = 1.25$, $p > 0.05$]. However, as expected, participants were more successful on easy trials (f2-f1 = ±4 Hz) as compared to difficult trials [f2-f1 = ±2 Hz; $F(1,22) = 101.64$, $p < 0.001$]. Similarly, we performed a 2 × 2 within-subjects ANOVA with factors 'response type' (button vs. saccade) and 'response cue' (before vs. after stimulus presentation) on the logit transformed PCRs, which revealed no significant differences (all $p > 0.05$, see **Table 1**).

On average, participants responded 430 ms after the 'go'-cue, i.e., after displaying the response mapping on the screen. Because we applied a forced-delay decision task, RTs were not expected to show large variability across different stimulus conditions. Accordingly, a within-subjects ANOVA with factors 'base stimulus frequencies' and 'difficulty' of the median RTs did not reveal any significant differences (all $p > 0.05$, see **Table 1**). The same analysis with the factors 'response type' and 'response cue' showed faster answers by button press than saccades [$F(1,22) = 24.82$, $p < 0.001$]. One reason for this difference was that detecting saccades accurately was slower than reading out button presses. Participants also gave faster responses when the response cue was delivered before stimulus presentation [$F(1,22) = 30.71$, $p < 0.001$, for a list of all RTs see **Table 1**].

TABLE 1 | Average task performance.

Behavioral performance		
Frequency (Hz)	**% Correct**	**RT (ms)**
15	67 (12)	437 (106)
19	69 (9)	430 (97)
23	71(9)	428 (93)
27	66 (7)	425 (93)
Total	**69 (7)**	**430 (97)**
f1-f2 (Hz)		
−4	69 (11)	432 (98)
−2	62 (9)	433 (101)
2	65 (9)	435 (100)
4	79 (11)	420 (90)
Response cue before		
Button press	69 (8)	379 (109)
Saccade	69 (7)	443 (91)
Response cue after		
Button press	68 (8)	419 (110)
Saccade	69 (8)	478 (99)

The top part shows the performance for the four base (f1) frequencies as proportion of correct responses (PCRs; in %) as well as the median reaction times (RTs) in milliseconds. The middle part depicts PCRs and RTs as a function of the difference between base (f1) and comparison (f2) frequency. The bottom part shows the performance for the different response modalities, separate for whether the response cue appeared before or after vibrotactile stimulation. All entries are followed by the corresponding standard deviation in brackets.

Stimulus-Evoked Fields

Stimulus evoked MEG activity from all planar gradiometers are depicted in **Figure 2A** for one exemplary stimulus pair (f1 = 23 Hz; f2 = 27 Hz). The vibrotactile stimulus evoked strong frequency-specific steady-state evoked fields (SSEFs), contralateral to the stimulated hand (**Figure 2B**). Source reconstruction localized the steady-state evoked response focally to the right somatosensory cortex, with a cluster spanning areas 3b, 1 and 2 (peak: 24, −38, 57). Crucially, evoked responses were limited to the duration of stimulus presentation and were absent during the retention interval.

We were interested whether subjects' performance was related to their steady-state evoked responses as previously reported with EEG (Spitzer et al., 2010). **Figure 2C** shows the grand average narrow band evoked activity at the frequency of f1 and f2 stimulation, computed over all stimulus conditions for equal subsets of correct and incorrect trials. The illustrated time-courses are based on averages from planar gradiometers over right somatosensory areas, where SSEFs were most pronounced. Statistical analysis revealed differences between correct and incorrect trials during both base (f1) and comparison (f2) stimulus presentation ($p < 0.05$). This difference is likely due to participants increased attention during correct trials, which has been shown to enhance somatosensory evoked potentials (Bardouille et al., 2010). Additionally, we tested whether individual SSEFs were related to behavioral performance across participants. The correlation between subject's PCRs and SSEF amplitude was not significant [Pearson's $r(21) = 0.34$, $p = 0.11$; **Figure 2D**], however, there was a trend toward stronger SSEFs in subjects with higher performance.

Induced MEG Responses

The overall induced responses observed in higher and lower frequencies pooled over all trials are illustrated in **Figure 3**. Transient and steady-state evoked potentials were eliminated by subtracting the average waveform before time-frequency transformation for each base and comparison frequency pair.

Because the piezoelectric stimulation device created an artifact that varied trial-by-trial, subtracting the average waveform left a residual artifact that was restricted to the time of stimulus presentation (**Figure 3B**).

In comparison to a prestimulus baseline, vibrotactile stimulation induced the typically observed changes in the beta band (15–25 Hz) over somatosensory areas (see Spitzer et al., 2010). During and immediately after stimulation, we observed a beta power decrease over bilateral somatosensory channels (**Figures 3B,C**; peak: 42, −26, 52), which was followed by a rebound, dominantly contralateral to the side of stimulation (**Figures 3B,D**; peak: 46, −34, 63). Moreover, alpha band (7–12 Hz) activity was increased during the retention phase in posterior channels (**Figures 3B,E**). Source reconstruction of this effect revealed a distributed activation pattern over visual regions that was most robust ipsilateral to the stimulated hand (peak: −12, −90, 45). Furthermore, this effect was more pronounced in correct than incorrect trials ($p_{FWE} < 0.05$). As visual input was inconsequential for task performance during this time, alpha power appears to reflect top-down inhibition of task-irrelevant cortical areas (Klimesch et al., 2007; Jensen and Mazaheri, 2010).

While there were no changes in induced gamma power (>40 Hz, **Figure 3A**) with respect to the prestimulus baseline, frontal gamma power between 70 and 110 Hz was related to task performance. In particular, we found higher broadband gamma band power for correct as compared with incorrect trials ($p_{FWE} < 0.01$). However, this effect neither correlated with changes in occipital alpha power across subjects, nor with participants' overall performance (both $p > 0.05$), as had been reported previously (Haegens et al., 2010).

Parametric Contrast of Induced Beta Oscillations

The central aim of this study was to identify changes in oscillatory power that scale with the stimulus held in WM throughout the delay period. **Figure 4** illustrates such a parametric WM effect for low frequencies (5–40 Hz). A cluster-based permutation test revealed TF windows in which the effect was statistically significant (**Figure 4A**). Interestingly, this analysis indicated two distinct clusters in the beta band (both $p_{FWE} < 0.05$), centered at the middle of the retention interval. One cluster spanned frequencies in the lower beta band (10–20 Hz) and showed the strongest modulation over bilateral parietal channels (**Figure 4E**). Source localization of this effect indicated focal activity in the right intraparietal sulcus of posterior parietal cortex (PPC; **Figure 4E**; peak: 50, −44, 53), an area closely linked to numerosity processing (Nieder, 2016). Markedly, the average time courses of lower beta power scaled monotonically with the frequency held in WM (**Figure 4D**), as confirmed by linear trend analysis (600–1050 ms, $p < 0.05$). The second cluster extended to the upper beta frequency range (30–35 Hz) and peaked in right frontal channels (**Figure 4C**). The most likely source of this effect was located in the right IFG of the lateral PFC (**Figure 4C**; peak: 48, 12, 35). Similar to the effect in the lower beta band, high beta power scaled with the remembered stimulus frequency throughout a large portion of the retention interval (**Figure 4B**).

To investigate a link to behavior, we compared the observed modulations of beta band power between correct and incorrect trials. When the analysis was based exclusively on incorrect trials, the observed parametric contrast did not reveal any significant effects. However, while analyses of only correct trials revealed the same pattern as the main analysis, the difference between correct and incorrect was not significant. Note that this analysis was limited to a fraction of trials to match the amount of correct with incorrect trials, which strongly reduced statistical power. **Figure 4F** illustrates an example of the performance related differences and displays the parametric contrast statistic at 30–35 Hz for equal-numbered subsets of correct and incorrect trials separately.

Parametric Modulations of Induced Gamma Activity by f1

The main focus of the present MEG study was the possible parametric modulation of higher frequency oscillations throughout f1 retention, complementing the previously established effects in lower frequencies with EEG. Statistical analysis of frequencies in the gamma band revealed a cluster of prefrontal channels, whose power at 74–90 Hz declined monotonically with increasing f1 frequency (**Figures 5A,E**; $p_{FWE} < 0.05$). Source reconstruction of the TF cluster identified the right IFG as the origin of this negative gamma band modulation (**Figure 5B**; peak: 50, −44, 53). In comparison with the high beta effect, which showed the opposite pattern (i.e., an increase with stimulus frequency), the modulation of gamma band activity was localized to more anterior and inferior areas, also reflecting the differences in their respective scalp topographies (viz. **Figures 4C**, **5B**). Linear trend analysis of the average power in this frequency range for each of the four f1 stimuli was significant between 550 and 800 ms after f1 onset (**Figure 5C**).

The separate analysis of equal-numbered subsets of correct and incorrect trials resulted in the same pattern as observed in lower frequencies. While an analysis based exclusively on correct trials appeared more similar to the effects of all trials (i.e., showed a modulation by f1), incorrect trials did not show this pattern. However, because this analysis was based upon random permutations of a fraction of trials, statistical power was strongly reduced and no significant differences manifested between the two subsets (**Figure 5D**).

DISCUSSION

In the present study, we recorded MEG in humans to determine the neural oscillations underlying vibrotactile frequency maintenance during WM. In a sequential frequency comparison task, we identified modulations of spectral power by the to-be-remembered vibrotactile stimulus frequency (i.e., f1) in the beta (at 10–20 and 30–35 Hz) and gamma (at 74–90 Hz) range during the WM period of the task. Oscillatory power in the beta band parametrically increased in parietal and prefrontal areas with

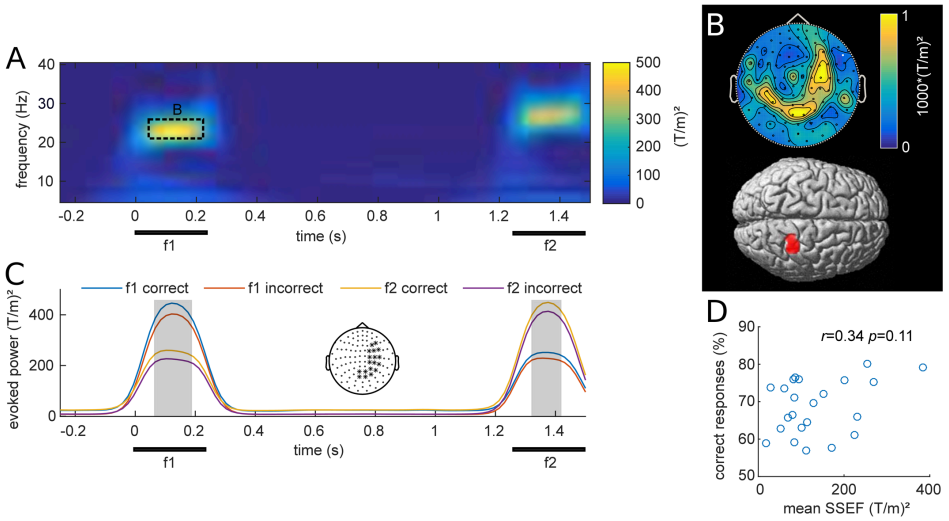

FIGURE 2 | (A) Grand average of stimulus evoked fields over all participants and planar gradiometers for an example stimulus pair (base = 23 Hz; comparison = 27 Hz). The steady-state evoked field (SSEF) at the time of f1 and f2 stimulation appears prominent in a narrow frequency band around the perceived vibrotactile frequency. **(B)** *Top*: Average topography of the SSEFs for all f1 stimuli. *Bottom*: Source reconstruction of the mean SSEF, weighted by relative amplitude, thresholded at $p < 0.001$ (uncorrected). Sources span the somatosensory areas 1, 2, and 3b. **(C)** SSEFs expressed as average of channels with strongest response during stimulus presentation (marked with * in topography), depicted in the center. The four time-courses show the mean narrow-band power around the frequencies of base (f1) and comparison (f2) stimuli for equal-numbered correct and incorrect trials. The gray shading indicates time points of significant difference between the two subsets from cluster analysis ($p_{FWE} < 0.05$). **(D)** Scatterplot of mean narrow-band SSEF amplitude and percent correct responses (PCR) for each subject. The correlation of these two metrics was not significant ($r = 0.34$, $p = 0.11$).

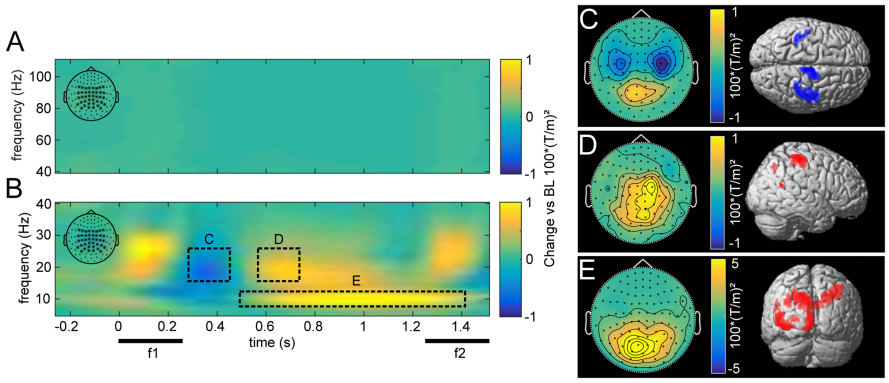

FIGURE 3 | Grand average induced power for high (40–110 Hz; **A**) and low frequencies (5–40 Hz; **B**), compared to pre-stimulus baseline for central parieto-occipital channels as marked in the top left corner. The dashed rectangles illustrate time-frequency windows with increases and decreases induced by stimulus presentation. Beta power first decreased after stimulus presentation **(C)**, then rebounded with an increase in right somatosensory areas, contralateral to the stimulated hand **(D)**. Alpha power was elevated throughout the delay period, most strongly in occipital areas **(E)**. **(C–E)** Show the topographies and source reconstructions ($p < 0.01$, uncorrected) of observed stimulus induced changes.

the magnitude of f1. In contrast, prefrontal gamma oscillations parametrically decreased with increasing f1.

The sequential frequency comparison task employed in this study required participants to maintain the stimulus frequency of the first stimulus (i.e., f1) in WM. Consistent with previous EEG studies of somatosensory WM (Spitzer et al., 2010; Spitzer and Blankenburg, 2011, 2012) we identified oscillations in the beta band (10–35 Hz) that encoded the frequency of f1 in a parametric manner during the delay period of the task. The parametric change of high beta power was localized to the IFG in full agreement with previous EEG (Spitzer et al., 2010), fMRI (Kostopoulos et al., 2007) and electrophysiological recordings (Romo et al., 1999; Brody et al., 2003) that demonstrated a crucial role of the IFG for parametric

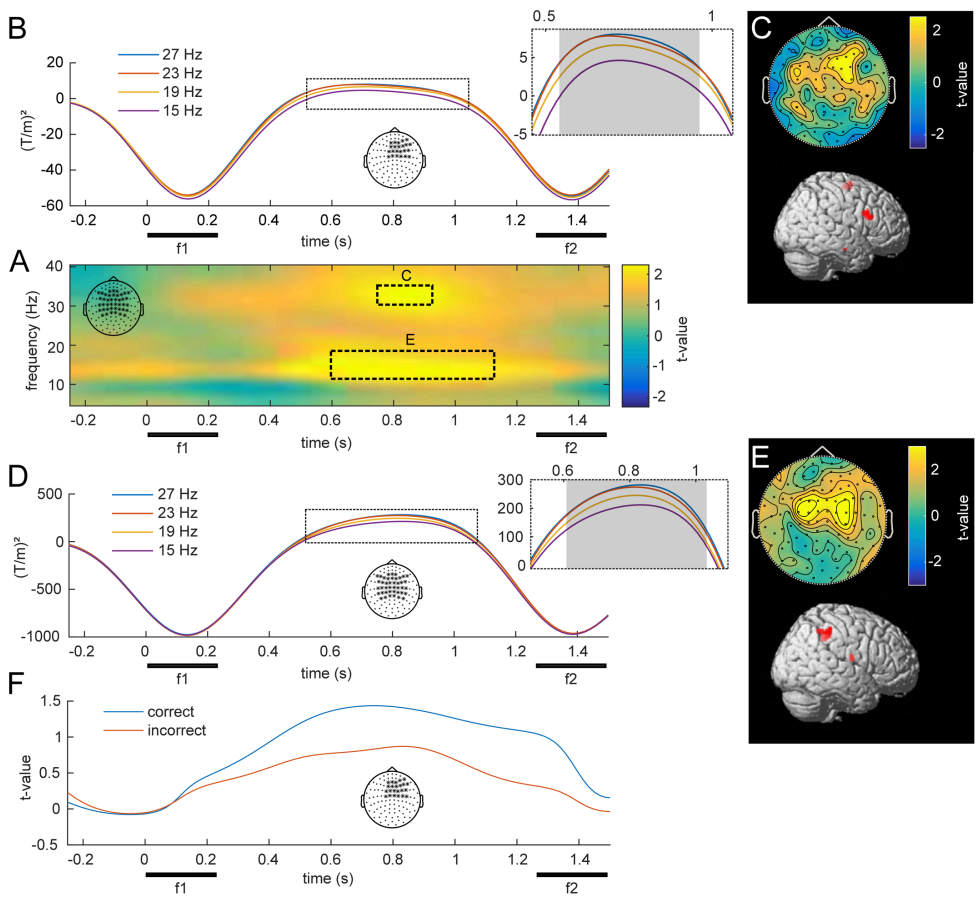

FIGURE 4 | Overview of low frequency oscillations modulated by f1. **(A)** Statistical parametric map of oscillatory power as a function of f1, averaged over bilateral fronto-parietal electrodes denoted in the top left corner. Statistical analysis revealed two separate clusters, one in a higher and one in a lower beta band ($p < 0.05$, FWE), which are marked with dashed lines. **(B)** Illustration of the average power at 30–35 Hz for the four f1 stimuli throughout the retention interval for right frontal channels. The gray area denotes a significant linear trend. **(C)** Topographical scalp distribution and corresponding source reconstruction of the TF cluster in the upper beta band as marked in **(A)**. **(D,E)** Time-course, topography and source reconstruction in analogy to **(B)** and **(C)** for the TF cluster in the lower beta band (10–20 Hz) as depicted in **(A)**. **(F)** Grand average time-course of WM effect in correct and incorrect trials over right frontal channels at 30–35 Hz.

somatosensory WM. Contrary to previous EEG recordings (Spitzer et al., 2010; Spitzer and Blankenburg, 2011, 2012), in which the skull typically acts like a low-pass filter (Pfurtscheller and Cooper, 1975), the observed effect extended above 30 Hz and might therefore be termed a change in the gamma, not the beta band.

Interestingly, we also observed modulations of high frequency gamma power in the right IFG. However, this effect displayed the opposite pattern of the parametric modulation of spectral power in the beta band, i.e., gamma band power decreased monotonically with stimulus frequency. The observed effect in the gamma band appeared in the same frequency range (74–90 Hz) as other correlates of WM in MEG (Kaiser et al., 2003; Fuentemilla et al., 2010; Haegens et al., 2010) and was estimated to be located slightly anterior to the high beta band modulation. Whereas the overall induced gamma power was additionally related to performance within subjects, it neither correlated with performance across subjects, nor with alpha power as was previously observed in a similar task by Haegens et al. (2010). The same study also observed a sustained broad band gamma increase in SII during the retention phase for which we found no evidence in the present study. The lack of such a sustained signal favors the notion that WM exhibits dynamic oscillatory changes – not sustained activity – as evidenced in single-cell recordings (cf. Shafi et al., 2007; Stokes et al., 2013; Lundqvist et al., 2016).

As signal detection with MEG depends on large-scale oscillatory changes, we speculate that our observations reflect a population-level correlate of the heterogeneous encoding as a complex pattern of increases and decreases in firing rate observed in single cells (Barak et al., 2010). This is in line with previous EEG studies (Spitzer and Blankenburg, 2011, 2012) hypothesizing

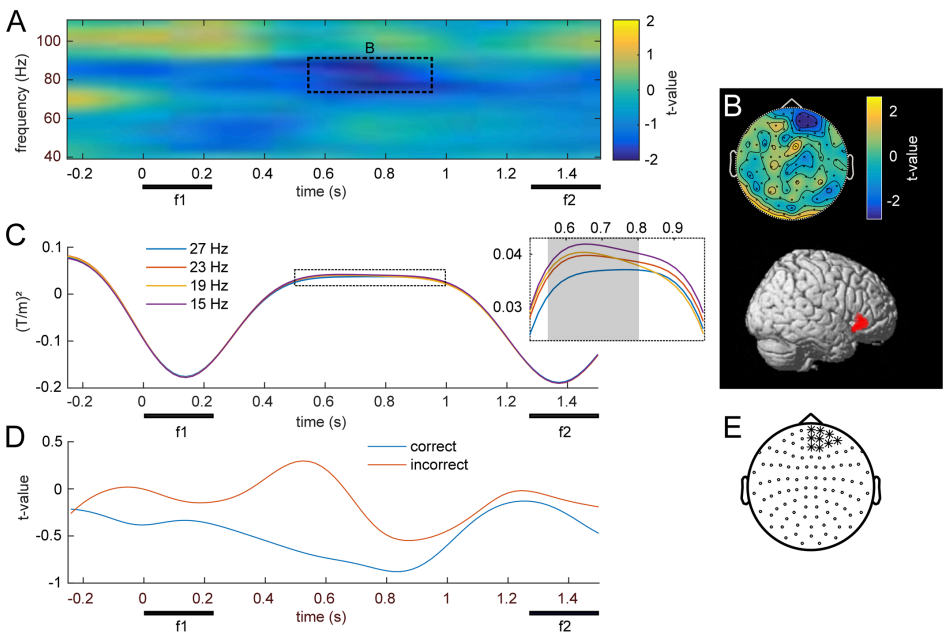

FIGURE 5 | Modulation of induced high frequency activity by f1. **(A)** Statistical parametric map of the linear contrast of the four base (f1) frequencies. The dashed rectangle marks the right frontal cluster ($p < .05$, FWE) for which **(B)** shows the scalp topography and corresponding source reconstruction. **(C)** Time-course of average stimulus induced power for the four different base (f1) stimuli; gray area denotes significant time points. **(D)** Grand-average time courses of gamma band power (74–90 Hz) for equal-numbered subsets of correct and incorrect trials. **(E)** Channels used for **(A–D)**, marked with *.

that parametric prefrontal WM effects may indicate an abstract internal scaling of analog quantity information, according to task demands. While the basis of this interpretation was confined to prefrontal oscillations in the beta band, the present results extend this view to prefrontal gamma. This is particularly interesting, because gamma amplitudes recorded with EEG, but not beta, have been found to predict neural responses from multiunit activity recordings in monkeys (Whittingstall and Logothetis, 2009), thus being more likely to represent commonalities between monkey and human research.

Contrary to previous EEG studies, we found that low beta band power (10–20 Hz) was also parametrically modulated by the stimulus frequency held in WM. Interestingly, this effect localized to the right intraparietal sulcus (IPS), an area well-established in its role for supramodal number processing (Eger et al., 2003; Castelli et al., 2006; Nieder, 2012). In particular, blood-oxygen-level dependent (BOLD) responses in the IPS can be used for multi-voxel pattern analysis to distinguish between quantities (Eger et al., 2009) and have been shown to activate in conjunction with inferior frontal areas in numerosity tasks (Piazza et al., 2007; Knops et al., 2014). The present results therefore join growing evidence that indicates a common representation of abstract quantity in the IPS and PFC.

It is unclear, however, why previous EEG studies (Spitzer et al., 2010, 2014; Spitzer and Blankenburg, 2011, 2012; Herding et al., 2016) did not detect the observed changes in the IPS. Besides the higher signal-to-noise ratio for shallow sources with MEG compared to EEG, one reason may be that MEG is more sensitive to sulcal than gyral sources, making the detection of oscillations from the intraparietal sulcus more likely than those from, e.g., the IFG (Hämäläinen et al., 1993; Goldenholz et al., 2009).

Notably, the parametric changes in low beta (10–20 Hz) included frequencies as low as those in the alpha range (8–12 Hz – also called 'mu'), which are commonly associated with the functional disengagement of particular brain areas (Klimesch et al., 2007). However, the low beta signal was parametrically modulated by the stimulus frequency, suggesting a feature-specific role of the underlying neural process. We suggest that our findings may be explained by frequency specific inhibitory processes in sensorimotor areas themselves, as proposed by the discrete coding and periodic replay hypothesis (Sandberg et al., 2003; Lundqvist et al., 2011), and might be an expression of passive maintenance states as theorized by the dynamic coding framework (Stokes, 2015). In agreement with this idea, the observed beta-gamma dynamics may reflect feature specific differences in brief beta and gamma bursts, which would agree with recent observations in monkeys (Lundqvist et al., 2016). Overall, it appears that an intricate interplay of beta and gamma oscillations in fronto-parietal areas underlies tactile WM, as has recently been observed for attention (van Ede et al., 2014).

In summary, we have shown that beta and gamma oscillations in the IFG parametrically encode stimulus features while

retaining vibrotactile frequencies in working memory. Interestingly, in contrast to increases in the beta band, gamma oscillations decreased with the to-be-maintained frequency. Additionally, we found a modulation of spectral power by stimulus frequency in a lower frequency range in the intraparietal sulcus, which underlines the close coupling of IPS and IFG for the processing of abstract quantities. Our findings suggest a functional role of neural oscillations for WM in a fronto-parietal network, with an extended role of beta and gamma oscillations for the somatosensory domain.

ETHICS STATEMENT

This study was carried out in conformance with the recommendations of the ethics committee of the Freie Universität Berlin with written informed consent from all subjects and in accordance with the Declaration of Helsinki.

AUTHOR CONTRIBUTIONS

AvL, JH, SL, TN, and FB: experiment design, data collection, data analysis, article preparation. BM and AV: data collection, data analysis, article preparation.

FUNDING

This work was supported by the German Research Foundation (DFG Grant GRK1589/2).

ACKNOWLEDGMENT

The authors thank Hermann Sonntag and Yvonne Wolff for help during data acquisition and Poppy Sharp for thoughts on the manuscript.

REFERENCES

Barak, O., Tsodyks, M., and Romo, R. (2010). Neuronal population coding of parametric working memory. *J. Neurosci.* 30, 9424–9430. doi: 10.1523/JNEUROSCI.1875-10.2010

Bardouille, T., Picton, T. W., and Ross, B. (2010). Attention modulates beta oscillations during prolonged tactile stimulation. *Eur. J. Neurosci.* 31, 761–769. doi: 10.1111/j.1460-9568.2010.07094.x

Bauer, M., Oostenveld, R., Peeters, M., and Fries, P. (2006). Tactile spatial attention enhances gamma-band activity in somatosensory cortex and reduces low-frequency activity in parieto-occipital areas. *J. Neurosci.* 26, 490–501. doi: 10.1523/JNEUROSCI.5228-04.2006

Benchenane, K., Tiesinga, P. H., and Battaglia, F. P. (2011). Oscillations in the prefrontal cortex: a gateway to memory and attention. *Curr. Opin. Neurobiol.* 21, 475–485. doi: 10.1016/j.conb.2011.01.004

Brainard, D. H. (1997). The psychophysics toolbox. *Spat. Vis.* 10, 433–436. doi: 10.1163/156856897X00357

Brody, C. D., Hernández, A., Zainos, A., and Romo, R. (2003). Timing and neural encoding of somatosensory parametric working memory in macaque prefrontal cortex. *Cereb. Cortex* 13, 1196–1207. doi: 10.1093/cercor/bhg100

Castelli, F., Glaser, D. E., and Butterworth, B. (2006). Discrete and analogue quantity processing in the parietal lobe: a functional MRI study. *Proc. Natl Acad. Sci. U.S.A.* 103, 4693–4698. doi: 10.1073/pnas.0600444103

Chandler, G., Hayes, D., Townsend, M., and Thwaites, A. (2015). *Technical Report: Testing and Operating the QuaeroSys Piezostimulator*. Cambridge: University of Cambridge. doi: 10.17863/CAM.12955

Delorme, A., and Makeig, S. (2004). EEGLAB: an open source toolbox for analysis of single-trial EEG dynamics including independent component analysis. *J. Neurosci. Methods* 134, 9–21. doi: 10.1016/j.jneumeth.2003.10.009

D'Esposito, M. (2007). From cognitive to neural models of working memory. *Philos. Trans. R. Soc. Lond. Biol. Sci.* 362, 761–772. doi: 10.1098/rstb.2007.2086

Eger, E., Michel, V., Thirion, B., Amadon, A., Dehaene, S., and Kleinschmidt, A. (2009). Deciphering cortical number coding from human brain activity patterns. *Curr. Biol.* 19, 1608–1615. doi: 10.1016/j.cub.2009.08.047

Eger, E., Sterzer, P., Russ, M. O., Giraud, A. L., and Kleinschmidt, A. (2003). A supramodal number representation in human intraparietal cortex. *Neuron* 37, 719–725. doi: 10.1016/S0896-6273(03)00036-9

Eickhoff, S. B., Stephan, K. E., Mohlberg, H., Grefkes, C., Fink, G. R., Amunts, K., et al. (2005). A new SPM toolbox for combining probabilistic cytoarchitectonic maps and functional imaging data. *Neuroimage* 25, 1325–1335. doi: 10.1016/j.neuroimage.2004.12.034

Friston, K. J., Harrison, L., Daunizaeu, J., Keibel, S. J., Phillips, C., and Trujillo-Barreto, N. J. (2008). Multiple sparse priors for the M/EEG inverse problem. *Neuroimage* 39, 1104–1120. doi: 10.1016/j.neuroimage.2007.09.048

Fuentemilla, L., Penny, W. D., Cashdollar, N., Bunzeck, N., and Duzel, E. (2010). Theta-coupled periodic replay in working memory. *Curr. Biol.* 20, 606–612. doi: 10.1016/j.cub.2010.01.057

Goldenholz, D. M., Ahlfors, S. P., Hämäläinen, M. S., Sharon, D., Ishitobi, M., Vaina, L. M., et al. (2009). Mapping the signal-to-noise-ratios of cortical sources in magnetoencephalography and electroencephalography. *Hum. Brain Mapp.* 30, 1077–1086. doi: 10.1002/hbm.20571

Haegens, S., Osipova, D., Oostenveld, R., and Jensen, O. (2010). Somatosensory working memory performance in humans depends on both engagement and disengagement of regions in a distributed network. *Hum. Brain Mapp.* 31, 26–35. doi: 10.1002/hbm.20842

Hämäläinen, M., Hari, R., Ilmoniemi, R. J., Knuutila, J., and Lounasmaa, O. V. (1993). Magnetoencephalography - theory, instrumentation, and applications to noninvasive studies of the working human brain. *Rev. Modern Phys.* 65, 413–497. doi: 10.1103/RevModPhys.65.413

Herding, J., Spitzer, B., and Blankenburg, F. (2016). Upper beta band oscillations in human premotor cortex encode subjective choices in a vibrotactile comparison task. *J. Cogn. Neurosci.* 28, 668–679. doi: 10.1162/jocn_a_00932

Jensen, O., and Mazaheri, A. (2010). Shaping functional architecture by oscillatory alpha activity: gating by inhibition. *Front. Hum. Neurosci.* 4:186. doi: 10.3389/fnhum.2010.00186

Jokisch, D., and Jensen, O. (2007). Modulation of gamma and alpha activity during a working memory task engaging the dorsal or ventral stream. *J. Neurosci.* 27, 3244–3251. doi: 10.1523/JNEUROSCI.5399-06.2007

Kaiser, J., Ripper, B., Birbaumer, N., and Lutzenberger, W. (2003). Dynamics of gamma-band activity in human magnetoencephalogram during auditory pattern working memory. *Neuroimage* 20, 816–827. doi: 10.1016/S1053-8119(03)00350-1

Kilner, J. M., Kiebel, S. J., and Friston, K. J. (2005). Applications of random field theory to electrophysiology. *Neurosci. Lett.* 374, 174–178. doi: 10.1016/j.neulet.2004.10.052

Klimesch, W., Sauseng, P., and Hanslmayr, S. (2007). EEG alpha oscillations: the inhibition-timing hypothesis. *Brain Res. Rev.* 53, 63–88. doi: 10.1016/j.brainresrev.2006.06.003

Knops, A., Piazza, M., Sengupta, R., Eger, E., and Melcher, D. (2014). A shared, flexible neural map architecture reflects capacity limits in both visual short-term memory and enumeration. *J. Neurosci.* 34, 9857–9866. doi: 10.1523/JNEUROSCI.2758-13.2014

Kostopoulos, P., Albanese, M. C., and Petrides, M. (2007). Ventrolateral prefrontal cortex and tactile memory disambiguation in the human brain. *Proc. Natl. Acad. Sci. U.S.A.* 104, 10223–10228. doi: 10.1073/pnas.0700253104

Lara, A. H., and Wallis, J. D. (2015). The role of prefrontal cortex in working memory: a mini review. *Front. Syst. Neurosci.* 9:173. doi: 10.3389/fnsys.2015.00173

Litvak, V., and Friston, K. (2008). Electromagnetic source reconstruction for group studies. *Neuroimage* 42, 1490–1498. doi: 10.1016/j.neuroimage.2008.06.022

Lundqvist, M., Herman, P., and Lansner, A. (2011). Theta and gamma power increases and alpha/beta power decreases with memory load in an attractor network model. *J. Cogn. Neurosci.* 23, 3008–3020. doi: 10.1162/jocn_a_00029

Lundqvist, M., Rose, J., Herman, P., Brincat, S. L., Buschman, T. J., and Miller, E. K. (2016). Gamma and beta bursts underlie working memory. *Neuron* 90, 152–164. doi: 10.1016/j.neuron.2016.02.028

Lutzenberger, W., Ripper, B., Busse, L., Birbaumer, N., and Kaiser, J. (2002). Dynamics of gamma-band activity during an audiospatial working memory task in humans. *J. Neurosci.* 22, 5630–5638.

Maris, E., and Oostenveld, R. (2007). Nonparametric statistical testing of EEG- and MEG-data. *J. Neurosci. Method* 164, 177–190. doi: 10.1016/j.jneumeth.2007.03.024

Nieder, A. (2012). Supramodal numerosity selectivity of neurons in primate prefrontal and posterior parietal cortices. *Proc. Natl. Acad. Sci. U.S.A.* 109, 11860–11865. doi: 10.1073/pnas.1204580109

Nieder, A. (2016). The neural code for number. *Nat. Rev. Neurosci.* 17, 366–382. doi: 10.1038/nrn.2016.40

Nolte, G. (2003). The magnetic lead field theorem in the quasi-static approximation and its use for magnetoencephalography forward calculation in realistic volume conductors. *Phys. Med. Biol.* 48, 3637–3652. doi: 10.1088/0031-9155/48/22/002

Oldfield, R. C. (1971). The assessment and analysis of handedness: the Edinburgh inventory. *Neuropsychologia* 9, 97–113. doi: 10.1016/0028-3932(71)90067-4

Oostenveld, R., Fries, P., Maris, E., and Schoffelen, J.-M. (2011). FieldTrip: open source software for advanced analysis of MEG, EEG, and invasive electrophysiological data. *Comput. Intell. Neurosci.* 2011:156869. doi: 10.1155/2011/156869

Pesaran, B., Pezaris, J. S., Sahani, M., Mitra, P. P., and Andersen, R. A. (2002). Temporal structure in neuronal activity during working memory in macaque parietal cortex. *Nat. Neurosci.* 5, 805–811. doi: 10.1038/nn890

Pfurtscheller, G., and Cooper, R. (1975). Frequency dependence of the transmission of the EEG from cortex to scalp. *Electroencephalogr. Clin. Neurophysiol.* 38, 93–96. doi: 10.1016/0013-4694(75)90215-1

Piazza, M., Pinel, P., Le Bihan, D., and Dehaene, S. (2007). A magnitude code common to numerosities and number symbols in human intraparietal cortex. *Neuron* 53, 293–305. doi: 10.1016/j.neuron.2006.11.022

Romo, R., Brody, C. D., Hernández, A., and Lemus, L. (1999). Neuronal correlates of parametric working memory in the prefrontal cortex. *Nature* 399, 470–473. doi: 10.1038/20939

Romo, R., and de Lafuente, V. (2013). Conversion of sensory signals into perceptual decisions. *Prog. Neurobiol.* 103, 41–75. doi: 10.1016/j.pneurobio.2012.03.007

Roux, F., and Uhlhaas, P. J. (2014). Working memory and neural oscillations: α-γ versus θ-γ codes for distinct WM information? *Trends Cogn. Sci.* 18, 16–25. doi: 10.1016/j.tics.2013.10.010

Sandberg, A., Tegnér, J., and Lansner, A. (2003). A working memory model based on fast Hebbian learning. *Network* 14, 789–802. doi: 10.1088/0954-898X_14_4_309

Shafi, M., Zhou, Y., Quintana, J., Chow, C., Fuster, J., and Bodner, M. (2007). Variability in neuronal activity in primate cortex during working memory tasks. *Neuroscience* 146, 1082–1108. doi: 10.1016/j.neuroscience.2006.12.072

Snyder, A. (1992). Steady-state vibration evoked potentials: descriptions of technique and characterization of responses. *Electroencephalogr. Clin. Neurophysiol.* 3, 257–268. doi: 10.1016/0168-5597(92)90007-X

Spitzer, B., and Blankenburg, F. (2011). Stimulus-dependent EEG activity reflects internal updating of tactile working memory in humans. *Proc. Natl. Acad. Sci. U.S.A.* 108, 8444–8449. doi: 10.1073/pnas.1104189108

Spitzer, B., and Blankenburg, F. (2012). Supramodal parametric working memory processing in humans. *J. Neurosci.* 32, 3287–3295. doi: 10.1523/JNEUROSCI.5280-11.2012

Spitzer, B., Gloel, M., Schmidt, T. T., and Blankenburg, F. (2014). Working memory coding of analog stimulus properties in the human prefrontal cortex. *Cereb. Cortex* 24, 2229–2236. doi: 10.1093/cercor/bht084

Spitzer, B., Wacker, E., and Blankenburg, F. (2010). Oscillatory correlates of vibrotactile frequency processing in human working memory. *J. Neurosci.* 30, 4496–4502. doi: 10.1523/JNEUROSCI.6041-09.2010

Stokes, M. G. (2015). 'Activity-silent' working memory in prefrontal cortex: a dynamic coding framework. *Trends Cogn. Sci.* 19, 394–405. doi: 10.1016/j.tics.2015.05.004

Stokes, M. G., Kusunoki, M., Sigala, N., Nili, H., Gaffan, D., and Duncan, J. (2013). Dynamic coding for cognitive control in prefrontal cortex. *Neuron* 78, 364–375. doi: 10.1016/j.neuron.2013.01.039

Tobimatsu, S., Zhang, Y. M., and Kato, M. (1999). Steady-state vibration somatosensory evoked potentials: physiological characteristics and tuning function. *Clin. Neurophysiol.* 110, 1953–1958. doi: 10.1016/S1388-2457(99)00146-7

van Ede, F., Szebenyi, S., and Maris, E. (2014). Attentional modulations of somatosensory alpha, beta and gamma oscillations dissociate between anticipation and stimulus processing. *Neuroimage* 97, 134–141. doi: 10.1016/j.neuroimage.2014.04.047

Whittingstall, K., and Logothetis, N. K. (2009). Frequencyband coupling in surface EEG reflects spiking activity in monkey visual cortex. *Neuron* 64, 281–289. doi: 10.1016/j.neuron.2009.08.016

Conflict of Interest Statement: The authors declare that the research was conducted in the absence of any commercial or financial relationships that could be construed as a potential conflict of interest.

Centro-parietal EEG potentials index subjective evidence and difficulty during perceptual decision making

Running title: Subjective evidence during decision making

Authors: Jan Herding[1,2], Simon Ludwig[1], Alexander von Lautz[1,2], Bernhard Spitzer[3], Felix Blankenburg[1,2,3]

[1]Neurocomputation and Neuroimaging Unit, Department of Education and Psychology, Freie Universität Berlin, Habelschwerdter Allee 45, 14195 Berlin

[2] Bernstein Center for Computational Neuroscience Berlin, Philippstr. 13, 10115 Berlin

[3]Center for Adaptive Rationality, Max Planck Institute for Human Development, Berlin, Germany.

Corresponding author: Jan Herding (jan.herding@gmail.com), Neurocomputation and Neuroimaging Unit, Department of Education and Psychology, Freie Universität Berlin, Habelschwerdter Allee 45, 14195 Berlin, +49 030 838 56693

Number of figures: 8
Number of tables: 1

Abstract

Recent studies suggest that a centro-parietal positivity (CPP) in the EEG signal tracks the absolute (unsigned) strength of accumulated evidence for choices that require the integration of noisy sensory input. Here, we investigated whether the CPP might also reflect the evidence for decisions based on a quantitative comparison between two sequentially presented stimuli (a signed quantity). We recorded EEG while participants decided whether the latter of two vibrotactile frequencies was higher or lower than the former in six variants of this task (n=116). To account for biases in sequential comparisons, we applied a behavioral model based on Bayesian inference that estimated subjectively perceived frequency differences. Immediately after the second stimulus, parietal ERPs reflected the signed value of subjectively perceived differences and afterwards their absolute value. Strikingly, the modulation by signed difference was evident in trials without any objective evidence for either choice and correlated with choice-selective premotor beta band amplitudes. Modulations by the absolute strength of subjectively perceived evidence – a direct indicator of task difficulty - exhibited all features of statistical decision confidence. Together, our data suggest that parietal EEG signals first index subjective evidence, and later include a measure of confidence in the context of perceptual decision making.

Keywords

decision making, EEG, P300, somatosensory, vibrotactile

Introduction

Recent studies have suggested a centro-parietal positivity (CPP) in the EEG signal (arguably identical to the classic P300 component) as a modality-independent proxy of accumulated evidence in perceptual decision making tasks (e.g., Kelly & O'Connell, 2015; Philiastides et al., 2014). In particular, when classifying a noisy sensory stimulus interval into one of two categories, the CPP increased faster and peaked earlier the weaker the noise was, i.e., the clearer the presented evidence (e.g., random dot motion (RDM) discrimination: Kelly & O'Connell, 2013; face-vs-car discrimination: Philiastides et al., 2014). Moreover, the CPP reached a fixed threshold at the time of the decision report, suggesting an accumulation-to-bound mechanism for response initiation (e.g., O'Connell et al., 2012; but see Philiastides et al., 2014). Together, these findings capture the hallmarks of popular sequential-sampling models of evidence accumulation (e.g., see Smith and Ratcliff, 2004), and may relate to similar, or even homologue neuronal processes as identified in the parietal cortex of non-human primates (e.g., Roitman and Shadlen, 2002; Gold and Shadlen, 2007; Shadlen and Kiani, 2013).

The link between decisional evidence and the CPP is not limited to decisions that require the accumulation of noisy sensory input over time. In an auditory four-stimulus oddball paradigm, the differences between 'deviant' and 'standard' stimuli (i.e., the evidence for a 'deviant' detection) modulated the CPP in the very same way as it was modulated by the strength of evidence in accumulation-based decisions (Twomey et al., 2015). Notably, the three 'deviant' stimuli in this task were always higher in pitch than the 'standard' stimulus, eliminating the necessity for participants to evaluate the sign of the difference (i.e., higher or lower) between 'deviant' and 'standard'.

In all of the aforementioned EEG studies, a parietal potential tracked the strength of evidence during perceptual decision making, however, without indicating for which choice alternative (i.e., unsigned evidence; e.g., Kelly and O'Connell, 2013; Philiastides et al., 2014). In the RDM task for instance, only

the proportion of coherently moving dots modulated the CPP, without differentiating between the directions in which the dots moved (Kelly and O'Connell, 2013). Here, we examined whether the CPP might also index the choice alternative, in addition to the strength of evidence, if we apply a sequential comparison task. In particular, does the CPP indicate the decision-relevant signed evidence for choices that involve a quantitative comparison? We used a classic vibrotactile two-alternative forced choice (2-AFC) task, in which participants compare two stimulus frequencies (f1 and f2) and decide whether the second one was higher or lower than the first one (comprehensive review on monkey electrophysiology in Romo and de Lafuente, 2013). In this paradigm, a choice-specific (i.e., binary) modulation of upper beta band (~20 – 30 Hz) amplitude in premotor cortex, decoupled from the motor response, was recently observed in human EEG recordings (Herding et al., 2016, 2017; Ludwig et al., 2018), replicating previous findings from monkey LFPs (Haegens et al., 2011, 2017). A representation of the graded differences between f1 and f2 (i.e., the signed evidence), however, has not yet been identified in the human EEG. For the current study, we pooled EEG data over six experiments, utilizing the same vibrotactile 2-AFC task while varying response modality, response timing, and response mapping (N = 116). We estimated subjective evidence and difficulty (i.e., the subjectively perceived signed and absolute difference, respectively, between f1 and f2) using a Bayesian inference model of choice behavior. This way, we accounted for known biases in sequential comparisons due to the so-called contraction-bias (e.g., Jou et al., 2004; Ashourian et al., 2011; Karim et al., 2012; Raviv et al., 2014) which is a direct consequence of the time-order effect/error (TOE; see Fechner, 1861; Woodrow, 1935; Hellström, 1985, 2003). Moreover, the behavioral model allowed us to derive a measure of confidence grounded in statistical decision theory (i.e., statistical decision confidence) obviating the need for subjective confidence reports. Using the behavioral model, we found that signals from the parietal cortex appeared to be first modulated by the subjectively

perceived signed difference, and later by the absolute value (i.e., the absolute strength of evidence).

Materials and Methods

Experimental Design

Participants: A total of 129 datasets were obtained from healthy, right-handed volunteers (21 – 40 years; 76 females) who participated in six different variants of the experiment. Most participants were students from the Freie Universität Berlin, and some participated in more than one variant of the experiment. All studies were approved by the local ethics committee at the Freie Universität Berlin, and participants gave written informed consent before an experiment started. Thirteen datasets were excluded due to chance-level behavioral performance (<55% correct answers) and/or excessive EEG artifacts, leaving 116 datasets for further analyses.

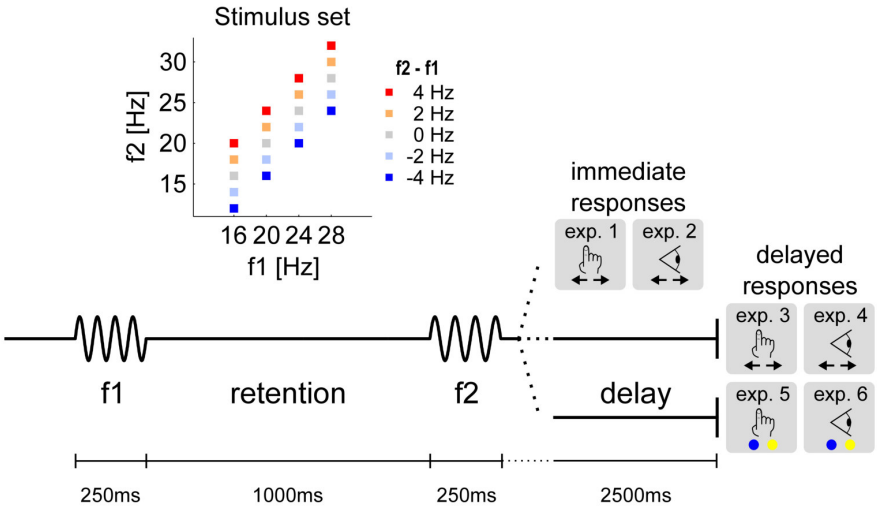

Figure 1 Task and stimuli. One after another, two vibrotactile stimuli with frequencies f1 and f2 were briefly presented to the left index finger of participants who had to decide whether f2 > f1 or f2 < f1. Response timing (immediate / delayed), response modality (saccade / button press), and response mapping (direction / color) varied over six variants of the task (exp. 1 – exp. 6). ***Inset****, The stimulus set that was used in all experiments, with the exception of zero-difference trials (gray) which were not used in exp. 1 and exp. 2. Each square represents one stimulus pair with f1 (x-axis) and f2 (y-axis). The color-code denotes the physical stimulus differences f2 – f1.*

Stimuli and behavioral task: In all six variants of the experiment, stimuli and comparison task were identical. Only the response modality and response timing varied across experiments (Figure 1). Supra-threshold vibrotactile stimuli with constant peak amplitude were applied to the left index finger using a piezoelectric Braille stimulator (QuaeroSys Medical Devices, Schotten, Germany). The stimuli consisted of amplitude-modulated sinusoids with a fixed carrier frequency of 133 Hz (137 Hz in Experiment 2). Amplitude-modulation of this carrier signal with frequencies between 12 – 32 Hz was used to create the sensation of tactile 'flutter' (see Talbot et al., 1968; Romo and Salinas, 2003), while limiting the spectrum of the physical driving signal to frequencies above 100 Hz (e.g., Tobimatsu et al., 1999). Thus, the risk of physical artifacts in the EEG analysis range of interest (<100 Hz) was minimized. The sound of the stimulator was masked by white noise of ~80 dB that was played throughout the experiment (e.g., see Spitzer et al., 2010; Spitzer and Blankenburg, 2011). Participants were comfortably seated ~60 cm in front of a TFT monitor. A fixation cross was displayed at the center of the screen to minimize eye movements. On each trial, two flutter stimuli were successively presented for 250 ms each (with frequencies f1 and f2), interleaved by a retention interval of 1000 ms (see Figure 1). The frequencies of the first stimulus (f1) were randomly drawn from 16, 20, 24 or 28 Hz, whereas f2 differed from f1 by +/- 2 or 4 Hz. In four variants of the experiment (Experiments 3 - 6), f2 was identical to f1 in 25% of the trials, without participants knowing. Participants were instructed to always decide whether f2 > f1 or f2 < f1.

In Experiments 1 and 2, participants indicated choices immediately after presentation of the second stimulus either by pressing one of two buttons with the right index or middle finger (Experiment 1), or by making a saccade to one of two target dots (Experiment 2). The target dots (diameter of ~0.5° visual angle) appeared on the left and on the right side of the screen (~12° visual angle off-center). Importantly, the response assignment of the two buttons and of the two saccade directions was

reversed for half of the participants. This way, the mapping of choices onto specific motor responses (which might have been associated with specific motor preparatory signals) was fully counterbalanced across participants (see also Herding et al., 2016, 2017). In Experiments 3 and 4, participants reported choices analogously to Experiments 1 and 2, however, only after a delay of 2500 ms. In Experiments 5 and 6, an additional mapping of choices onto a color-code (blue vs. yellow) was required to report decisions after the delay. In the experiments with delayed responses (Experiments 3 – 6), 2000 ms after the presentation of f2, a blue and a yellow target dot (diameter of ~1° visual angle) appeared on the left and on the right side of the screen (fully counterbalanced across trials; ~12° visual angle off-center). In Experiments 3 and 4, the colors of the dots were irrelevant, and participants selected targets based on a fixed association between direction and choices (counterbalanced across participants). In Experiments 5 and 6, each color was associated with one of the two choice options (counterbalanced across participants). Participants selected a target based on its location (Experiments 3 and 4) or color (Experiments 5 and 6) after another 500 ms either by pressing the left-arrow or right-arrow button with the right index or middle finger (Experiments 3 and 5, see Ludwig et al., 2018), or by making a saccade onto the target (Experiments 4 and 6). See Figure 1 for a graphical summary of the experimental designs.

In Experiments 1 and 2, participants received performance feedback after each trial, and completed seven blocks of 160 f1-vs-f2 comparisons (each block lasted ~15 minutes including eye-tracker calibration) for a total of 1120 trials. In Experiments 3 – 6, feedback based on the performance for trials with f1 ≠ f2 was provided after each block, and participants completed eight blocks of 128 frequency comparisons (each block lasted ~12 minutes including eye-tracker calibration) for a total of 1024 trials. Before each experiment, participants performed ~50 practice trials.

Note that the influence of the different response conditions was not subject to the current study.

Oscillatory signatures in the EEG signal that are related to these response manipulations have been reported elsewhere (Herding et al., 2016; Herding et al., 2017; Ludwig et al., 2018).

Eye-tracking: In Experiment 2, a Tobii T60 eye-tracker (Tobii Technology, Danderyd, Sweden) was used to record eye movements of participants during each trial (binocular sampling at 60 Hz). The T60 is integrated into a 17'' TFT monitor and is able to track participants that are comfortably seated in front of the monitor (i.e., no chin rest required). In Experiments 4 and 6, eye movements were recorded (monocular sampling at 500 Hz) using an EyeLink 1000 Desktop Mount with a chin rest (SR Research, Ottawa, Canada). Online evaluation of the participants' gaze directions was implemented with custom code using the Tobii toolbox and psychtoolbox 3 for MATLAB (Brainard, 1997; Cornelissen et al., 2002). Thus, we were able to monitor that participants kept the gaze on the central fixation cross during each trial (with tolerance of ~3° visual angle) and displayed a warning message if this was not the case ("Please keep fixation throughout the trial"). Additionally, we read out participants' choices (200 ms fixation on target dot) and provided performance feedback online, either after each trial (experiment 2) or after each block (experiments 4 and 6). To maintain a high tracking accuracy, the eye-tracker was calibrated before the beginning of each block using a standard 5-dot (Tobii T60) or 9-dot (EyeLink 1000) calibration procedure.

Statistical Analysis

Behavioral model of choices and confidence: In order to explain the observed choice pattern, we fitted a Bayesian inference model to individual behavioral data, and thereby, estimated subjectively perceived frequency differences (SPFDs; Figure 2A, for details see Herding et al., 2016; see also Ashourian and Loewenstein, 2011; Sanchez, 2014). In brief, the model targets to account for a known

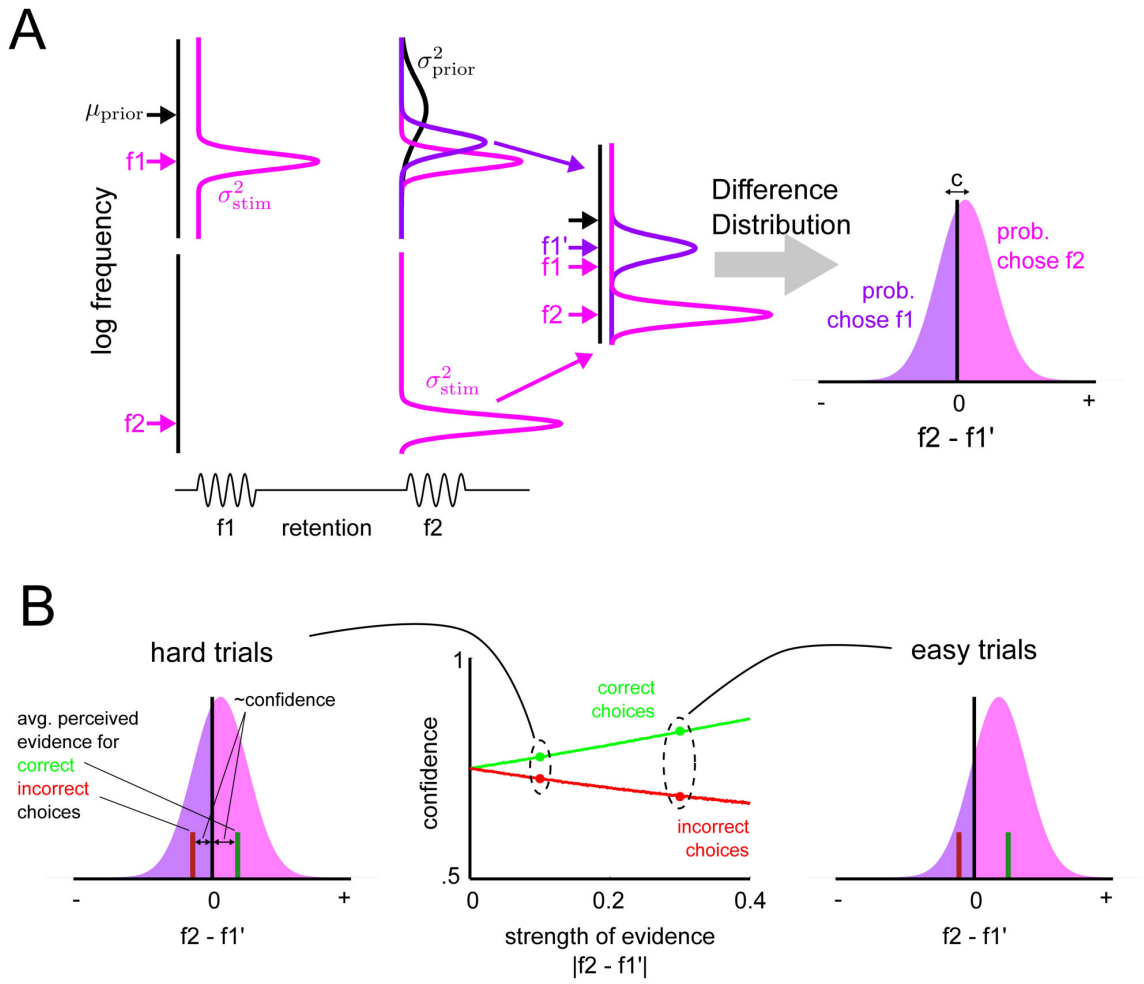

Figure 2 Behavioral model for choices and confidence. ***A****, Graphical illustration of the behavioral model based on Bayesian inference. Y-axes display frequencies on a logarithmic scale. Top: Representation of f1 during different stages of the task. Pink distribution represents the likelihood function of f1. Black distribution is the prior centered on the stimulus set. Purple distribution is the posterior of f1 with shifted mean f1'. Lower: The likelihood of f2 (pink distribution) is used for the comparison with the posterior of f1. Subtracting the posterior of f1 from the likelihood of f2, yields a difference distribution which is used to fit the probability to chose f1 to the behavioral data of each participant by optimizing* σ^2_{stim}, σ^2_{prior}, *and decision criterion* c. ***B****, Intuition of statistical decision confidence. The distance between perceived evidence and decision criterion is proportional to confidence. Average perceived evidence is displayed separately for correct and incorrect trials (green and red bar, respectively). Difference distribution for hard (f2 – f1' = 0.1) and easy (f2 – f1' = 0.3) trials illustrate that confidence increases with evidence strength for correct trials but decreases for incorrect trials.*

bias in sequential comparisons (e.g., see Hellström, 1985, 2003; Ashourian and Loewenstein, 2011). That is, participants tend to compare f2 not only with the physical value of f1, but also with the average frequency of all presented stimuli, as if the representation of f1 is subject to a contraction towards the mean (hence, the term 'contraction bias', see e.g., Jou et al., 2004; Preuschhof et al., 2010; Ashourian and Loewenstein, 2011; Karim et al., 2012; Raviv et al., 2014; see time-order effect for underlying core principle: e.g., Fechner, 1820; Woodrow, 1935, Hellström, 1985). In other words, the quantity that drives choices in the given task is best described by the difference between f2 and a representation of f1 that deviates from its physical value toward the mean frequency of the stimulus set. In our model, we introduce this shifted quantity – which we will call f1' – as a weighted average of the mean of all stimulus frequencies and the physical value of f1 – implemented in terms of Bayesian inference. In particular, f1' is the expected value of the Gaussian posterior distribution of f1, assuming a Gaussian prior centered on the frequencies of the stimulus set (see Figure 2A). The model was fitted to the choices of individual participants by optimizing three free parameters (i.e., variance of stimulus likelihood σ^2_{stim}, prior variance σ^2_{prior}, and a decision criterion *c*) using variational Bayes as implemented in the VBA toolbox (Daunizeau et al., 2014). In order to assess the model's goodness-of-fit, we computed Bayes Factors (BFs) to compare each model fit with a "null" model in which decisions were based on the physical stimulus differences (i.e., f2 – f1). Notably, the model of SPFDs as well as the "null" model followed Weber-Fechner's law and implemented the representation of frequency values on a logarithmic scale (see Herding et al., 2016).

Based on the individual model fits, we quantified the SPFD for each stimulus pair by the difference f2 – f1', yielding 16 SPFD values for Experiments 1 and 2, and 20 SPFD values for Experiments 3 – 6. At the same time, the difference distribution between the likelihood of f2 and the posterior of f1 (centered on f1') additionally allowed us to compute a measure of confidence based on statistical

decision theory (e.g., Drugowitsch, 2016; Hangya et al., 2016; Sanders et al., 2016; Figure 2B). The difference distribution describes the distribution of percepts that are associated with a given stimulus pair, i.e., with the SPFD between both stimuli. According to statistical decision theory (or signal detection theory), a single percept can be conceived as a sample *d* from this distribution, and a choice based on this very percept depends on where the sample is located with respect to a decision criterion *c* (i.e., choose f2 > f1 if $d > c$). The distance between the sample and the criterion (i.e., $|d - c|$) can be transformed into the probability of a correct response given the percept *d*, which in turn is a measure for confidence (Lak et al., 2014; Urai et al., 2017; Figure 2B). For each participant, we estimated average confidence based on this approach for SPFDs on the interval [-0.4, 0.4]. For each SPFD on this interval, we drew 100,000 samples from the individual difference distributions (i.e., based on the estimated parameters), and computed the associated confidence for each sample. Confidence values were then averaged separately for correct and incorrect trials. Since results were roughly symmetric across zero, the average confidence was grouped according to absolute values of SPFDs (e.g., -0.2 and 0.2), and respective mean values were computed. The illustration in Figure 2B was obtained by simulating data from an unbiased observer (c=0) with $\sigma^2_{stim} = 0.05$ and $\sigma^2_{prior} = 0.347$.

EEG recording and analysis: In all experiments, EEG (ActiveTwo; BioSemi) was recorded at 2048 Hz (offline down-sampled to 512 Hz) from 64 electrodes positioned in an elastic cap according to the extended 10-20 system. Individual electrode locations for each participant were obtained prior to the experiments using a stereotactic electrode-positioning system (Zebris Medical GmbH, Isny, Germany). Additional electrodes were used to register the horizontal and vertical electrooculogram (hEOG and vEOG). For preprocessing, EEG data were high- and low-pass filtered using a non-causal FIR filter (with cut-off frequencies of 0.1 and 30 Hz, respectively), and re-referenced to a common average montage.

Eye blink artifacts in the EEG data were corrected using adaptive spatial filtering based on individual calibration data informed by the vEOG signal (see Ille et al., 2002). For experiment 2, in which participants gave immediate responses by saccades, we used the same approach informed by the hEOG signal to remove artifacts of horizontal saccades from the EEG signal. The artifact-free EEG data were segmented into epochs from -2250 to 2000 ms relative to the presentation time of the second stimulus in order to examine evoked EEG responses after the second stimulus as well as to compute control analyses after the first stimulus. Noisy trials were identified by careful visual inspection and were excluded from further analysis (14.8 % of trials on average). The remaining single-trial data were baseline-corrected relative to the 100 ms preceding stimulus onset. All analyses were done in MATLAB (The MathWorks) using custom code, functions of the SPM12 toolbox (Wellcome Department of Cognitive Neurology, London; www.fil.ion.ucl.ac.uk/spm), and the FieldTrip toolbox for EEG/MEG data (Radboud University Nijmegen, Donders Institute; fieldtrip.fcdonders.nl).

Multiple regression and group-level analysis: For each participant, we implemented a multiple regression analysis of the preprocessed single-trial EEG data. At each time point, we regressed the EEG data onto the SPFDs (i.e., f2 – f1') and their absolute values (i.e., |f2 – f1'|) over trials, separately for correct and incorrect choices. The resulting regression coefficients quantified how strongly the trial-specific values of the regressors (i.e., f2 – f1' and |f2 – f1'|) were related to trial-by-trial variability in the EEG data. To identify time periods and channels for which this relation was consistently different from zero across participants, we used cluster-based permutation testing (Maris and Oostenveld, 2007). That is, we compared the summary statistics of the observed data (one-sample t-test of regression coefficients across all data sets at each time point) with a distribution of summary statistics obtained from 500 randomly sign-flipped permutations. A cluster was defined as a

group of adjacent time points that all exceeded a cluster-defining threshold of $p_{threshold} < 0.005$ (uncorrected). Clusters that exceeded a cluster-based family-wise error (FWE) corrected threshold of $p_{FWE} < 0.05$ (corrected for time and channels) were considered statistically significant.

Event-related potentials (ERPs): To visualize the effects identified in the statistical analysis as classic ERPs, we binned the individual 16 values of SPFDs (i.e., differences of log-transformed stimulus frequencies; one per stimulus pair with f1 ≠ f2) into six discrete levels across participants (i.e., [< -0.18]; [-0.18 to -0.09]; [-0.09 to 0]; [0 to 0.09]; [0.09 to 0.17]; [> 0.17]). The grand average ERPs were computed separately for each level. We defined the six levels symmetrically around a SPFD of zero (corresponding to chance-level performance), and in such a way that each participant had at least one stimulus pair per level. Since SPFDs were generally small for trials with identical stimuli (i.e., f1 = f2), we used only four levels for the computation of ERPs in these trials (i.e., [< -0.09]; [-0.09 to 0]; [0 to 0.09]; [> 0.09]). Note that by binning the data into discrete levels of SPFDs, the high precision of utilizing subjective measures for a single-trial analysis is lost for the visualization of the ERPs.

Source reconstruction: The cortical sources of the observed modulations on the scalp-level were localized using the 3D source reconstruction routines provided by SPM12 (Friston et al., 2006). Based on the individually recorded electrode positions for each participant, a forward model was constructed using an 8196-point cortical mesh of distributed dipoles perpendicular to the cortical surface of a template brain (see Friston et al., 2006). The lead field of the forward model was computed using the three-shell Boundary Elements Method (BEM) EEG head model available in SPM12. Multiple sparse priors (Friston et al., 2008) under group constraints (Litvak and Friston, 2008) were applied to invert the forward model. For model inversion, we used a representative time

interval (i.e., -200 to 1500 ms relative to f2) of ERPs that were computed separately for each level of SPFDs (see ERPs above) drawing on all trials including those with identical stimuli (i.e., f1 = f2). The results of the inversion were summarized in six corresponding 3D images (i.e., one for each level of SPFDs) that reflected source activity averaged over a time window of interest. In particular, summary images were computed for an early (250 to 500 ms) and a late (500 to 800 ms) time window capturing the two effects observed at the scalp level (i.e., modulation by signed evidence and strength of evidence, respectively). For each time window, contrasting the 3D images within each participant analogously to the sensor space analysis served as an estimate for subject-specific source locations of both effects. The results of conventional group-level statistical analyses of these source images (see Litvak et al., 2011) are displayed at a significance level of $p < 0.001$ (uncorrected). Anatomical references for source estimates were established on the basis of the SPM anatomy toolbox (Eickhoff et al., 2005) where possible.

Single-trial correlation of CPP and upper beta band amplitude: In order to explore the relationship between the CPP and premotor choice-specific upper beta band amplitude (see Herding et al., 2016, 2017; Ludwig et al., 2018), single-trial correlations between these two measures were computed. Notably, only for experiments 1 and 2; as these experiments required immediate responses, and hence, a direct transformation of evidence into a motor response. For each participant, the magnitude of the CPP in every trial was specified by a single value for the early and for the late effect, respectively. In particular, the single-trial EEG signal from electrode CPz was averaged over a brief time period during which a modulation of the CPP by the signed values of SPFDs (i.e., 250 – 500 ms) or by its absolute values (i.e., 500 – 800 ms) was observed. Additionally, a measure of the upper beta band amplitude in electrodes over premotor areas was computed for each trial. Using response-

locked time-frequency representations of the single-trial data (reported in Herding et al., 2016, 2017), average beta band amplitude was computed over a time-frequency cluster that exhibited a significant modulation by participants' choices (i.e., electrodes FC2, FCz, and C2; 20 – 30 Hz; -750 to -350 ms from responses for experiment 1, see Herding et al., 2016; electrodes FC2 and FC4, 24 – 32 Hz, -750 to -450 ms from responses for experiment 2, see Herding et al., 2017). We used correct and incorrect trials to compute the single-trial correlations for each participant. The correlation coefficients from both experiments were pooled (N = 45), and a one-sample t-test was computed to assess whether a consistent correlation was present across participants.

Results

Behavioral Results

Pooled over all experiments, participants made 72.5% correct choices on average. To test whether performance varied across the six experiments and across the different frequency differences, we performed a two-way repeated measures ANOVA on proportions of correct responses (PCRs) with between-subject factor 'Experiment' (experiments 1 – 6), and within-subject factor 'Frequency Difference' (-4, -2, 2, and 4 Hz stimulus difference). We used logit-transformed PCRs to account for non-normally distributed residuals. The analysis revealed no significant performance differences between experiments (main effect 'Experiment', $p = 0.125$; interaction 'Experiment' x 'Frequency Difference', $p = 0.182$). Within each experiment, PCRs varied significantly with the factor 'Frequency Difference' ($p < 0.001$). For further scrutinization of this effect, we computed post-hoc paired t-tests for each study separately to evaluate the influence of difficulty (+/- 4 Hz vs. +/- 2 Hz differences), and sign of the frequency differences (positive vs. negative differences). As expected, a larger proportion of trials were judged correctly when the (physical) f2 − f1 frequency difference was ±4 Hz compared with trials where the difference was only ±2 Hz in all experiments (all $p < 0.001$; paired t-test; see difficulty effect, Table 1). In experiments 1 and 2, we additionally observed more correct responses for positive compared with negative frequency differences ($p = 0.03$, and $p = 0.002$; paired t-test; see sign effect, Table 1) which might be attributed to an observed response bias toward "f2 > f1" choices in these two experiments (mean criterion shifts: 0.116 and 0.126 with $p = 0.029$ and $p = 0.002$; one-sample t test). Moreover, the analysis of median response times (RTs) from these two experiments revealed that participants responded faster when choosing "f2 > f1" as compared to choosing "f2 < f1" for correct choices (Experiment 1: 798 ms vs. 855 ms , $p<0.001$, paired t-test, see Herding et al., 2016; Experiment 2: 548 ms vs. 599 ms, $p = 0.001$, paired t-test, see Herding et al., 2017) and vice

versa for incorrect choices (Experiment 1: 952 ms vs. 903 ms, p = 0.014, paired t-test, see Herding et al., 2016; Experiment 2: 665 ms vs. 605 ms, p = 0.002, paired t-test, see Herding et al., 2017). RTs from Experiments 3 – 6 did not show any systematic variations and are difficult to interpret, because of the delayed decision reports.

	Frequency difference of stimuli (f2 – f1) in Hz					
	-4	-2	2	4	difficulty effect	sign effect
Exp.1	74.8 ±6.3	63.4 ±5.5	68.9 ±4.0	85.0 ±2.9	p < 0.001	p = 0.030
Exp. 2	75.9 ±4.4	64.7 ±3.5	70.8 ±4.4	86.1 ±4.3	p < 0.001	p = 0.002
Exp. 3	74.3 ±6.1	64.2 ±6.0	65.2 ±5.2	78.1 ±5.7	p < 0.001	p = 0.615
Exp. 4	77.7 ±8.8	65.4 ±7.7	66.2 ±5.5	79.8 ±6.6	p < 0.001	p = 0.871
Exp. 5	78.8 ±5.5	66.6 ±4.2	67.8 ±4.5	81.1 ±5.8	p < 0.001	p = 0.388
Exp. 6	74.2 ±5.9	63.1 ±4.3	66.9 ±5.3	80.6 ±5.0	p < 0.001	p = 0.067
pooled	**75.9 ±2.4**	**64.5 ±2.0**	**67.7 ±1.9**	**81.8 ±2.0**	**p < 0.001**	**p < 0.001**

Table 1 Proportion of correct responses (PCRs) in % as a function of the physical frequency difference f2 – f1 for each experiment. Mean values ± 95% confidence interval are shown. 'Difficulty effect' compares easy (+/- 4 Hz) and difficult (+/- 2 Hz) trials in a paired t-test. 'Sign effect' compares trials with a positive (2 and 4 Hz) and negative (-4 and -2 Hz) frequency difference in a paired t-test. PCRs were logit-transformed before testing, due to non-normally distributed residuals.

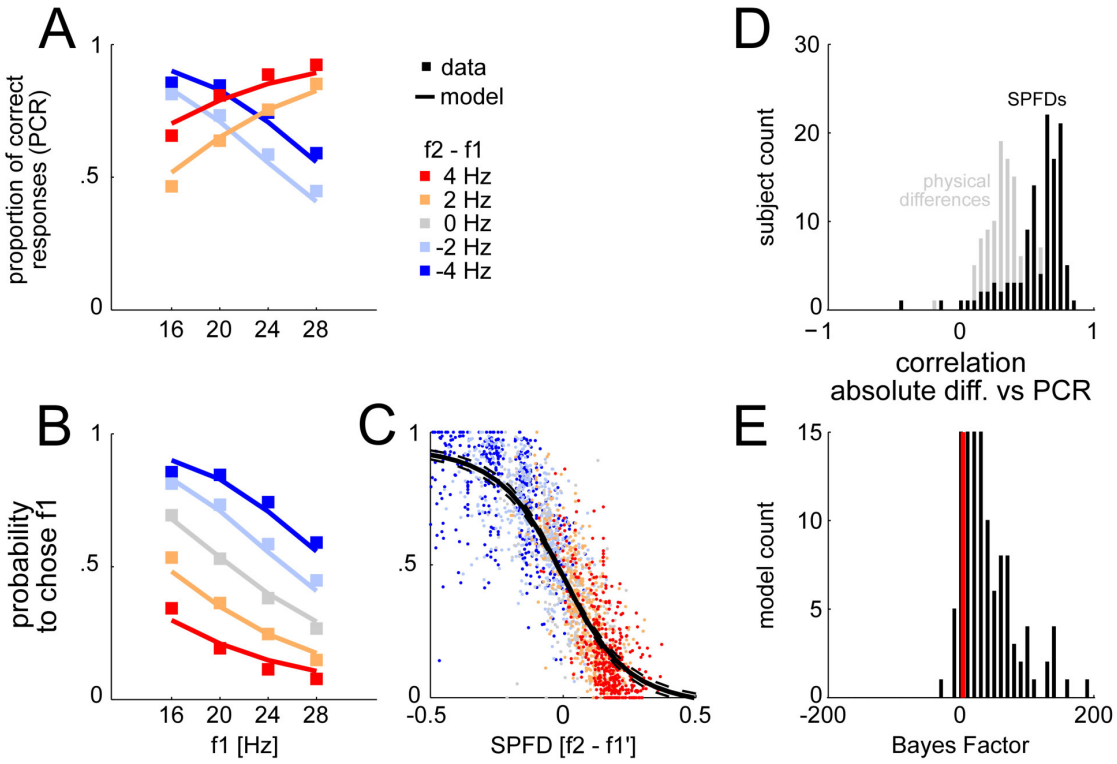

Figure 3 Behavioral and modeling results. ***A****, Grand average of observed (squares) and modeled (lines) proportions of correct responses (PCRs) plotted separately for each f1 (x-axis) and each physical stimulus difference f2 – f1 (color-code).* ***B****, Same as in A, but for probabilities to choose f1. Note that the blue squares/lines are identical as in A, and the red squares/lines correspond to 1-PCRs from A.* ***C****, Probabilities to choose f1 for each stimulus pair of each participant (dots), color-coded for physical stimulus differences (f2 – f1), and plotted against subjectively perceived frequency differences (SPFD; f2 – f1'). The solid black line represents the modeled probability to choose f1, averaged over all participants +/- 95% confidence interval (dashed lines).* ***D****, Histogram of correlation coefficients from all participants obtained from correlating absolute physical differences (|f2-f1|) with PCRs (gray), and from correlating absolute values of SPFDs (|f2-f1'|) with PCRs (black).* ***E****, Histogram of Bayes factors (BFs), comparing the SPFD model with a "null" model (based on physical stimulus differences) for each participant. Red line marks threshold for positive evidence in favor of SPFD model (BF > 3).*

Bayesian inference model yields good approximations for signed subjective evidence and experienced difficulty

As known from many 2-AFC studies that require the comparison of two sequentially presented stimuli, participants typically show a very particular choice pattern due to the contraction bias/TOE (e.g., Preuschhof et al., 2010; Ashourian et al., 2011; Karim et al., 2012; see squares in Figure 3A and

B), which we also observed in the current data. That is, for trials with f2 > f1 (i.e., f2 - f1 = +2 Hz or +4 Hz), participants performed better with increasing f1, whereas for trials with f2 < f1 (i.e., f2 - f1 = -2 Hz or -4 Hz), the opposite was true (Figure 3A). In other words, the probability to choose f1 decreased with increasing f1 for all frequency differences (interestingly also for those trials with no frequency difference; Figure 3B). Our previously proposed Bayesian inference model (Herding et al., 2016) can account for this choice pattern (lines in Figures 3A and B). Moreover, with the individually estimated SPFDs (i.e., f2 – f1') we obtained a subjective, fine-grained measure that reliably predicted participants' choices. Hence, we used the signed SPFDs as a proxy for signed subjective evidence towards a decision in this task (Figure 3C). Computing Bayes factors (BFs) to formally assess the quality of our Bayesian model provided positive evidence (BF > 3) in favour of the SPFD model for 91.4 % of the participants (106/116), and strong evidence (BF > 20) for 87.9 % (102/116; Figure 3E). Accordingly, the absolute values of the SPFDs (i.e., |f2 - f1'|) correlated significantly more with participants PCRs than the absolute values of the physical differences (i.e., |f2 – f1|), rendering SPFDs an improved predictor of subjectively experienced difficulty (paired t-test, $p < 0.001$; Figure 3D).

Parietal ERP first reflects signed subjective evidence and then absolute strength of evidence

We computed a multiple regression analysis on the total EEG data using the signed SPFDs (i.e., f2 – f1') as well as their absolute values (i.e., |f2 – f1'|) as single-trial regressors. This way, we could independently assess correlations of scalp potentials with signed subjective evidence and with the absolute strength of evidence. For a first analysis, we used trials in which objective sensory evidence was present (i.e., physically different stimuli with f2 ≠ f1; >80 % of all trials). For correct decisions, we found that a centro-parietal positive ERP after the second stimulus was positively correlated with signed subjective evidence early on (168 – 709 ms, 35 electrodes, strongest in P1, Pz, CPz, CP4, CP2,

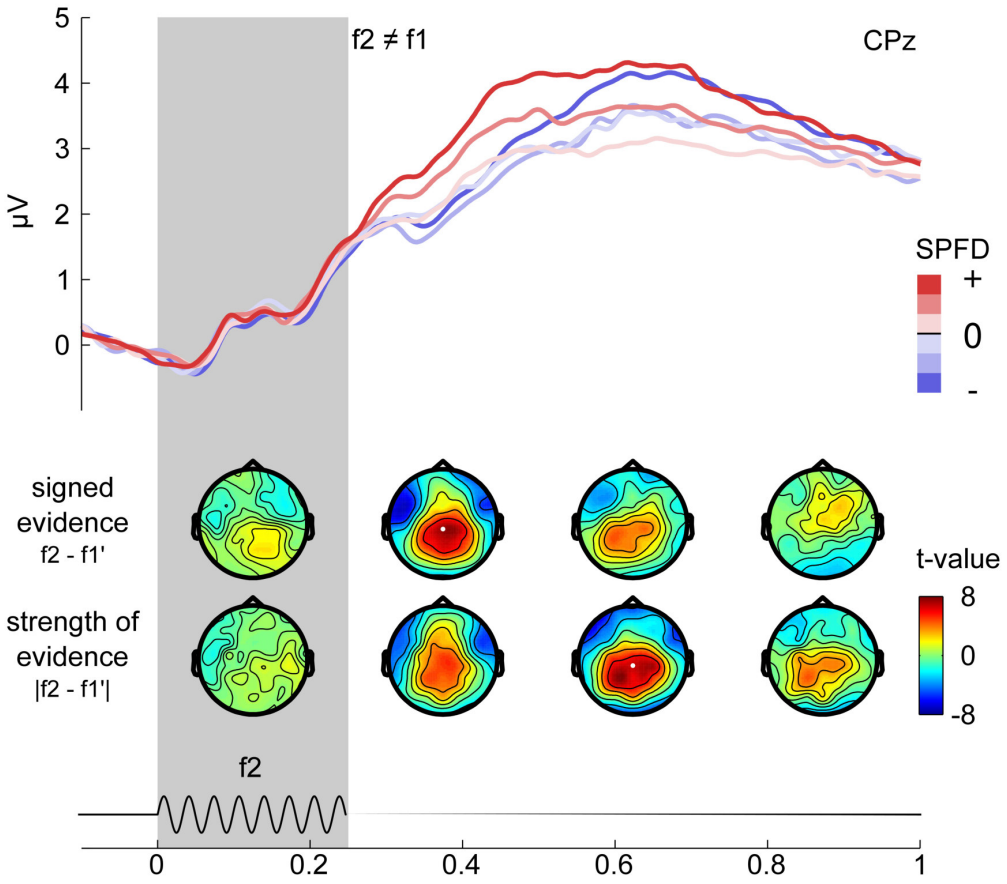

Figure 4 CPP is first modulated by signed subjective evidence and then by the absolute value, displayed for trials with available physical evidence (i.e., f2 ≠ f1) from all experiments. ***Lower****, Scalp topographies of t-values reflecting group-level statistics for modulations by signed subjective evidence (f2 - f1') and by the absolute strength of evidence (|f2 – f1'|). Displayed topographies are averages over 250 ms windows, starting at 0 with the onset of the second stimulus. The modulation by signed subjective evidence peaks clearly earlier (250 – 500 ms topography) than the modulation by the absolute strength of evidence (500 – 750 ms topography).* ***Upper****, ERPs from electrode CPz (white dot in scalp topographies), are computed separately for six levels of SPFDs, and display a modulation by the signed values of the SPFDs and then by the absolute values of the SPFDs.*

and P2 with p_{FWE} = 0.002; Figure 4). Later, however, the same ERP was positively correlated with the absolute strength of the evidence (273 – 953 ms, 33 electrodes, strongest in P1, CPz, Cz, C2, CP2, and P2 with p_{FWE} = 0.002; scalp topographies in Figure 4). The overall profile of the underlying ERP strongly resembled the classic P300 or CPP (see time courses in Figure 4). Please note that the time courses of the grand average ERPs per binned SPFD level provide a much coarser view on the underlying effects

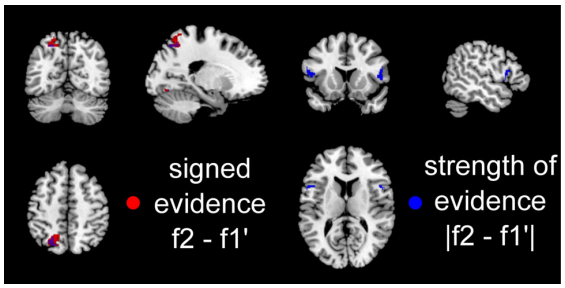

Figure 5 Source reconstructions for the early CPP modulation by signed subjective evidence (red), and the late modulation by the absolute strength of evidence (blue).

as compared to the statistical t-maps, because the fine-grained information contained in subject-specific SPFDs is lost for the ERP visualization. For incorrect decisions, the above-mentioned modulations by subjective evidence vanished (all $p_{FWE} > 0.05$), however, the overall profile of the ERP remained unchanged conforming to the shape of a typical P300/CPP. Directly comparing the modulations between correct and incorrect decisions revealed significant differences (i.e., interaction effects) in both the modulation by signed subjective evidence (326 – 367 ms and 418 – 455 ms, electrodes P1, P3, P5, PO7, and PO3 with $p_{FWE} = 0.022$ and $p_{FWE} = 0.032$) and in the modulation by absolute strength of evidence (723 – 750 ms, electrodes CP5, P7, PO7, O1, Iz, and O2 with $p_{FWE} = 0.028$). In sum, parietal ERPs reflected the signed and absolute subjective evidence only for correct trials – and significantly more than for incorrect trials. Hence, a faithful representation of the subjective evidence is tightly linked to correct decisions, implying the behavioral relevance of these effects.

The significant positive correlations in centro-parietal electrodes in correct trials (both with signed and absolute values of SPFDs) were accompanied by significant negative correlations in bilateral fronto-temporal electrodes for all described effects, hinting at the rough orientation of underlying dipole generators (see scalp topographies in Figure 4). In general agreement with the scalp topographies, the reconstructed source locations suggest that the modulation by signed subjective

evidence originates from left superior parietal lobule (SPL; Brodman area 7A; MNI peak coordinates: -24, -62, 54) in the posterior parietal cortex (PPC; Figure 5). On a considerably lower significance level ($p < 0.05$; uncorrected), also the right SPL is implicated as a likely source. The modulation by the absolute strength of subjective evidence additionally suggested probable sources in bilateral inferior frontal gyrus (IFG, Brodman area 44/45, MNI peak coordinates: -54/+48, 14, 12; Figure 5).

We challenged our findings in a series of control analyses to exclude confounding factors as the driving forces behind the observed effects. First and foremost, we examined whether the observed modulations of parietal ERPs were driven by the outermost stimulus pairs alone. That is, in the given stimulus set, some choices could have been based on exceptionally high or low f2 alone, possibly associated with qualitatively distinct percepts. We excluded these outermost stimuli from the stimulus set and repeated the multiple regression analysis on the remaining subset of data (inset Figure 6). Notably, the subset only included trials in which any f2 could lead to either choice (i.e., f2 alone did not predict the correct decision in these trials), resulting in markedly reduced trial numbers for the analysis (i.e., 450-700 per subject). Nevertheless, the results were qualitatively identical to those obtained when using the full set (compare Figure 4 and 6). After the presentation of f2, the ERP was first modulated by the signed subjective evidence (295 – 578 ms, 24 electrodes, strongest in Pz, CPz, CP1, CP2, P1, and P3 with $p_{FWE} = 0.002$) and then by the absolute strength of evidence for correct decisions (486 – 676 ms, 14 electrodes, strongest in CPz, Pz, POz, CP1, CP2, and P1 with $p_{FWE} = 0.002$), but not for incorrect decisions (no clusters). A significant difference between correct and incorrect trials was only observed for the modulation by absolute strength of evidence (602 – 654 ms, electrodes P1, P3, PO7, PO3, POz, and PO4 with $p_{FWE} = 0.026$). With respect to the computation of ERPs, excluding the outermost stimuli led to fewer trials falling into the most extreme bins of SPFDs (see ERPs in Material and Methods). In particular, this concerned large negative and large positive

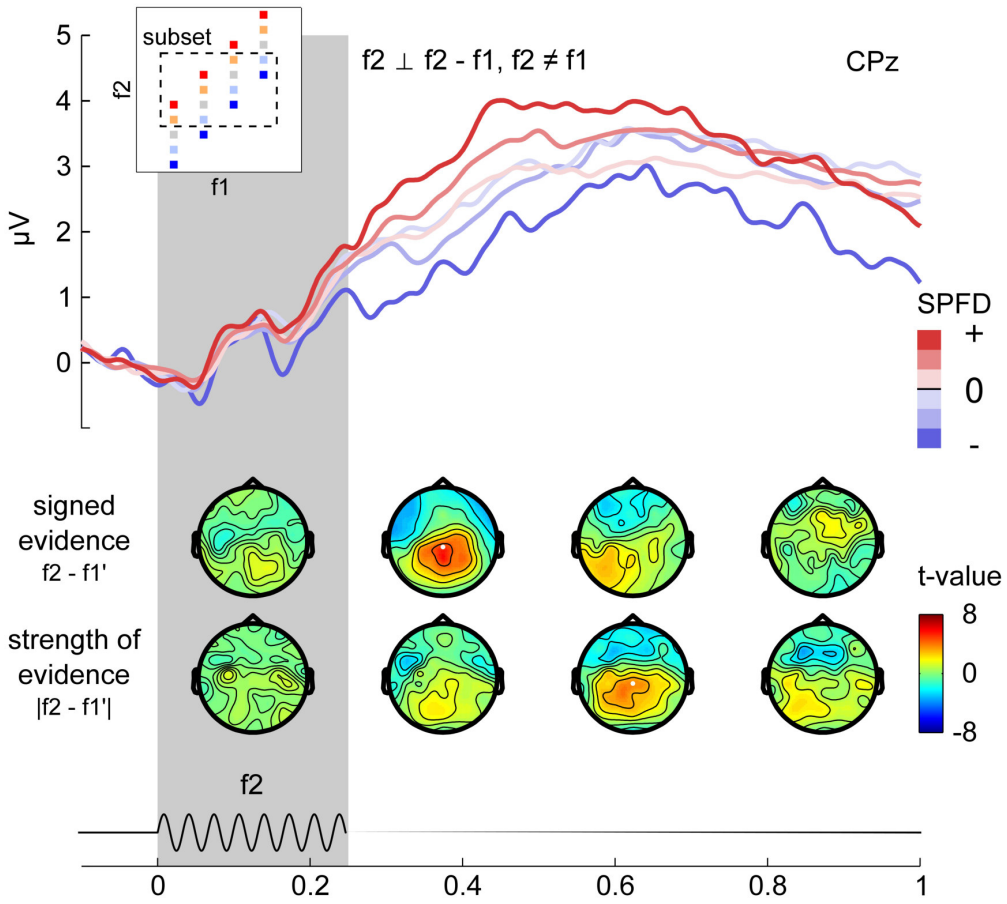

Figure 6 CPP modulation persists when using a subset of trials in which f2 alone does not predict decision outcome (i.e., f2 and f2 – f1 are orthogonal). Inset in upper left corner highlights the stimulus pairs that were used for this analysis (see also Figure 1). Same conventions as in Figure 4. Note that only the grand average ERPs for the most negative and most positive level of SPFDs (dark blue and dark red) were affected by using a reduced dataset (see text for details).

SPFDs (dark blue and dark red in upper panel of Figure 6) with 26 and 78 participants respectively contributing data to the grand average ERPs (i.e., 35 trials per individual ERPs on average). For comparison, all 116 participants contributed individual ERPs (based on 67 trials on average) to the grand average for the remaining levels of SPFDs. Again, note that the computation of classic ERPs only served displaying purposes. The statistical analysis was based on single-trials (i.e., not binned into discrete levels of SPFDs), and was hence unaffected by any imbalances in trial numbers per discrete levels of SPFDs. Taken together, this analysis ruled out that the outermost stimulus pairs alone

accounted for the observed modulations in the EEG signal.

In a further control analysis, we focused on the observation that for some participants SPFDs were distributed asymmetrically around zero due to an overall response bias. As a consequence, the corresponding absolute values were not fully independent from the signed SPFDs. We therefore orthogonalized the absolute values with respect to the signed SPFDs by subtracting the individual mean before computing the multiple regression and again obtained qualitatively identical results (modulation by signed SPFDs: 264 – 537 ms, 29 electrodes, strongest in Pz, CPz, POz, CP2, CP4, and P1 with $p_{FWE} = 0.002$; modulation by absolute values of SPFDs: 279 – 947 ms, 32 electrodes, strongest in Pz, CPz, CP1, CP2, P1, and P3 with $p_{FWE} = 0.002$).

Next, we explored whether the EEG signal was possibly also affected after the first stimulus by the quantity that had to be kept in working memory (i.e., in analogy to the presumed subjective difference quantity on which the decision is based). That is, we studied whether we could find a parietal potential that was modulated by f1 in a similar way as the ERPs after f2 were modulated by SPFDs. We did not find any comparable effect (i.e., no cluster with comparable spatial and temporal configuration; for a similar result, see Spitzer et al., 2016).

Finally, when examining the data from each experiment (see Materials and Methods) separately, we found a highly similar pattern of modulations by subjective evidence as with the pooled data. In all experiments, the ERP was first modulated by the signed subjective evidence, and then by the strength of subjective evidence for correct (all effects with $p_{FWE} < 0.014$, except for Experiment 3, with $p_{FWE} = 0.178$ and $p_{FWE} = 0.248$ for the early and late modulation, respectively), but not for incorrect decisions (no clusters in parietal electrodes, except for Experiment 2 showing a negative modulation by the absolute strength of evidence with $p_{FWE} = 0.018$). Note that for Experiments 1 and 2, RTs indicated that participants responded faster for “f2 > f1” choices as compared with “f2 < f1” choices even when

considering only trials from the subset shown in Figure 6, while for Experiments 3 – 6, RTs were uninformative due to the delayed response paradigm. As a consequence, the observed modulation by signed SPFDs (i.e., higher ERP for positive SPFDs as compared with negative SPFDs immediately after f2) might be explained by faster unfolding decision processes for choices of "f2 > f1". In particular, the observed effect might reflect that the 'classic' CPP, only tracking absolute strength of evidence, started earlier for positive SPFDs than for negative SPFDs. However, since we only have meaningful RT data for two out of six experiments, we can neither confirm nor rule out the possibility that variations in the onset of the CPP explain the observed modulation by signed SPFDs.

Signed subjective evidence modulates parietal ERPs even during judgements of physically identical stimulus pairs

We repeated the multiple regression analysis with signed SPFDs and their absolute values as regressors, however, this time only using trials without any physical evidence for one or the other choice. In other words, we only used trials with two identical stimuli (i.e., f1 = f2: 12 Hz vs 12 Hz, 16 Hz vs 16 Hz, 20 Hz vs 20 Hz, 24 Hz vs 24 Hz). Crucially, although the physical difference f2 – f1 is always zero for these trials, the individually estimated SPFDs yielded non-zero values for each stimulus pair. This is a direct consequence of the known biases in choice behavior that are typically observed in sequential comparison tasks (i.e., comparing f2 with mean-biased f1' instead of the physical value of f1). Based on the non-zero SPFDs, we were hence able to divide trials according to decisions that were in line with the estimated SPFDs (i.e., SPFD < 0: f1 chosen, and SPFD > 0: f2 chosen), and those that were not (i.e., SPFD < 0: f2 chosen, and SPFD > 0: f1 chosen). This way, we could divide trials into "consistent" and "inconsistent" with respect to the model outcome. Remarkably, for "consistent" decisions, we found a qualitatively similar positive correlation of ERPs with signed SPFDs as for correct

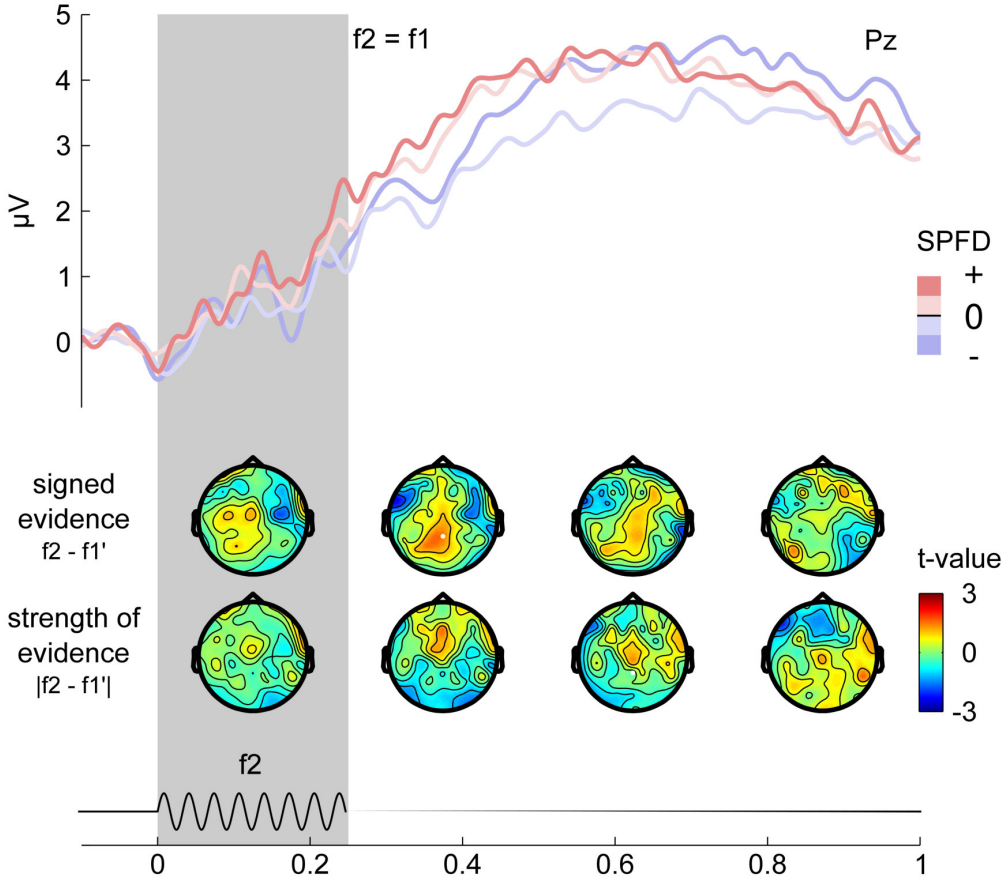

Figure 7 CPP is modulated by signed subjective evidence even in the absence of physical evidence (i.e., f2 = f1). Same conventions as in Figure 4. ***Lower****, the modulation by subjective evidence peaks in the same time window as the modulation for trials with f2 ≠ f1 (250 – 500 ms topography) and displays a similar topography (see Figures 4 and 6). A modulation by the absolute strength of evidence is not observed. Note the different scale of t-values.* ***Upper****, ERPs from electrode Pz (white dot in scalp topographies) are computed separately for four levels of SPFDs and display a weak modulation by the signed values of the SPFDs. Note that a considerably reduced set of trials (25% of all presented trials) and participants (Experiments 3 – 6; 73/116 participants) was available for this analysis.*

trials in which physical evidence for a decision was actually present (236 – 246 ms, electrodes PO3, POz, Pz, CP6, CP4, CP2, P2, P4, P6, P8, and PO8, $p_{cluster}$ = 0.016, FWE corrected, Figure 7). For decisions identified as "inconsistent", no such correlation was found. A comparison between "consistent" and "inconsistent" trials revealed that the modulation of ERPs by signed subjective evidence was significantly different (i.e., an interaction effect) between both sets of trials (322 – 338 ms, electrodes

P3, P5, PO3, Oz, POz, Pz, P2, P8, PO8, and PO4, $p_{cluster}$ = 0.044, FWE corrected). Notably, the separation of trials into these two sets was solely based on the modeled SPFDs, and yet, we were able to observe a significant difference in the EEG signal. However, the absolute values of the SPFDs did not modulate the CPP in trials with identical stimuli. Only a more anterior cluster became statistically significant for "consistent" decisions (268 – 279 ms, electrodes F1, F3, Fz, F2, F4, FC2, and FCz, $p_{cluster}$ = 0.03, FWE corrected), however, this effect did not differ between "consistent" and "inconsistent" trials.

Modulation by absolute strength of evidence relates to statistical decision confidence

That the CPP was correlated with the absolute values of SPFDs may suggest that this modulation could be linked with the level of confidence in a decision. To explore such potential relationship, we checked whether the late CPP conforms with the predictions of "statistical decision confidence" (see Drugowitsch, 2016; Hangya et al., 2016; Sanders et al., 2016). In this framework, confidence exhibits four key characteristics that can be tested without the need for explicit confidence ratings, simply based on statistical decision theory: (1) confidence is positively correlated with PCRs; (2) confidence increases with evidence strength for correct choices, but decreases for incorrect choices (see Figure 2B for intuition); (3) when (almost) no evidence is available (i.e., in very hard trials), confidence exhibits the same intermediate level for correct and incorrect choices; (4) for the same strength of evidence, high-confidence trials still yield higher PCRs than low-confidence trials.

Concerning (1), as reported in our main results, we found that the late CPP was positively correlated with the absolute values of SPFDs, which in turn were highly correlated with PCRs (Figure 3D). For (2) and (3) we extracted single-trial amplitudes of the CPP (mean amplitude between 500 and 800 ms after f2 in electrode CPz), and grouped these amplitudes according to the discrete levels of absolute

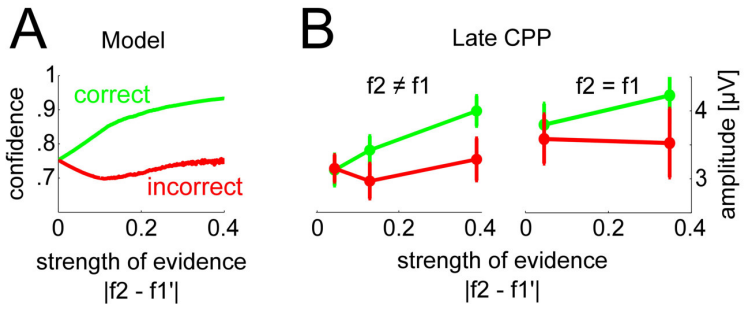

Figure 8 Late CPP corresponds to statistical decision confidence. ***A****, Average statistical decision confidence based on simulations from behavioral models of each participant. Confidence increases with evidence strength (i.e., |f2 – f1'|) for correct trials and decreases (initially) for incorrect trials. For very hard trials (|f2 – f1'| = 0), confidence is at the same intermediate level for correct and incorrect trials.* ***B****, Average amplitude (+/- standard error of mean) of late CPP (500 – 800 ms) exhibits same pattern as predicted by simulations shown in A, for trials with and without objective evidence (i.e., f2 ≠ f1 and f2 = f1, respectively).*

SPFDs separately for correct and incorrect trials (i.e., three levels for trials with f2 ≠ f1: [0 to 0.09]; [0.09 to 0.17]; [> 0.17]; two levels for trials with f2 = f1: [0 to 0.09]; [> 0.09]). As predicted by statistical decision confidence, we found that the CPP amplitude increased with evidence strength for correct trials, and (initially) decreased for incorrect trials, in remarkable alignment with the average confidence computed from individual model fits (Figure 8A, B). Moreover, for the most difficult trials (i.e., least evidence strength), the CPP amplitude was at the same intermediate level for correct and incorrect trials (Figure 8B). Notably, predictions (2) and (3) were also reflected in CPP amplitudes when considering only trials with f2 = f1 (Figure 8B, right panel). Lastly, we did a median split of our data based on CPP amplitudes to simulate a division into high- and low-confidence trials (4). We compared PCRs between high- and low-amplitude trials for each of the three levels of evidence strength (i.e., [0 to 0.09]; [0.09 to 0.17]; [> 0.17]), and found that for the intermediate and high level of evidence strength, PCRs were significantly higher in trials with a high CPP amplitude as compared to trials with a low CPP amplitude (paired t-test, both $p < 0.001$). Taken together, the late CPP in the present dataset fulfils all requirements posed by statistical decision theory for a measure of

confidence.

Parietal ERPs correlate with upper beta band amplitude over effector-specific premotor areas

Finally, we explored whether the observed modulation of ERPs was related to choice-specific modulations of upper beta band amplitude over premotor areas previously identified in the same data (i.e., experiments 1 and 2 as reported in Herding et al., 2016, 2017). In this earlier work, beta band power was shown to be higher for "f2 > f1" choices as compared to "f2 < f1" choices, regardless of whether the choice was correct or incorrect. Indeed, we found a positive correlation between the amplitude of parietal ERPs during the early modulation by signed SPFDs and the beta band amplitude (one-sample t-test across single-trial correlations of participants, mean rho = 0.03, $p < 0.001$). Notably, we obtained the same positive correlation when considering data from both experiments separately (experiment 1: mean rho = 0.03, $p = 0.016$; experiment 2: mean rho = 0.02, $p = 0.002$). The late CPP (i.e., during the modulation by absolute SPFDs) was also positively correlated with single-trial beta band amplitudes (mean rho = 0.02, $p = 0.006$). However, when considering both experiments separately, only data from experiment 1 showed a significant positive correlation (mean rho = 0.02, $p = 0.02$), but not data from experiment 2 (mean rho = 0.01, $p = 0.15$). Importantly, average response times in experiments 1 and 2 (~ 862 ms and ~ 603 ms) intersected with the timing of the late CPP (i.e., 500 – 800 ms after f2) and thus render a causal relation between this late component and choice-specific upper beta band amplitude unlikely. For the early parietal signal (i.e., 250 – 500 ms after f2), on the other hand, a causal role in choice selection seems chronologically possible. However, such potential causality remains to be thoroughly investigated in future studies.

Discussion

In the current study, we investigated human ERP signals during the comparison of two sequentially presented vibrotactile stimuli (with frequencies f1 and f2). We pooled a sizeable amount of data (N = 116) over six different variants of this task, varying in response modality, response timing, and response mapping, whereas stimuli and comparison task remained unchanged. Despite the variations, we consistently found that ERPs after the second stimulus were first modulated by the signed subjective evidence in favour of the ensuing decision (i.e., signed SPFDs), and later by the absolute strength of evidence (i.e., absolute values of SPFDs). Notably, both modulations were only observed for correct decisions, linking a successful discrimination of f1 and f2 with a faithful representation of the perceived stimulus difference (i.e., SPFDs) in the parietal cortex. Even in the absence of any objective differences between f1 and f2 (i.e., f1 = f2), ERPs indexed the signed values of SPFDs, but not their absolute values. This observation implies that parietal signals may index endogenous evidence for subsequent decisions beyond what has been observed in the CPP (see CPP in the absence of stimuli in O'Connell et al., 2012). Accordingly, we found a correlation between the early ERP effect and choice-selective upper beta band amplitudes in effector-specific premotor areas. The late modulation by the absolute values of SPFDs on the other hand seemed to index the amount of evidence for a decision, which we related to the concept of statistical decision confidence. The putative neuronal sources of both early and late ERP modulation were located in SPL (Brodman area 7A; primarily in the left hemisphere), whereas the late modulation by absolute differences additionally exhibited likely sources in bilateral IFG (Brodman area 44/45).

Several studies of the broadband human EEG signal have shown that the CPP reflects the accumulated evidence for perceptual decisions which require the integration of noisy sensory input over time for immediate and delayed responses (e.g., O'Connell et al., 2012; Kelly and O'Connell, 2013; Philiastides

et al., 2014, Twomey et al., 2016). These findings might be directly linked to seminal work on visual perceptual decision making in monkeys that implicated the PPC as a key site for evidence accumulation (see Shadlen and Kiani, 2013). A recent study showed that also in other tasks, i.e., in a classic oddball paradigm, the CPP, or rather the P300, was modulated by the evidence in favour of a successful 'deviant' detection (i.e., a modulation by the difference between 'deviant' and 'standard' stimulus; Twomey et al., 2015). The topography and evolution of the present ERP modulations match these reports. Yet, all previous studies that associated the CPP with decisional evidence, found a modulation of the CPP by the evidence *within* a single choice category, but never a modulation by evidence *across* choice alternatives (e.g., O'Connell et al., 2012; Kelly and O'Connell, 2013; Philiastides et al., 2014; Twomey et al., 2015; Twomey et al., 2016). That is, the CPP was shown to track the strength of available evidence, albeit concealing for which choice alternative. In particular, Kelly and O'Connell (2013) showed that only the proportion of coherent motion, independent of direction (i.e., leftward or rightward), modulated the CPP in an RDM task (see also Twomey et al., 2016). Moreover, Philiastides et al. (2014) were able to discriminate different levels of presented evidence based on a parietal potential (i.e., likely the CPP), no matter whether an image of a face or a car was shown. However, a classification between faces and cars was not possible. In the current study, we report for the first time that parietal signals were modulated by both the amount of evidence and the choice alternative at the same time (i.e., by signed evidence in form of SPFDs). Only later, the absolute strength of evidence alone (i.e., absolute values of SPFDs; independent of the specific choice category) was reflected by the CPP as known from previous work. We propose that the early modulation by the signed values of SPFDs indexes the evidence on which a decision was based. The late modulation by the absolute values of SPFDs, on the other hand, might refer to the strength of evidence for a decision, which appears closely related to confidence. Given the observed differences

in RTs between both choice alternatives (i.e., faster RTs for “f2 > f1” choices) in two out of six experiments, another possible explanation for the reported effects is that we observed the ‘classic’ CPP, however, with different onset times depending on the subsequent choice. In particular, this could implicate that one choice alternative (“f2 > f1”) was processed faster than the other (“f2 < f1”), possibly hinting at a preferred/default choice.

Yet, our findings do not entirely correspond to the ’classic’ CPP, as we did not observe a saturation of the CPP at a fixed threshold, but rather a modulation by subjective task difficulty (cf. Kelly and O’Connell, 2013; but see Philiastides et al. 2014). A further investigation of this relationship revealed that the modulation by absolute values of SPFDs complied in all respects with the definition of statistical decision confidence (see Drugowitsch, 2016; Hangya et al., 2016; Sanders et al., 2016). Importantly, in line with the classic definition of confidence, statistical decision confidence refers to the probability that a choice is correct (given the evidence) and was recently shown to align with human confidence judgements (Sanders et al., 2016). That is, this framework allows to infer confidence levels even in the absence of explicit confidence ratings. That the CPP, or rather the P300, might indicate confidence has been suggested for a long time (e.g., Squires et al., 1973; Sutton et al., 1982; Curran, 2004), and has recently been reiterated. Gherman and Philiastides (2015), for instance, reported a higher amplitude of the CPP for choices that were made with high certainty as compared to choices with low certainty (see also Philiastides et al., 2014). Moreover, although the CPP has been typically reported to reach a fixed level at the time of the response report (see Kelly and O’Connell, 2015; but Philiastides et al., 2014), when considering false alarm trials, a clearly lower amplitude was observed, possibly indexing lower confidence in those trials (Figure 2C in O’Connell et al., 2012). The lack of differences in CPP amplitudes at response time for the remaining results might be related to the task demands per se. By applying continuous task designs (e.g., O’Connell et al., 2012, Kelly and

O'Connell, 2013), decision-unrelated stimulus evoked EEG signals were elegantly avoided, however, an additional level was added to the task, requiring the detection of stimuli. This might have led to a rather constant level of confidence before committing to a decision (see Discussion in Philiastides et al., 2014). The reconstructed sources of the confidence-related signal in bilateral IFG appear unusual at first glance, however, recent fMRI studies also implicated the IFG in the processing of confidence (Hebart et al., 2016; Sherman et al., 2016).

Finally, the present vibrotactile 2-AFC task has been used extensively by Romo and colleagues during electrophysiological recordings from monkeys (reviewed in Romo and deLafuente, 2013). In this research, premotor areas were identified as one of the first sites to show decision-related firing rate patterns that encoded the differences between f1 and f2 (Hernández et al., 2002, 2010; Romo et al., 2004). Furthermore, a choice-specific (i.e., binary) amplitude modulation of large-scale upper beta band oscillations (~20 – 30 Hz) in premotor areas was recently identified in monkey local field potentials (Haegens et al., 2011) as well as in human EEG data (Herding et al., 2016, 2017; Ludwig et al., 2018). With the current results, we might thus provide first evidence for a previously missing EEG signature that indexes the fine-grained subjective evidence in favour of the ensuing choices. Given the stimulus-locked early onset of the ERP modulation by signed evidence, the response-locked character of the beta band modulation, the conceptually reasonable gradient (i.e., choices are based on evidence), and the source locations of both findings (i.e., evidence in parietal cortex and choice in premotor cortex), we presume that parietal ERPs precede and potentially drive the beta band effect. In fact, using the data from Experiments 1 and 2 with immediate responses (i.e., with a direct translation from evidence to choices), we found a positive correlation between single-trial parietal ERP magnitude (during the early modulation by signed evidence) and the level of beta band amplitude (during the choice modulation). However, since the data could only be pooled from two

out of six experiments, this possible connection between CPP and beta band amplitude deserves a more thorough investigation in future research.

To conclude, our data corroborate the notion of the CPP tracking evidence in perceptual decision making (see Kelly and O'Connell, 2015). Using a vibrotactile 2-AFC comparison task, we could show, however, that this signal may have additional features depending on task demands. Our results revealed that parietal ERPs first index signed subjective evidence, and only later the absolute strength of evidence. Given that this observation cannot be attributed to differences in the processing time of evidence accumulation for both choice alternatives, we propose that the early modulation reflects the quantity on which a decision is based, whereas the late modulation indexes the amount of evidence or even confidence. In the context of the vibrotactile 2-AFC task, our findings suggest that the fine-grained signed evidence that is reflected early in the parietal cortex might index the input to more categorical choice representations, e.g., in effector-specific premotor areas (see Haegens et al., 2011; Herding et al., 2016, 2017; Ludwig et al., 2018).

Acknowledgements

This work was supported by the Deutsche Forschungsgemeinschaft (DFG, GRK1589/1). We thank Ulf Toelch for useful comments on the manuscript.

References

Ashourian P, Loewenstein Y. 2011 Bayesian inference underlies the contraction bias in delayed comparison tasks. PLoS One 6.

Baranski J V, Petrusic WM. 1998. Probing the locus of confidence judgments: experiments on the time to determine confidence. J Exp Psychol Hum Percept Perform 24:929–945.

Brainard DH. 1997. The Psychophysics Toolbox. Spat Vis 10:433–436.

Cornelissen FW, Peters EM, Palmer J. 2002. The Eyelink Toolbox: Eye tracking with MATLAB and the Psychophysics Toolbox. Behav Res Methods, Instruments, Comput 34:613–617.

Curran T. 2004. Effects of attention and confidence on the hypothesized ERP correlates of recollection and familiarity. Neuropsychologia 42:1088–1106.

Daunizeau, J, Adam, V, Rigoux, L. 2014. VBA: A Probabilistic Treatment of Nonlinear Models for Neurobiological and Behavioural Data. *PLoS Computational Biology*, *10*, e1003441.

Drugowitsch, J. 2016. Becoming confident in the statistical nature of human confidence judgments. Neuron, 90(3), 425-427.

Eickhoff SB, Stephan KE, Mohlberg H, Grefkes C, Fink GR, Amunts K, Zilles K. 2005. A new SPM toolbox for combining probabilistic cytoarchitectonic maps and functional imaging data. Neuroimage 25:1325–1335.

Fechner GT. 1860. Elemente der Psychophysik. Leipzig: Breitkopf & Härtel.

Festinger L. 1943. Studies in decision: I. Decision-time, relative frequency of judgment, and subjective confidence as related to physical stimulus difference. J Exp Psychol 32:291–306.

Friston K, Harrison L, Daunizeau J, Kiebel S, Phillips C, Trujillo-Barreto N, Henson R, Flandin G, Mattout J. 2008. Multiple sparse priors for the M/EEG inverse problem. Neuroimage 39:1104–1120.

Friston K, Henson R, Phillips C, Mattout J. 2006. Bayesian estimation of evoked and induced responses. Hum Brain Mapp 27:722–735.

Gherman S, Philiastides MG. 2015. Neural representations of confidence emerge from the process of decision formation during perceptual choices. Neuroimage 106:134–143.

Gold JI, Shadlen MN. 2007. The neural basis of decision making. Annu Rev Neurosci 30:535–574.

Haegens S, Nácher V, Hernández A, Luna R, Jensen O, Romo R. 2011. Beta oscillations in the monkey sensorimotor network reflect somatosensory decision making. PNAS 108:10708–10713.

Haegens S, Vergara J, Rossi-Pool R, Lemus L, Romo R. 2017. Beta oscillations reflect supramodal information during perceptual judgment. PNAS 114:13810-13815.

Hangya B, Sanders JI, Kepecs A. 2016. A mathematical framework for statistical decision confidence. Neural Computation 28:9, 1840-1858.

Hebart MN, Schriever Y, Donner TH, Haynes JD. 2016. The Relationship between Perceptual Decision Variables and Confidence in the Human Brain. Cereb Cortex 26:118–130.

Hellström A. 2003. Comparison is not just subtraction: effects of time- and space-order on subjective stimulus difference. Percept Psychophys 65:1161–1177.

Hellström Å. 1985. The time-order error and its relatives: Mirrors of cognitive processes in comparing. Psychol Bull 97:35–61.

Herding J, Spitzer B, Blankenburg F. 2016. Upper Beta Band Oscillations in Human Premotor Cortex Encode Subjective Choices in a Vibrotactile Comparison Task. J Cogn Neurosci 28:668–679.

Herding J, Ludwig S, Blankenburg F. 2017. Response-modality-specific encoding of human choices in upper beta-band oscillations during vibrotactile comparisons. Frontiers in Human Neuroscience.

Hernández A, Nácher V, Luna R, Zainos A, Lemus L, Alvarez M, Vázquez Y, Camarillo L, Romo R. 2010. Decoding a perceptual decision process across cortex. Neuron 66:300–314.

Hernández A, Zainos A, Romo R. 2002. Temporal evolution of a decision-making process in medial premotor cortex. Neuron 33:959–972.

Ille N, Berg P, Scherg M. 2002. Artifact correction of the ongoing EEG using spatial filters based on artifact and brain signal topographies. J Clin Neurophysiol 19:113–124.

Jou J, Leka GE, Rogers DM, Matus YE. 2004. Contraction bias in memorial quantifyingjudgment: Does it come from a stable

compressed memory representation or a dynamicadaptation process? Am J Psychol. 117(4):543–564.

Karim M, Harris JA, Morley JW, Breakspear M. 2012. Prior and present evidence: How prior experience interacts with present information in a perceptual decision making task. PLoS One 7.

Kelly SP, O'Connell RG. 2013. Internal and external influences on the rate of sensory evidence accumulation in the human brain. J Neurosci 33:19434–19441.

Kelly SP, O'Connell RG. 2015. The neural processes underlying perceptual decision making in humans: Recent progress and future directions. J Physiol 109:27–37.

Litvak V, Friston K. 2008. Electromagnetic source reconstruction for group studies. Neuroimage 42:1490–1498.

Litvak V, Mattout J, Kiebel S, Phillips C, Henson R, Kilner J, Barnes G, Oostenveld R, Daunizeau J, Flandin G, Penny W, Friston K. 2011. EEG and MEG data analysis in SPM8. Comput Intell Neurosci 2011:852961.

Ludwig S, Herding J, Blankenburg F. 2018. Oscillatory EEG signatures of postponed somatosensory decisions. Hum Brain Mapp. 2018; 00:1–14. Maris E, Oostenveld R. 2007. Nonparametric statistical testing of EEG- and MEG-data. J Neurosci Methods 164:177–190.

Mazurek ME, Roitman JD, Ditterich J, Shadlen MN. 2003. A Role for Neural Integrators in Perceptual Decision Making. Cereb Cortex 13:1257–1269.

O'Connell RG, Dockree PM, Kelly SP. 2012. A supramodal accumulation-to-bound signal that determines perceptual decisions in humans. Nat Neurosci 15.

Philiastides MG, Heekeren HR, Sajda P. 2014. Human Scalp Potentials Reflect a Mixture of Decision-Related Signals during Perceptual Choices. J Neurosci 34:16877–16889.

Preuschhof C, Schubert T, Villringer A, Heekeren HR. 2010. Prior Information biases stimulus representations during vibrotactile decision making. J Cogn Neurosci 22:875–887.

Roitman JD, Shadlen MN. 2002. Response of neurons in the lateral intraparietal area during a combined visual discrimination reaction time task. J Neurosci 22:9475–9489.

Romo R, de Lafuente V. 2013. Conversion of sensory signals into perceptual decisions. Prog Neurobiol 103:41–75.

Romo R, Hernández A, Zainos A. 2004. Neuronal correlates of a perceptual decision in ventral premotor cortex. Neuron 41:165–173.

Romo R, Salinas E. 2003. Flutter discrimination: neural codes, perception, memory and decision making. Nat Rev Neurosci 4:203–218.

Sanchez G. 2014. Real-time electrophysiology in cognitive neuroscience: towards adaptive paradigms to study perceptual learning and decision making in humans.

Sanders JI, Hangya B, Kepecs A. 2016. Signatures of a Statistical Computation in the Human Sense of Confidence. Neuron 90: 499-506.

Shadlen MN, Kiani R. 2013. Decision making as a window on cognition. Neuron 80:791–806.

Sherman MT, Seth AK, Kanai R. 2016. Predictions Shape Confidence in Right Inferior Frontal Gyrus. J Neurosci 36:10323–10336.

Singer T, Critchley HD, Preuschoff K. 2009. A common role of insula in feelings, empathy and uncertainty. Trends Cogn Sci 13:334–340.

Smith PL, Ratcliff R. 2004. Psychology and neurobiology of simple decisions. Trends Neurosci 27:161–168.

Spitzer B, Blankenburg F. 2011. Stimulus-dependent EEG activity reflects internal updating of tactile working memory in humans. PNAS 108:8444–8449.

Spitzer B, Blankenburg, F, Summerfield, C. 2016. Rhythmic gain control during supramodal integration of approximate number. Neuroimage, 129, pp. 470-479

Spitzer B, Wacker E, Blankenburg F. 2010. Oscillatory correlates of vibrotactile frequency processing in human working memory. J Neurosci 30:4496–4502.

Spitzer, B., Waschke, L., Summerfield, C. (2017). Selective overweighting of larger magnitudes during noisy numerical comparison. Nature Human Behaviour, 0145 (2017).

Squires KC, Hillyard SA, Lindsay PH. 1973. Vertex potentials evoked during auditory signal detection : Relation to decision criteria *. Percept Psychophys 14:265–272.

Sutton S, Rouchkin DS, Munson R, Kietzman ML, Hammer M. 1982. Event related potentials in a two-interval forced choice decision task. Percept Psychophys 32:360–374.

Talbot W, Darian-Smith I, Kornhuber H, Mountcastle V. 1968. The sense of flutter-vibration: comparison of the human capacity with response patterns of mechanoreceptive afferents from the monkey hand. Neurophysiology 31:301–334.

Tobimatsu S, Zhang YM, Kato M. 1999. Steady-state vibration somatosensory evoked potentials: physiological characteristics and tuning function. Clin Neurophysiol 110:1953–1958.

Twomey DM, Kelly SP, O'Connell RG. 2016. Abstract and Effector-Selective Decision Signals Exhibit Qualitatively Distinct Dynamics before Delayed Perceptual Reports. J Neurosci 36:7346–7352.

Twomey DM, Murphy PR, Kelly SP, O'Connell RG. 2015. The classic P300 encodes a build-to-threshold decision variable. Eur J Neurosci 42:1636–1643.

Urai AE, Braun A, Donner TH. 2017. Pupil-linked arousal is driven by decision uncertainty and alters serial choice bias. Nature Communications 8:14637.

Vickers D. 1979. *Decision processes in visual perception*. New York, NY: Academic Press.

Woodrow H. 1935. The effect of practice upon time-order errors in the comparison of temporal intervals. Psychol Rev 42:127–152.

Neuronal signatures of a random-dot motion comparison task

Authors: Alexander von Lautz, Jan Herding, Felix Blankenburg

Neurocomputation and Neuroimaging Unit, Department of Education and Psychology, Freie Universität Berlin, Habelschwerdter Allee 45, 14195 Berlin

Bernstein Center for Computational Neuroscience Berlin, Philippstr. 13, 10115 Berlin

Corresponding author: Alexander von Lautz (alexander.von-lautz@bccn-berlin.de), Neurocomputation and Neuroimaging Unit, Department of Education and Psychology, Freie Universität Berlin, Habelschwerdter Allee 45, 14195 Berlin, +49 030 838 56693

Declarations of Interest: none

Abstract

The study of perceptual decision making has made significant progress owing to major contributions from two experimental paradigms: the working memory influenced sequential comparison task for vibrotactile, haptic stimuli and the random-dot motion task in the visual domain requiring evidence accumulation over time. On the one hand, electrophysiological recordings in nonhuman primates and humans have identified changes in firing rates and power modulations of beta band oscillations with the vibrotactile frequencies held in working memory, as well as with the mental operation required for decision making. On the other hand, firing rates and centro-parietal potentials were found to increase to a fixed level at the time of responding during the random-dot motion task, possibly reflecting an underlying evidence accumulation mechanism until a decision threshold is met. Here, to bridge these two paradigms, we presented two visual random-dot motion stimuli in a sequential comparison task while recording EEG from human volunteers. We identified a modulation of prefrontal beta band power that scaled with the level of dot motion coherence of the first stimulus during a short retention interval. Furthermore, beta power in premotor areas was modulated by participants' choices approximately 700 ms before responses were given via button press. At the same time, dot motion patches of the second stimulus evoked a pattern of broadband centro-parietal signal build-up till responses were made, whose peak varied with trial difficulty. Hence, we show that known modulations of beta power during working memory and decision making extend from the vibrotactile to the visual domain and provide support for the notion of evidence accumulation as an unconfined decision-making mechanism generalizing over distinct decision types.

Keywords:

Random-dot motion, working memory, decision making, EEG, centro-parietal positivity, beta oscillations, sequential comparison

1. Introduction

The study of perceptual decision making investigates how the brain translates sensory information to inform decisions (Heekeren et al., 2008; Shadlen & Kiani, 2013). Investigations into the neural basis of this process have made significant progress with the use of two tasks: (1) the sequential vibrotactile frequency comparison (SFC) task and (2) the visual random-dot motion (RDM) task (for review, see: Gold & Shadlen, 2007).

In vibrotactile SFC experiments non-human primates are tasked with the differentiation of two sequentially presented somatosensory stimuli, f1 and f2, who are set apart by a short working memory (WM) delay. After both vibrotactile frequencies are presented, decisions about whether f2 was higher or lower than f1 are reported by button press. Single-cell recordings in monkeys demonstrate that while retaining f1 in working memory, neural activity in the PFC is parametrically modulated by the to-be-maintained frequency, both in firing rate (Romo et al., 1999) and small neuronal populations' states (Barak et al., 2010). Moreover, following perception of f2, firing rates in the medial and ventral premotor cortex (m/vPMC) reflect the mental calculation f2-f1 necessary to perform the task (Romo et al., 2004; Hernandez et al., 2002). Analogous human M/EEG recordings have found corresponding parametric modulations in prefrontal beta band power with the frequency held in working memory (Spitzer et al., 2010; Spitzer & Blankenburg, 2011; von Lautz et al., 2017; Ludwig et al., 2018) and recently a choice-selective beta power change during the formation of a decision in this paradigm (Herding et al., 2016, 2017; Ludwig et al., 2018).

The second task, the discrimination of random-dot motion, requires participants to detect the overall motion direction of a field of moving dots by accumulating across the entire field and report the perceived motion direction via oculomotor responses. This decision process is

driven by orientation selective neurons in the middle temporal area (MT) which projects to response related areas, such as the lateral intraparietal area (LIP), frontal eye fields (FEF), superior colliculus (SC) and dorsolateral prefrontal cortex (dlPFC) (Ditterich et al., 2003; Kim & Shadlen, 1999; Ratcliff et al., 2003; Shadlen & Newsome, 1996, 2001). Examining broadband signals of the human EEG during a variety of similar paradigms revealed a centro-parietal positivity (CPP; in fact, the classic P300; see Twomey et al., 2015) that built-up until the time of responding and exerted a pattern reflecting the rate of evidence accumulation during single trials (O'Connell et al., 2012; Kelly and O'Connell, 2013; Philiastides et al., 2014).

Together, these studies from the vibrotactile and the visual domain have identified distinct regions that seem to be involved in the respective decision-making processes. The observed discrepancies can most likely be attributed to the differences in sensory and response modalities that are usually employed in either paradigm. However, despite the progress on a theoretical level (Gold & Shadlen, 2007; Wang, 2012; Romo & de Lafuente, 2013; Murakami & Mainen, 2015) and the proposal of an intentional framework of decision making which might be able to bridge the gap between these two lines of research (Shadlen et al., 2008), experimental progress has been slow. Curiously, until now human neuroimaging studies have neither investigated the SFC task with RDM stimuli nor the RDM task with vibrotactile stimuli (but see pupil dilation: Urai et al., 2017; monkey LFP: Wimmer et al., 2016). This is particularly surprising, because there is evidence that the SFC task can be applied to other sensory domains (Spitzer & Blankenburg, 2012) and motion direction can be perceived from tactile inputs (van Kemenade et al., 2014; Krebber et al., 2015).

Here, we take a first step to reconcile these two avenues of research experimentally by using the classic visual random-dot motion stimuli in a sequential comparison task. While measuring EEG, we consecutively presented two random-dot stimuli and gave participants the task of comparing the magnitude of coherent motion. We hypothesize that the magnitude of motion coherence held in WM is reflected by a parametric modulation of prefrontal beta power and that beta oscillations encode the choice (S2>S1, S2<S1) prior to responding. Moreover, we expect the RDM stimuli to elicit typical responses from occipital channels during stimulus perception and a modulation of the CPP build-up by the amount of available decision evidence. Notably, the decision evidence in the current paradigm is not solely determined by the coherence level of a single RDM stimulus, but by the difference in coherent motion between two RDM stimuli.

2. Materials and Methods

2.1. Participants

Twenty-nine healthy volunteers (20-34 years; 14 female) participated in the study after providing written informed consent. Participants received recompense of 10€ per hour. One participant was excluded from the analysis because of EEG equipment failure during recording. The local ethics committee at the Freie Universität Berlin approved the study.

2.2. Procedure

Volunteers were asked to observe two consecutively presented random-dot motion stimuli and to indicate whether the second stimulus (S2) displayed more or less coherent motion than the first stimulus (S1) (Figure 1). Importantly, participants were asked to compare only the amount of coherent motion, while the motion direction was not relevant for the task

and could be upwards or downwards. A trial began by a fixation period of 1 s, which was followed by the first RDM stimulus for 0.5 s. After a 1 s delay, a second RDM stimulus appeared for another 0.5 s. Participants then judged whether S2 displayed more coherently moving dots as compared to S1 by pressing a button with their right hand. One half of the participants indicated S2>S1 and S2<S1 by a button press with their middle and index finger, respectively, while the other half responded vice versa. After indicating their choice, participants were informed whether the decision was correct by a color change of the fixation cross (green or red) for 0.3 s. The next trial started after a variable period of 1-1.5 s. Participants were asked to keep their eyes fixated on the central cross throughout the experiment.

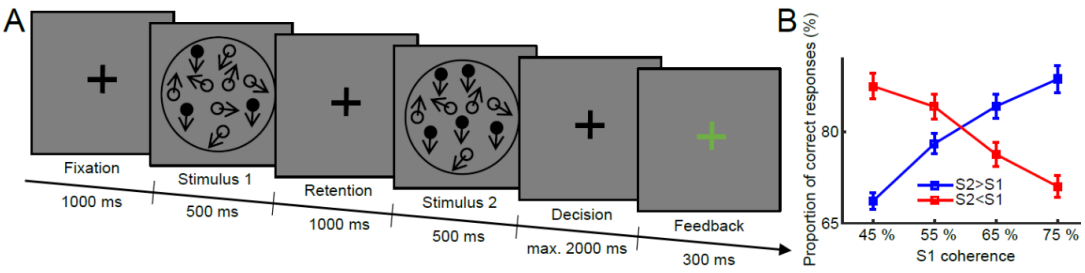

Figure 1: (A) Trial design. A trial started with a 1000ms fixation period, after which two random-dot motion patches were presented in succession with a delay period of 1000ms. Each stimulus was on screen for 500ms and consisted of randomly moving dots, out of which a portion moved non-randomly in the same direction. Participants indicated which of the two patches had more coherent motion while the direction was irrelevant for the task. After responding, participants got feedback by a red or green fixation cross. (B) Overall proportion of correct responses per S1 coherence level for the two possible choices (blue or red). If the coherence level of the second stimulus was higher (choice S2>S1, blue), participants performed better for high coherence S1 trials. If the second stimulus was lower (choice S2<S1, red), higher S1 coherence reduced performance. This is a manifestation of the time-order effect, also termed contraction bias.

After practicing for 64 trials during the EEG setup, participants performed 1024 trials divided into eight blocks with short breaks in between blocks. Participants were instructed to respond as quickly as possible without making errors. Response times (RTs) were defined as the duration between S2 onset and the button press. If a response took longer than 1.5 s, the fixation cross would flicker to remind participants to respond quickly. These slow trials

and very fast responses during S2 presentation (<100 ms after S2 offset) were excluded from subsequent data analyses. The overall recording time was about 70 minutes.

2.3. Stimuli

The stimuli were generated using MATLAB R2014a (The MathWorks), employing the variable coherence random dot motion (VCRDM) library for the Psychtoolbox (Brainard, 1997). In a dimly lit room, the stimuli were presented on a TFT monitor (refresh rate: 60 Hz) that was placed 65 cm away from the upright sitting participant.

Random dot stimuli were displayed within a circular aperture with a diameter of 5° visual angle (dva). The placement of dots in each RDM patch followed the standard VCRDM procedure, which utilizes three independent sets of dots. These are presented for one frame at a time and are displaced every three frames. For example, dot group one moves on frames 1, 4, 7..., while group two is modulated only on frames 2, 5, 8… etc. These three sets are crucial, because while they give the percept of continuous movement, it not possible to track a single dot on screen. In the standard dot motion detection task, each dot has a small likelihood of moving coherently, however, the majority is redrawn at a random location. Here, we used a different implementation in which all dots always move coherently, but in random directions (as in Hebart et al., 2012). Only the number of dots moving either upwards or downwards was modulated. Hence, if the coherence level was e.g. “45% up”, for every 100 dots, 45 dots consistently moved upwards, while the remaining 55% moved in random directions. When a dot moved outside the aperture, it was replaced on the opposite boundary with the same inherent motion. The number of dots was fixed at ~2.5 dots/dva² on screen at a time. Individual dots had a size of ~0.05 dva² and the motion speed was fixed

149 at 3 deg/s. All these parameters were thoroughly tested to minimize the percept of fuzziness
150 inherent to random dot motion displays.

151 On each trial, the coherence level for the first stimulus (S1) was randomly set to 45%, 55%,
152 65%, or 75%, and the coherence level of the second stimulus (S2) varied by ±10 or ±20 %.
153 The direction of coherent motion was either up- or downwards and was independent
154 between both RDM patches. Both the proportion of coherent motion and the motion
155 direction were fully counterbalanced throughout the experiment.

156 ## 2.4. Behavioral Model

157 In sequential comparison tasks, the discriminability of stimuli is heavily influenced by the
158 order in which the two stimuli are presented. This effect is known as the time-order
159 error/effect (TOE; e.g., Fechner, 1820; Woodrow, 1935; Hellström 1985, 2003) or
160 contraction bias. In particular, for a given set of stimuli, participants seem to compare the
161 second stimulus not only with the physical properties of the first stimulus, but also with the
162 average percept from the given stimulus set (Ashourian & Lowenstein, 2011; Karim et al.,
163 2012). In Bayesian terms, participants seem to form a prior which is centered on the mean of
164 the stimulus set and compare the second stimulus with a representation of the first stimulus
165 that was computed by Bayesian inference (i.e., the posterior of the first stimulus). As a
166 consequence, the representation of the first stimulus is shifted towards the overall mean of
167 the stimulus set and can account for the observed behavior associated with the TOE. Here,
168 we used such a Bayesian inference model with a Gaussian prior centered on the set of all
169 coherence levels. The prior variance, stimulus likelihood variance and decision criterion were
170 estimated from the choices of individual participants using variational Bayes with the VBA
171 toolbox (Daunizeau et al., 2014). To quantify the subjectively perceived coherence difference

172 (SPCD) for every trial and each participant, we defined the expected value of the posterior
173 distribution as the mean-shifted percept of S1 (denoted as S1') to compute S2-S1' (for a
174 more detailed description see Herding et al., 2016 and Sanchez, 2014). The computation of
175 SPCD yielded 16 individual values for each participant that were summarized in six bins
176 representing easy, medium and hard trials (for either choice) to allow for a comparison
177 across the group.

178 ## 2.5. EEG recording and data processing

179 Sixty-four active electrodes were placed in the extended 10-20 system to record EEG
180 (ActiveTwo, BioSemi) at 2048 Hz. In addition, four electrodes measured the vertical and
181 horizontal electrooculogram (vEOG, hEOG). Each cap was centered on the head and every
182 participants' electrode placement was measured in 3D with a stereotactic electrode-
183 positioning system (Zebris Medical GmbH, Isny, Germany). Each recording was
184 downsampled to 512 Hz, re-referenced to a common average montage and then bandpass
185 filtered between 0.1 and 96 Hz. Line noise at 50 Hz was removed by an additional linear filter
186 using the discrete Fourier transform. The vEOG recording was used to calibrate an adaptive
187 spatial filter that reflected individual eye blinks. These templates were used to inform the
188 removal of eye-blinks (Ille et al., 2002). The blink-free data was cut into epochs of -3 to +3 s
189 relative to S2 onset to investigate stimulus processing and working memory effects. To
190 examine decision-related activity, we alternatively epoched the data with respect to the
191 time of response on each trial. A final visual inspection of each individual trial ensured the
192 removal of artefactual and noisy trials (~16% of trials removed).

193 For time-frequency (TF) analysis, the Fourier transform of the epoched data was computed
194 separately for low (5-48Hz) and high (40-80Hz) parts of the frequency spectrum. For low

frequencies we used an adaptive sliding window of 5 cycles per frequency at 2 Hz steps and multiplied a Hann taper to the data prior to Fourier transformation (i.e., TF bin = 2 Hz x 25ms). For higher frequencies, we used a multitaper approach based on Slepian sequences with a fixed length of 200 ms at steps of 4 Hz (i.e., TF bin = 4 Hz x 25ms). All data analysis was performed using FieldTrip (Radboud University Nijmegen, Donders Institute; fieltriptoolbox.org) and SPM12 (Wellcome Department of Cognitive Neurology, London, UK; www.fil.ion.ucl.ac.uk/spm).

2.6. Statistical Analysis

The response-locked and S2-locked data were analyzed in analogy. In case of TF transformed data, response-locked TF maps were square root transformed and smoothed with a 3 Hz x 300 ms full width at half maximum Gaussian kernel, reducing between-subject variance (Kilner et al., 2005). To identify the difference between decisions (S2>S1 vs. S2<S1) we performed a general linear model (GLM) analysis with the factors “S2 more/less than S1” and “correct/incorrect” (2x2). Then, we contrasted the individual subject’s averages to map the difference between choices. These individual time courses or TF maps then underwent a cluster-based permutation test procedure (Maris and Oostenveld, 2007). The resulting test statistic identifies clusters of strong activity differences and corrects for the family-wise error (FWE) level over channel, time and when applicable also frequency ($p_{cluster}<0.05$). The analysis of S2-locked data followed the same procedure but included a baseline correction to the prestimulus fixation period (-.65 to -.15 s relative to S1 onset) instead of a square root transformation. The GLM factor in addition to correctness was in this case the parametric modulation of S1 coherence level at four levels [45% 55% 65% 75%], which was then zero-

mean contrasted [-1.5 -0.5 0.5 1.5]. Hence, the S2-locked contrast shows the parametric modulation of neural activity by the coherence level of S1.

2.7. Source Reconstruction

The scalp-level effects identified in the previous step were localized in the cortex using the individually recorded electrode positions for each participant and routines applying 3D source reconstruction with multiple sparse priors (MSP) provided by SPM12 (Friston et al., 2006). First, we constructed a forward model using an 8196-point cortical mesh of dipoles distributed perpendicular to a template brain's cortical surface. A three-shell Boundary Elements Method (BEM) EEG head model was used to compute the lead field. Source inversion of the forward model was computed using MSP (Friston et al.,2008) under group constraints (Litvak & Friston, 2008). This was done for each condition for the significant time-frequency window from sensor-level analysis. The source inverted 3D images of each condition were then contrasted in analogy to sensor space analysis and subsequently used for statistical analysis on the group level (cf. Litvak et al., 2011). Mass-univariate statistical testing resulted in significance tests for all voxels. For illustration purposes, we display the significant voxels of each analysis at $p<0.05$ (uncorrected), indicating the most likely sources of the FWE-corrected sensor level analysis. The above-threshold sources were attributed to anatomical landmarks by employing SPM anatomy toolbox (Eickhoff et al., 2005).

3. Results

3.1. Behavior

Overall, participants responded correctly in 78.5 (7.1) % of trials and with an average RT of 838 (29) ms across conditions (Table 1). A repeated-measures ANOVA of median RTs with the factors "difficulty" (±20% versus ±10% dot-motion coherence) and "sign" (S1>S2 versus S1<S2) identified behavioral differences arising from the tasks' difficulty and the direction of choice. We performed the same analysis on the logit-transformed proportion of correct responses, which was only modulated by the difficulty of the coherence comparison and not the sign. Thus, participants were overall faster when choosing S2<S1, independent of whether their choice was correct. To establish that this difference was not explained by the counterbalanced finger assignment across participants for either S1>S2 or S1<S2, we calculated between groups t-tests for reaction time and performance, which were not significant (RT: T(13)=1.37, p=0.19; PCR: T(13)=0.14, p=0.89). To exclude the possibility that different motion directions influenced behaviour, we compared performance between up- and downward motion (RT: T(27)=1.29, p=0.21; PCR: T(27)=0.98, p=0.34).

	Coherence level difference (S2-S1)				Difficulty effect	Sign effect	Interaction
	-20%	-10%	10%	20%	F(1, 27)	F(1, 27)	F(1, 27)
PCR (%)	86.3 (6.6)	70.7 (6.6)	71.7 (7.8)	85.15 (7.3)	242.4*, p<0.001	0.1, p=0.907	3.8, p=0.061
RT (ms)	805 (27)	837 (27)	855 (30)	834 (29)	8.1* p=0.008	35.1*, p<0.001	3.2, p=0.083

Table 1: Proportion of correct responses and reaction times for the physical coherence difference S2-S1. Mean values with SD are shown in the left part, the effects are the result of an ANOVA with difficulty and sign as factors. The analysis of difficulty compares the easy (±20) with hard (±10%) trials, the sign effect the positive (+10% and +20%) with the negative (-10% and -20%) coherence difference. As expected, participants were better and faster on easy trials. Interestingly, while participants performed equally on positive and negative trials, they were faster on negative trials (S2<S1). There was no interaction between difficulty and sign.

257 Furthermore, we tested whether volunteers performed better in those trials in which the
258 direction of both S1 and S2 was the same, compared to those where dot-motion was
259 different (RT: T(27)=0.13, p=0.90; PCR: T(2.79), p=0.009). Hence, while there were no
260 differences between stimulus directions, participants responded more often correct, but
261 equally fast, when both RDM stimuli had the same inherent motion.

262 Interestingly, we observed a pronounced time-order effect/error (contraction bias) that is
263 characteristic for sequential comparison tasks (see Fig.1B; Herding et al., 2016, 2017; Karim
264 et al.,2012; Ashourian & Loewenstein, 2011; Preuschhof et al., 2010; Woodrow, 1935;
265 Fechner, 1860). In particular, we observed an increase in correct S1<S2 choices with higher
266 S1 stimulus coherence, concurrent with an increase in correct S1>S2 choices with decreasing
267 S1 coherence. This pattern indicates that participants might compare S2 with a
268 representation of S1 that regressed to the mean of the stimulus set (S1'). To account for this
269 substantial effect on performance, we used a behavioral model that estimates the
270 subjectively perceived coherence difference (S2-S1'; SPCD) for each participant and all
271 choices (see Methods: Behavioral model).

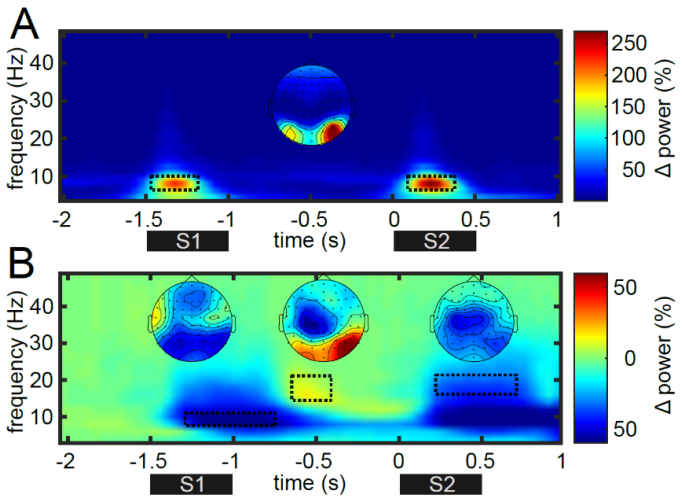

Figure 2: Stimulus-evoked and task induced time-frequency maps. (A) Grand average of relative change in stimulus-evoked power at 5-48Hz with respect to prestimulus baseline. Data is collapsed over all channels; the topography corresponds to the TF windows during stimulus presentation marked below. (B) Grand average of task induced power, expressed as the change in power to a prestimulus baseline. The topographies reflect the time-frequency window marked in the boxes below.

3.2. Overall stimulus responses

As a first EEG analysis step, we verified that our novel task design showed well-documented patterns in response to random-dot motion stimuli presentation. Figure 2A illustrates the TF representation of overall changes in stimulus-evoked power relative to a prestimulus baseline. Most notably, alpha (7-13 Hz) power increased after stimulus onset, most pronounced in right occipital channels. Grand-average induced power (Fig.2B) showed an established pattern of alpha power decreases after stimulus onset relative to the prestimulus baseline (e.g., de Lange et al., 2013; all $p_{FWE}<0.05$). Starting about 0.1 s after each stimulus onset, occipital channels showed this alpha decrease while dot-motion was onscreen, with a dimming of the effect after (e.g. 0.5-1 s after S1). While alpha power was decreased throughout the task, power in the lower beta band at 16-22 Hz first decreased during stimulus presentation but rebounded in right occipital channels after the RDM pattern disappeared (0.3 - 0.6 s after S1). Then, during the perception of S2 and the start of decision processes, we observed a decrease in beta power over contralateral (left) premotor

cortex, mimicking effects previously observed in the somatosensory SFC tasks (Herding et al., 2016) that fit with choice-related beta modulations associated with button presses (Donner et al., 2009; de Lange et al., 2013). This was particularly interesting, because beta band oscillations at 15-25 Hz are typically associated with sensorimotor processing (e.g., Bauer et al., 2006; van Ede et al., 2011; Pfurtscheller, 1981) and while we did not observe the same pattern as tactile comparison tasks elicit, our subsequent working memory and decision making effects mirrored somatosensory modulations in the beta band (Spitzer et al., 2010; Spitzer & Blankenburg, 2011, 2012; Herding et al., 2016, 2017; Ludwig et al., 2018; von Lautz et al., 2017), indicating a role for this frequency band beyond somatosensory processes.

3.3. Parametric working memory of S1 stimulus coherence

One of the central findings of previous somatosensory working memory M/EEG studies is the parametric modulation of oscillatory power in the beta band as a function of the vibrotactile frequency held in WM (Spitzer et al., 2010; von Lautz et al., 2017). Here, we focused on an analogous stimulus property – the level of dot-motion coherence. The TF map in Figure 3 depicts the parametric contrast of the four motion coherence levels (45%, 55%, 65%, 75%) during stimulus retention. The permutation test procedure identified a cluster from right prefrontal channels in the beta band (18-26Hz) that was modulated by the to-be-remembered stimulus coherence 0.4-0.8 s after S1 offset ($p_{FWE}<0.05$). Source reconstruction of this cluster with the same parametric constrast placed this effect in the bilateral inferior frontal gyrus (peak MNI: +42,+36,+14; Fig. 3C). Notably, the timecourse of this frontal beta band modulation (Fig 3D) showed an overall increase in ERS at the center of the working memory interval whose peak was monotonically greater for higher stimulus coherences held in working memory, as indicated by linear trend analysis (0.45-0.7s, all time bins $p<0.05$).

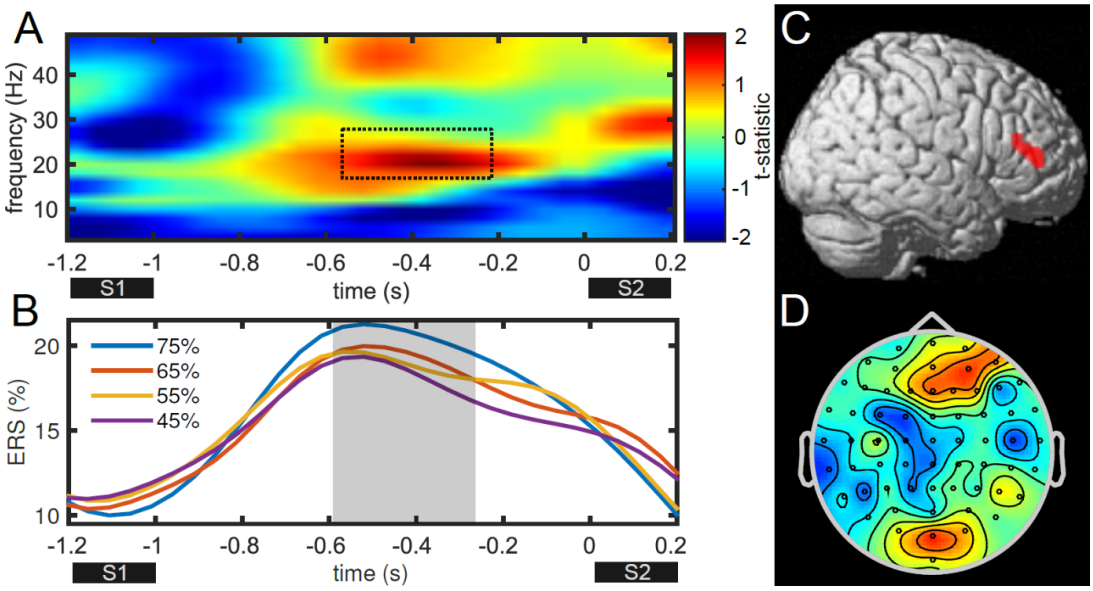

Figure 3: TF analysis and source reconstruction reveal parametric representation in right prefrontal beta band. (A) Time-frequency map of the zero-mean contrast of low to high coherence levels (45-75%) across channels F4 and AF4. (B) Time course of the average beta band per S1 coherence level during the retention interval. The grey mark depicts significant time points of linear trend analysis (p<0.05). (C) Source reconstruction of the beta band effect identified with nonparametric cluster analysis marked in A. The most likely source of this prefrontal effect was found in the right IFG. The red marking shows the thresholded 3D source (p<0.05, uncorrected). (D) Topography of the cluster identified in A, corresponding to the source reconstruction in C.

Exploratory analysis of higher frequencies (>48Hz) revealed a parametric modulation of gamma power at 55-65 Hz throughout the whole WM interval ($p_{FWE}<0.05$; Supplementary Figure 1A). Interestingly, while beta power increased with stimulus frequency, gamma power decreased. The source of this activity was localized to a large portion in the right inferior frontal gyrus (IFG; peak MNI: +52,+24,+0) (Supplementary Figure 1C). However, the analysis of the gamma band timecourse revealed that the highest coherence condition alone was mainly driving this effect (Supplementary Figure 1B).

Unexpectedly, we identified a cluster of centro-parietal channels whose lower beta power was modulated by S1 stimulus coherency ($p_{FWE}<0.05$, Supplementary Figure 1D). The timecourse of this effect (Supplementary Figure 1E) showed the same beta power peak as observed in higher beta frequencies (cf. Fig. 3D), however, displaying a monotonic decrease with higher stimulus coherence (linear trend 0-0.15 s and 0.5-0.65 s, at $p_{FWE}<0.05$). Source

reconstruction revealed bilateral area 4a of the primary motor cortex as the origin of this negative modulation (peak MNI: +4, -36, +66) and the precuneus (peak MNI: -16, -54,+68; Supplementary Figure 1F).

3.4. Beta band indexes subsequent choice

To investigate the oscillatory signatures underlying decision making we contrasted trials by participants' choices – S2 > S1 vs. S2 < S1. This analysis revealed a central cluster in frequencies of 20-30 Hz at 0.9-0.6 s before answering ($p_{FWE}<0.05$). The focal pattern in topography (Fig, 4 C) as well as source reconstruction (Fig. 4, B) pinpointed the location of this effecgt to bilateral (pre-) motor cortices (Area 4a, peak MNI: -6, -14, 72).

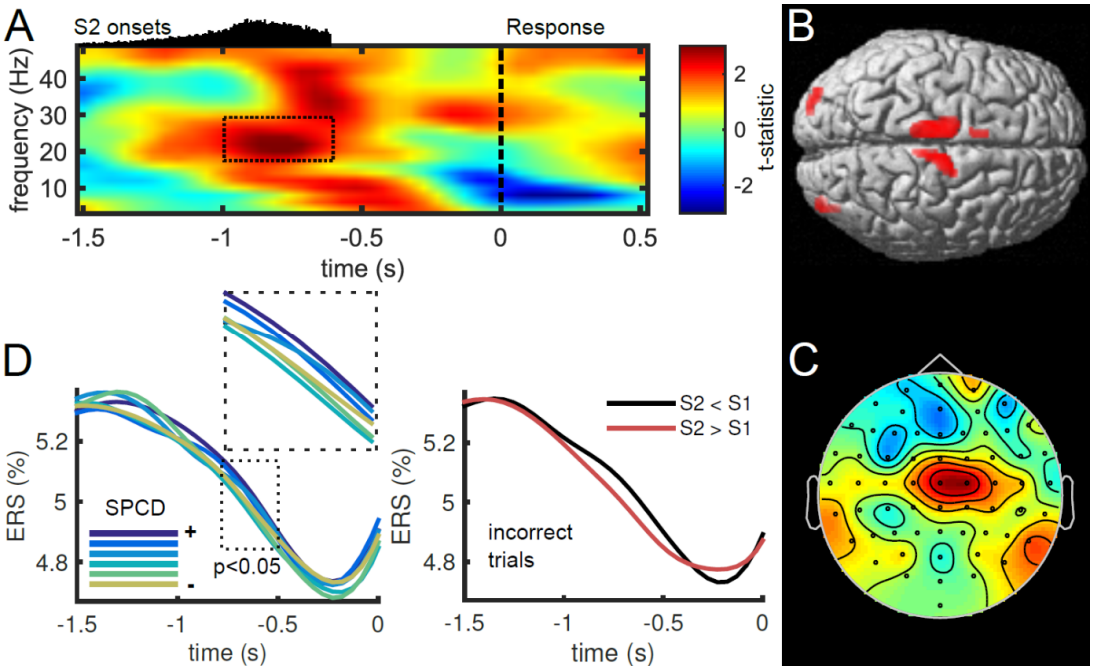

Figure 4: Choice-modulated power in upper beta band. (A) Time-frequency representation of response-locked power in t-values of choice contrast (S2>S1 vs. S2<S1) averaged over electrodes Cz and C2. Histogram above the TF map depicts the distribution of S2 onsets. Nonparametric cluster analysis revealed a modulation of the beta band by choice, marked here with the black box. (B) Result of 3D source reconstruction of the significant cluster marked in the time-frequency window in A. The effect was rendered on a T1 standard brain, red marks the areas of most likely sources, thresholded at p<0.05 uncorrected. (C) Topography of the central cluster marked by the box in A. (D) Left: Time course of beta band power from central channels grouped by the subjectively perceived coherence difference (SPCD) in six levels. Inset zooms into the significant time window, showing a binary split between higher and lower perceived coherence differences. Right: Time course of beta power as on the left for incorrect trials, split into S2 higher or lower than S1, and showing the opposite pattern (n.s.).

We applied our model of subjectively perceived coherence difference (SPCD) that accounts for the time-order effect on every trial to the analysis of the average central beta band time course. The resulting trials were binned in six groups, from perceiving much more coherency in S2 than S1 to the opposite. Figure 3B illustrates the beta band modulation by each separate SPCD bin, indicating a stronger central beta for S2>S1 trials 0.9-0.5 s before responding. If this beta band effect reflects subjects' choice, incorrect trials are expected to show the inverse pattern, because participants chose the opposite answer. Analysis of the average beta band time courses did indeed indicate this opposite pattern (Figure 4C), but was not significantly modulated, likely due to the small amount of incorrect choices.

3.5. Centro-parietal positivity

We used the subjectively perceived coherence differences (i.e. S2-S1') estimated for each trial as regressors for the analysis of stimulus- and response-locked epochs (Fig. 5, *top* and *bottom* respectively). Thus, we contrasted not only trials by participants' choice, but also by how difficult each choice was in turn.

A positive modulation of centro-parietal ERPs after S2 onset was clearly visible over a set of 17 electrodes marked in the scalp topography in Figure 5 ($p_{FWE}<0.001$), closely matching the classic P300 and typical CPP topographies. We collapsed analyses across both up- and downward motion as there was no influence on CPP amplitude, latency and topography (all $p>0.05$). In general, the CPP built up shortly after stimulus onset (0.2s) and flattened out immediately after stimulus offset (0.5 s).

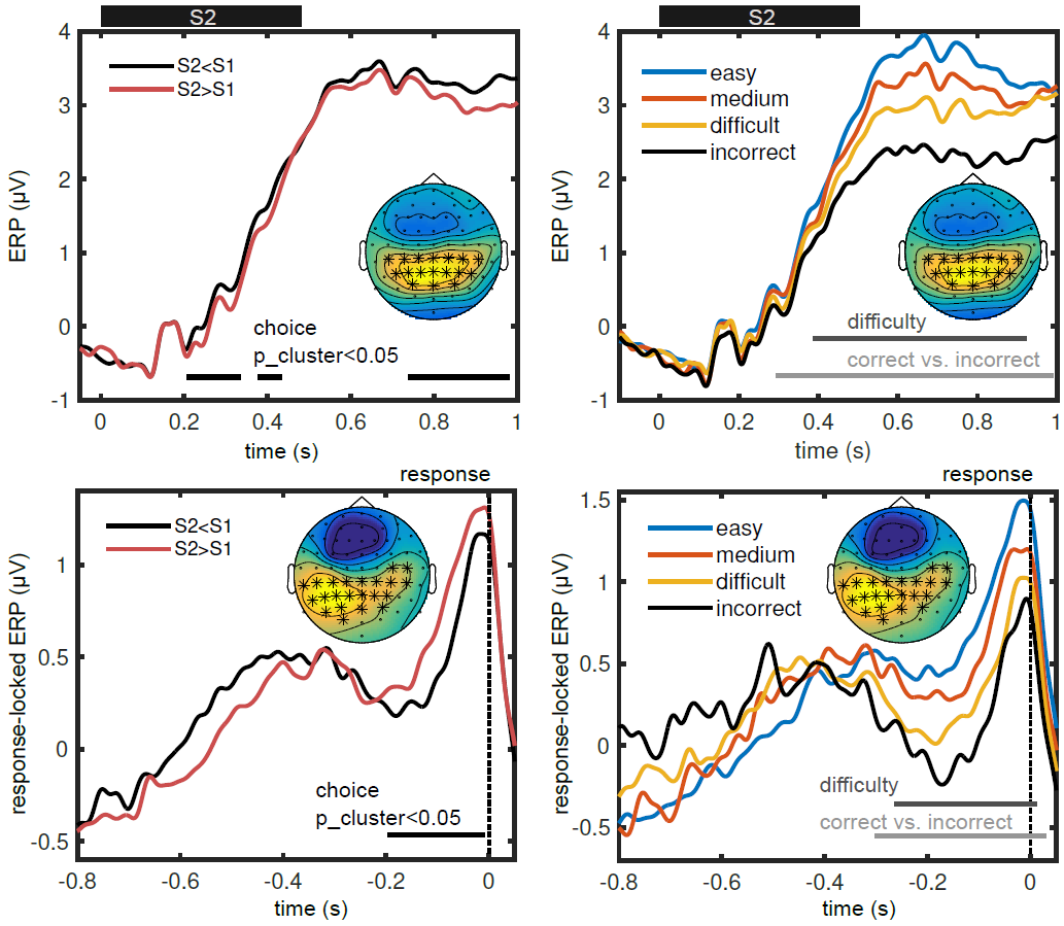

*Figure 5 Centro-parietal signal increases with perception of S2 and reaches maximum with response. Top: S2-locked broadband EEG response from channels marked in topography with *. The left part shows time courses of each possible choice, S2>S1 and S2<S1, the right part the modulation by model-based estimates of subjectively perceived coherence difference (SPCD), split into easy, medium, difficult and incorrect trials. Bottom: Same as in figures above, but for response-locked signals and channels from the positive cluster marked in the topography with *. Channels marked in topographies in all plots are those that were significantly modulated for more than 50% of time in significant time window ($p_{FWE}<0.05$). Black and grey lines show the significant time windows from the cluster-based permutation analysis for choice (left) and difficulty as well as of correct vs. incorrect trials respectively (right).*

Comparing choices of S2>S1 with S2<S1 revealed a modulation of the CPP between 0.2-0.4 s after S2 onset and a later, likely response related difference starting after 0.75s (thresholded at $p_{FWE}<0.05$, Fig.5, *top left*). The observation that responses of S2<S1 were slightly faster (see Table 1), may therefore be explained by faster CPP build-up. Subsequently, we split correct trials into subjectively perceived bins of 'easy', 'medium', and 'hard' trials with our behavioral model. The top right part of Figure 5 illustrates that the CPP increased in

proportion to the strength of S2-S1' coherence difference and correspondingly had a higher peak level (0.4-0.92s, $p_{FWE}<0.05$). We were interested, whether this pattern extended to incorrect trials, and found a slower build-up and lower peak CPP as early as 0.3s after stimulus onset when compared to the average correct response (threshold at $p_{FWE}<0.05$).

Analogous analysis of response-locked data revealed a build-up of centro-parietal signals from 22 channels that was most pronounced over left posterior parietal areas ($p_{FWE}<0.001$, Fig.5 topography, *bottom*). Contrary to S2-locked signals this accumulation of signal peaked with the response button press and dropped to baseline levels shortly after. Subjects' choices modulated this signal, with an increased CPP build-up for S2>S1 trials in the last 200 ms before responding ($p_{FWE}<0.05$). Split into bins of 'easy', 'medium' and 'hard' trials, we found a proportional CPP peak at response that scaled with difficulty and was reduced in incorrect trials (both thresholded at $p_{FWE}<0.05$).

To underline that these effects may represent a decision variable and not sensory evidence in the motion perception of RDM stimuli, we investigated the build-up of CPP relative to S2 stimulus coherence, as this could represent an accumulation of sensory evidence for the stimulus coherence level rather than the decision of S2-S1' observed previously. We constructed a parametric contrast of the eight levels (25%, 35%, …, 95%) of S2 coherence and tested this against zero with the same permutation test procedure as in previous analyses. This investigation did not indicate any effect of S2 stimulus coherence on the CPP time course (all clusters $p_{FWE}>0.05$). Since the S2 coherence is confounded with the difficulty of the task-relevant S2-S1 calculation, we also applied this analysis to the S1 coherence, again with no significant results (all clusters $p_{FWE}>0.05$). While not essential for the present study, these control analyses on our particular task give further evidence that the CPP may

reflect a true ‘decision variable’ that tracks decision-relevant evidence and not just sensory input.

4. Discussion

We investigated the neural processes underlying working memory and perceptual decisions using a sequential random-dot motion (RDM) coherence comparison task. We identified modulations of the beta band during the retention interval of the task and during the formation of a decision: first, in prefrontal areas, beta band power increased monotonically with the coherence level held in working memory. Second, in premotor and motor areas, participants' choices modulated beta power before responding by button press. Additionally, the CPP tracked the accumulation of decision-relevant evidence, reflecting the subjectively perceived coherence differences between the two RDM patches, indexing the trial difficulty. Our results suggest that inferior frontal (WM), posterior parietal (CPP), and motor regions (choice) work together to maintain and evaluate decision related stimulus features independent of sensory modality.

In remarkable agreement with previous reports of vibrotactile parametric working memory recorded with MEG, EEG, and fMRI in humans (von Lautz et al., 2017; Spitzer et al., 2010; Kostopoulos et al., 2007; Wu et al., 2018) and single-cell recordings in nonhuman primates (e.g., Romo et al., 1999), we observed a monotonic scaling of beta band power in the right IFG with the RDM coherence held in working memory. Moreover, the observed frequency range (18-26 Hz) and the precise location within the IFG matches results from a visual flicker frequency task more closely than similar tactile or auditory recordings (see Spitzer & Blankenburg, 2012; Wu et al., 2018). In particular, a recent fMRI decoding study employing an SFC task across sensory modalities found WM content-specific activity in the right IFG for both visual and tactile working memory (Wu et al., 2018). Interestingly, in an exploratory analysis we observed a concurrent decrease of prefrontal gamma power with the coherence

440 retained in working memory (supplementary Figure 1E-H). This pattern of beta and gamma
441 power was also recently observed with MEG (von Lautz et al., 2017) and is a known correlate
442 of WM (Fuentemilla et al., 2010; Haegens et al., 2010). In contrast to MEG however, EEG
443 may be ill-suited for investigations of high gamma frequencies, because the skull acts as a
444 low-pass filter (Nunez, 1981). Moreover, the observed decrease appeared to be mostly
445 driven by the lowest S1 coherence level alone and may therefore not be as reliable as
446 previous MEG recordings. Together, our findings provide further evidence for a modality
447 independent role of prefrontal beta oscillations for parametric working memory that may be
448 a feature of passive maintenance states interrupted by brief gamma bursts as observed
449 recently during monkey recordings (Lundqvist et al., 2016; Sherman et al., 2016; Stokes,
450 2015).

451 In sequential comparison tasks, it is assumed that decisions are the result of mentally
452 calculating stimulus 2 – stimulus 1. Choice-related neural activity is expected to reflect the
453 resulting sign (+/-) of this subtraction. Fitting with this notion, we found a modulation of
454 beta oscillatory power by choice in central regions associated with the response-button
455 press, for which source reconstruction estimated premotor and motor regions as the most
456 likely sources. This supports the idea that that neural responses of decision processes are
457 exhibited in those parts of the brain where subsequent responses are put into action
458 (Shadlen et al., 2008). Our findings agree with vibrotactile comparison tasks in both non-
459 human primates and humans (Haegens et al., 2011; Herding et al., 2016; Ludwig et al.,
460 2018), where power in the upper beta band from bilateral pre-motor areas was modulated
461 by subjects' choices before responding. Remarkedly, the same pattern appears to be
462 response-modality specific, as Herding and colleagues (2016, 2017) had participants respond
463 by either button press or saccades and found distinct sources of this effect in premotor areas

464 and FEF, respectively. Moreover, firing rate changes reflecting the signed difference between
465 vibrotactile frequencies, f2-f1, have been recorded in medial and ventral PMC when
466 monkeys responded by button press (Hernández et al., 2002, 2010; Romo et al., 2004).
467 Crucially, these studies all used vibrotactile stimuli. In contrast, our present results are the
468 first to demonstrate choice encoding in the beta band from motor areas for a visual
469 sequential comparison task.

470 Interestingly, recordings during sequential comparisons of visual RDM stimuli have been
471 made in monkey lPFC, where firing rates reflect task-relevant sensory, memory and decision
472 processes (Zaksas & Pasternak, 2006; Hussar & Pasternak, 2012, 2013). Additionally,
473 Wimmer et al., (2016) analyzed LFPs during the same task and found that beta power
474 encoded the task-relevant S1 feature during the working memory delay, matching the
475 present findings (Fig. 3). Moreover, broadband LFP activity reflected the difference between
476 S2 and S1, first in proportion to the stimulus difference (S2-S1), then as an index of choice.
477 While not in the same area, these effects are similar to previous sensorimotor LFP recordings
478 during a vibrotactile version (Haegens et al., 2011) and have been theorized to communicate
479 in a top-down fashion with MT and motor areas in a hierarchical network (Wimmer et al.,
480 2015). Agreeing with this idea, we speculate that the present findings complement previous
481 single-cell recordings by showing the analogous modulatory effects in synchronized neuronal
482 population activity.

483 Our findings in the beta band also provide further evidence for a generalized, supramodal
484 role for the beta band in encoding task-relevant quantitative information (Spitzer et al.,
485 2014; Spitzer & Blankenburg, 2012; Herding et al., 2016). In this view (for review, see Spitzer
486 & Haegens, 2017), beta band amplitude may reflect quantities at different times of such

487 comparison tasks in distinct brain areas, i.e. lPFC during parametric coherence level
488 retention (Barak et al., 2010; Brody et al., 2003; Romo et al., 1999) and PMC during decision
489 making (Haegens et al., 2011; Herding et al., 2016; Hernández et al., 2002), as a dynamic,
490 short-lived brain state for endogenous information processing. Additionally, in a recent EEG
491 study using an SFC task with delayed decision reports, Ludwig et al. (2018) demonstrated
492 that premotor beta power only indexed choices when a specific motor mapping was
493 provided during the decision delay, thereby further extending this view to necessitate
494 immediate task-relevance of the encoded choice. In the present design, both working
495 memory and decision information were immediately pertinent to the task, as the retention
496 interval was short with one second and the decision was not delayed, but responses given
497 immediately. Therefore, our task is suitable to investigate whether we can extend our
498 understanding of this quantity- and choice-related signal to the visual domain, providing
499 evidence for a common quantitative task-relevant code in the beta band irrespective of
500 sensory modality. Additionally, the decision variable reflected the calculation of S2-S1 and
501 not the accumulation of evidence for a particular motion direction directly, as in the typical
502 RDM paradigm. We therefore speculate that when applying the present task to recordings in
503 nonhuman primates, we may be able to separate the sensory and perceptual aspects of
504 decision making and relate them to the functioning of MT and LIP/VIP neurons (cf. Huk et al.,
505 2017; Katz et al., 2016). Such recordings may also serve to better understand the association
506 of beta amplitude and decision accuracy, as previous MEG recordings have indicated that
507 beta may reflect the accuracy and not the content of upcoming perceptual reports (Donner
508 et al., 2007), for which we found no evidence here.

509 Complementing these oscillatory changes, a number of recent studies have suggested that
510 the CPP - a broadband signal in the human EEG - tracks the accumulated evidence for

perceptual decisions that require sequentially sampling and integrating input over time (Kelly & O'Connell, 2013; Philiastides et al., 2014; Twomey et al., 2015). This activity may directly reflect known single-cell firing variability in the PPC with an accumulation of evidence in the form of a decision variable (for review, see Gold & Shadlen, 2007; Shadlen & Kiani, 2013). The present findings agree with these earlier reports of the CPP and extend the view of the CPP as a token of the current state of decision making. Exceptionally, in our novel task the tracking of the CPP represented not the accumulation of evidence for a certain coherence level or direction, but embodied the imminent decision process, i.e., evidence accumulation for the difference between S1 and S2. Furthermore, we observed a scaling of the CPP with respect to the subjectively perceived coherence difference, and thus the difficulty of the trials. This in turn may indicate that the peak of the CPP (or P300) is related to a participants' confidence in the decision, as previously observed in RDM paradigms with other electrophysiological or neuroimaging methods (Hebart et al., 2016; Kiani & Shadlen, 2009; Ding & Gold, 2012).

Interestingly, we encountered no absolute bound of CPP at the time of the response, as has been observed in recent studies with RDM patches (O'Connell et al., 2012; Kelly & O'Connell, 2013). On the contrary, our investigations agree with findings from face/house decision tasks, where scalp potentials appear to be parametrically scaled by the amount of sensory evidence at the time of choice (Philiastides et al., 2014). Our observations can be explained by a diffusion-to-bound model with collapsing bounds (for an overview, see O'Connell et al., 2018), where the amount of sensory evidence as indexed by the CPP required for a decision decreases over time and is therefore lower for the more difficult, slower trials at the time of response. However, we did not observe a more gradual build-up of CPP for more difficult trials, but rather a small decrease in CPP 200 ms before the participant responded.

Therefore, the CPP appears not to index the accumulation of evidence for a single stimulus direction as in classic RDM paradigms, but the difference in coherence between two of them. Indeed, it may be that the lagged build-up is also a feature of a sensory process in RDM tasks, as this effect was also not observed in a face/house distinction task (cf. Philiastides et al., 2014). To fully understand what the CPP represents, the relation between the CPP in a comparison task and its counterpart with a single RDM stimulus should be investigated directly, and differences and common components (e.g., with cross-classification) investigated.

In conclusion, beta power scaled parametrically with the random dot motion coherence in right prefrontal areas during stimulus retention, then indexed the choice before responding. These effects mirror findings from the well-studied vibrotactile domain with human M/EEG and single-cell recordings in nonhuman primates. Moreover, the CPP accrued before responding and was influenced by the subjectively perceived difficulty on each trial. Notably, the CPP was not affected by RDM motion perception, but changed with the task of comparing two stimuli, indicating a close relationship to the decision variable. The present findings are a first step to unite major lines of decision making paradigms across sensory domains, with findings pointing to an extended role for the beta band during working memory and decision making and to further insights into the CPP as an index of evidence accumulation.

Acknowledgements

The authors thank Laurence Hunt, Maria Rüsseler and Timo Schmidt for helpful suggestions.

Funding

This work was supported by Deutscher Akademischer Austauschdienst and the German Research Foundation (DFG Grant GRK1589/2).

Conflict of interest

None

References

Ashourian P., Loewenstein Y. (2011). Bayesian inference underlies the contraction bias in delayed comparison tasks. PLoS One, 6, e19551.

Bauer, M., Oostenveld, R., Peeters, M., & Fries, P. (2006). Tactile spatial attention enhances gamma-band activity in somatosensory cortex and reduces low-frequency activity in parieto-occipital areas. Journal of Neuroscience, 26, 490–501.

Barak, O., Tsodyks, M., and Romo, R. (2010). Neuronal population coding of parametric working memory. J. Neurosci. 30, 9424–9430. doi: 10.1523/JNEUROSCI.1875-10.2010

Brainard, D. H. (1997). The psychophysics toolbox. Spat. Vis. 10, 433–436. doi: 10.1163/156856897X00357

Brody, C. D., Hernández, A., Zainos, A., and Romo, R. (2003). Timing and neural encoding of somatosensory parametric working memory in macaque prefrontal cortex. Cereb. Cortex 13, 1196–1207. doi: 10.1093/cercor/bhg100

Buchholz, V. N., Jensen, O., and Medendorp, W. P. (2014). Different roles of alpha and beta band oscillations in anticipatory sensorimotor gating. Front. Hum. Neurosci. 8:446. doi: 10.3389/fnhum.2014.00446

Daunizeau, J., Adam, V., & Rigoux, L. (2014). VBA: A probabilistic treatment of nonlinear models for neurobiological and behavioural data. PLoS Computational Biology, 10, e1003441.

H. van Dijk, J.M. Schoffelen, R. Oostenveld, O. Jensen (2008). Prestimulus oscillatory activity in the alpha band predicts visual discrimination abilityJ. Neurosci., 28 (2008), pp. 1816-1823

Ding L, Gold JI. 2012. Neural correlates of perceptual decision makingbefore, during, and after decision commitment in monkey frontaleyefield. Cereb Cortex. 22:1052–1067.

Ditterich J, Mazurek ME, Shadlen MN (2003). Microstimulation of visual cortex affects the speed of perceptual decisions. Nat Neurosci. 6:891–898.

Donner TH, Siegel M, Fries P, Engel AK (2009). Buildup of choice-predictive activity in human motor cortex during perceptual decisionmaking. Curr Biol 19:1581–1585.

Donner TH, Siegel M, Oostenveld R, Fries P, Bauer M, Engel AK (2007). Population activity in the human dorsal pathway predicts the accuracy of visual motion detection. J. Neurophysiol., 98, pp. 345-359

Van Ede, F., de Lange, F., Jensen, O., & Maris, E. (2011). Orienting attention to an upcoming tactile event involves a spatially and temporally specific modulation of sensorimotor alpha- and beta-band oscillations. Journal of Neuroscience, 31, 2016–2024.

Eickhoff, S. B., Stephan, K. E., Mohlberg, H., Grefkes, C., Fink, G. R., Amunts, K., et al. (2005). A new SPM toolbox for combining probabilistic cytoarchitectonic maps and functional imaging data. Neuroimage 25, 1325–1335. doi: 10.1016/j.neuroimage.2004.12.034

597 Fuentemilla, L., Penny, W. D., Cashdollar, N., Bunzeck, N., and Duzel, E. (2010). Theta-coupled
598 periodic replay in working memory. Curr. Biol. 20, 606–612. doi: 10.1016/j.cub.2010.01.057

599 Litvak, V., Mattout, J., Kiebel, S., Phillips, C., Henson, R., Kilner, J., (2011). EEG and MEG data analysis
600 in SPM8. Computational Intelligence and Neuroscience, 2011, 852961.

601 Fechner, G. T. (1860). Elemente der Psychophysik. Leipzig: Breitkopf & Härtel.

602 Friston, K., Harrison, L., Daunizeau, J., Kiebel, S., Phillips, C., Trujillo-Barreto, N., (2008). Multiple
603 sparse priors for the M/EEG inverse problem. Neuroimage, 39, 1104–1120.

604 Friston K, Henson R, Phillips C, Mattout (2006) Bayesian estimation of evoked and induced responses.
605 JHum Brain Mapp. Sep; 27(9):722-35.

606 Gold JI, & Shadlen MN (2007). The neural basis of decision making. Annual Review of
607 Neuroscience,30, 535-574.

608 Haegens S, Nácher V, Hernández A, Luna R, Jensen O, Romo R (2011). Beta oscillations in the monkey
609 sensorimotor network reflect somatosensory decision making. *PNAS* 108:10708–10713.

610 Haegens, S., Osipova, D., Oostenveld, R., and Jensen, O. (2010). Somatosensory working memory
611 performance in humans depends on both engagement and disengagement of regions in a distributed
612 network. Hum. Brain Mapp. 31, 26–35. doi: 10.1002/hbm.20842

613 Hämäläinen, Matti & Hari, Riitta & Ilmoniemi, Risto J. & Knuutila, Jukka & Lounasmaa,Olli V.. 1993.
614 Magnetoencephalography—theory, instrumentation, and applications tononinvasive studies of the
615 working human brain. Reviews of Modern Physics. Volume65, Issue 2. 413-497. ISSN 0034-6861
616 (printed). DOI: 10.1103/revmodphys.65.413.

617 S. Hanslmayr, A. Aslan, T. Staudigl, W. Klimesch, C.S. Herrmann, K.H. BaumlPrestimulus oscillations
618 predict visual perception performance between and within subjectsNeuroimage, 37 (2007), pp. 1465-
619 1473

620 Hebart MN, DonnerTH, Haynes J-D (2012). Human visual and parietal cortex encode visual choices
621 independent of motor plans. Neuroimage. 63:1393–1403.

622 Hebart MN, Schriever Y, Donner TH, Haynes J-D (2016). The relationship between perceptual decision
623 variables and confidence in the human brain. Cereb. Cortex 26,118–130

624 Heekeren, H. R., Marrett, S., and Ungerleider, L. G. (2008). The neural systems that mediate human
625 perceptual decision making. Nat. Rev. Neurosci. 9, 467–479. doi: 10.1038/nrn2374

626 Hellström Å. (2003). Comparison is not just subtraction: effects of time- and space-order on
627 subjective stimulus difference. Percept Psychophys 65:1161–1177.

628 Hellström Å. (1985). The time-order error and its relatives: Mirrors of cognitive processes in
629 comparing. Psychol Bull 97:35–61.

630 Herding J, Ludwig S, Blankenburg F (2017) Response-modality-specific encoding of human choices in
631 upper beta-band oscillations during vibrotactile comparisons. Frontiers in Human Neuroscience
632 11.

633 Herding J, Spitzer B, Blankenburg F (2016). Upper Beta Band Oscillations in Human Premotor Cortex
634 Encode Subjective Choices in a Vibrotactile Comparison Task. *Journal of Cognitive Neuroscience,* 1–
635 12.

636 Hernández, A., Nácher, V., Luna, R., Zainos, A., Lemus, L., Alvarez, M., (2010). Decoding a perceptual
637 decision process across cortex. Neuron, 66, 300–314.

638 Hernández, A., Zainos, A., & Romo, R. (2002). Temporal evolution of a decision-making process in
639 medial premotor cortex. Neuron, 33, 959–972.

640 Horwitz, G. D., and Newsome, W. T. (1999). Separate signals for target selection and movement
641 specification in the superior colliculus. Science 284, 1158–1161. doi: 10.1126/science.284.5417.1158

642 Huk, A. C., Katz, L. N. & Yates, J. L. The Role of the lateral intraparietal area in (the study of) decision
643 making. Annu Rev Neurosci. 40, 349–372 (2017).

644 Ille N., Berg P., Scherg M. (2002). Artifact correction of the ongoing EEG using spatial filters based on
645 artifact and brain signal topographies. J. Clin. Neurophysiol. 19 113–124. 10.1097/00004691-
646 200203000-00002

647 Karim M., Harris J. A., Morley J. W., Breakspear M. (2012). Prior and present evidence: How prior
648 experience interacts with present information in a perceptual decision making task. PLoS One, 7,
649 e37580.

650 Katz, L., Yates, J., Pillow, J. W., and Huk, A. (2016). Dissociated functional significance of choice-
651 related activity across the primate dorsal stream. *Nature* 535, 285–288. doi: 10.1038/nature18617

652 Kelly, S. P., and O'Connell, R. G. (2013). Internal and external influences on the rate of sensory
653 evidence accumulation in the human brain. J. Neurosci. 33, 19434–19441. doi:
654 10.1523/JNEUROSCI.3355-13.2013

655 van Kemenade BM, Seymour K, Wacker E, Spitzer B, Blankenburg F, Sterzer P (2014). Tactile and
656 visual motion direction processing in hMT+/V5. NeuroImage, 84, pp. 420-427

657 Kiani R, Shadlen MN (2009). Representation of confidence associated with a decision by neurons in
658 the parietal Cortex. Science. 324:759–764.

659 Kilner, J. M., Kiebel, S. J., and Friston, K. J. (2005). Applications of random field theory to
660 electrophysiology. Neurosci. Lett. 374, 174–178. doi: 10.1016/j.neulet.2004.10.052

661 Kim J. N., Shadlen M. N. (1999). Neural correlates of a decision in the dorsolateral prefrontal cortex
662 of the macaque. *Nat. Neurosci.* 2 176–185. 10.1038/5739

663 Kostopoulos, P., Albanese, M. C., and Petrides, M. (2007). Ventrolateral prefrontal cortex and tactile
664 memory disambiguation in the human brain. Proc. Natl. Acad. Sci. U.S.A. 104, 10223–10228. doi:
665 10.1073/pnas.0700253104

666 Krebber, M., Harwood, J., Spitzer, B., Keil, J., Senkowski, D. (2015). Visuotactile motion
667 congruence enhances gamma-band activity in visual and somatosensory cortices.
668 Neuroimage, 117, 160-169.

669 de Lange FP, Rahnev DA, Donner TH, Lau H (2013) Prestimulus oscillatory activity over motor cortex
670 reflects perceptual expectations. The Journal of Neuroscience. 33: 1400-10. PMID 23345216 DOI:
671 10.1523/JNEUROSCI.1094-12.2013

672 von Lautz AH, Herding J, Ludwig S, Nierhaus T, Maess B, Villringer A, Blankenburg F (2017). Gamma
673 and Beta Oscillations in Human MEG Encode the Contents of Vibrotactile Working Memory. *Frontiers*
674 *Human Neuroscience* 11:576.doi: 10.3389/fnhum.2017.00576

675 Litvak, V., & Friston, K. (2008). Electromagnetic source reconstruction for group studies. Neuroimage,
676 42, 1490–1498.

677 Litvak, V., Mattout, J., Kiebel, S., Phillips, C., Henson, R., Kilner, J., (2011). EEG and MEG data analysis
678 in SPM8. Computational Intelligence and Neuroscience, 2011, 852961.

679 Ludwig S, Herding J, Blankenburg F. (2018). Oscillatory EEG signatures of postponed somatosensory
680 decisions. Hum Brain Mapp. 1–14. https://doi.org/10.1002/hbm.24198

681 Lundqvist, M., Rose, J., Herman, P., Brincat, S. L., Buschman, T. J., and Miller, E. K. (2016). Gamma
682 and beta bursts underlie working memory. Neuron 90, 152–164. doi: 10.1016/j.neuron.2016.02.028

683 Maris E, Oostenveld R, (2007). Nonparametric statistical testing of EEG- and MEG-data. J. Neurosci.
684 Method 164, 177–190. doi: 10.1016/j.jneumeth.2007.03.024

685 Wang XJ, (2012). Neural dynamics and circuit mechanisms of decision-making. Curr Opin Neurobiol
686 22:1039–1046. 10.1016/j.conb.2012.08.006

687 Newsome, W. T., Britten, K. H. & Movshon, J. A. Neuronal correlates of a perceptual decision. Nature
688 341, 52–54 (1989)

689 Nunez, P. L. (1981) Electric fields of the brain: The neurophysics of EEG. Oxford University Press.

690 O'Connell RG, Dockree PM, Kelly SP (2012). A supramodal accumulation-to-bound signal that
691 determines perceptual decisions in humans. Nat Neurosci 15:1729–1735

692 O'Connell, R. G., Shadlen, M. N., Wong-Lin, K. & Kelly, S. P. (2018). Bridging Neural and
693 Computational Viewpoints on Perceptual Decision-Making. Trends Neurosci.
694 doi:10.1016/j.tins.2018.06.005

695 Pfurtscheller, G. (1981). Central beta rhythm during sensorimotor activities in man.
696 Electroencephalography and Clinical Neurophysiology, 51, 253–264.

697 Pfurtscheller G, Lopes da Silva FH (1999). Event-related EEG/MEG synchronization and
698 desynchronization: basic principles Clin. Neurophysiol. 110 1842–57

699 Philiastides, M., Heekeren, H. R., Sajda, P. (2014). Human Scalp Potentials Reflect a Mixture of
700 Decision-Related Signals during Perceptual Choices. The Journal of Neuroscience, 34(50), 16877-
701 16889; doi: 10.1523/JNEUROSCI.3012-14.2014.

702 Preuschhof, C., Schubert, T., Villringer, A., & Heekeren, H. R. (2010). Prior information biases stimulus
703 representations during vibrotactile decision making. Journal of Cognitive Neuroscience, 22, 875–887.

704 Ratcliff R, Cherian A, Segraves M. (2003) A comparison of macaque behavior and superior colliculus
705 neuronal activity to predictions from models of simple two-choice decisions. Journal of
706 Neurophysiology. 90:1392–1407.

707 Romo, R., Brody, C. D., Hernández, A., & Lemus, L. (1999). Neuronal correlates of parametric working
708 memory in the prefrontal cortex. *Nature,* 399(6735), 470–473.

709 Romo, R., and de Lafuente, V. (2013). Conversion of sensory signals into perceptual decisions. Prog.
710 Neurobiol. 103, 41–75. doi: 10.1016/j.pneurobio.2012.03.007

711 Romo, R., Hernández, A., & Zainos, A. (2004). Neuronal correlates of a perceptual decision in ventral
712 premotor cortex. Neuron, 41, 165–173.

713 Sanchez, G. (2014). Real-time electrophysiology in cognitive neuroscience: Towards adaptive
714 paradigms to study perceptual learning and decision making in humans. PhD thesis, Université
715 Claude Bernard Lyon 1, France.

716 Shadlen MN, Kiani R (2013). Decision making as a window on cognition. Neuron 80:791–806.

717 Shadlen MN, Kiani R, Hanks TD, Churchland AK (2008). Neurobiology of decision making: An
718 intentional framework. In C. Engel & W. Singer (Eds.), Strüngmann Forum reports. Better than
719 conscious? Decision making, the human mind, and implications for institutions (pp. 71-101).
720 Cambridge, MA, US: MIT Press.

721 Shadlen MN, Britten KH, Newsome WT, Movshon JA (1996): A computational analysis of the
722 relationship between neuronal and behavioral responses to visual motion. J Neurosci. 16:1486–1510.

723 Shadlen MN, Newsome WT (2001) Neural basis of a perceptual decision in the parietal cortex (area
724 LIP) of the rhesus monkey. J Neurophysiol. 86:1916–1936

725 Sherman M. A., Lee S., Law R., Haegens S., Thorn C. A., Hämäläinen M. S., et al. (2016). Neural
726 mechanisms of transient neocortical beta rhythms: converging evidence from humans,
727 computational modeling, monkeys, and mice. PNAS 113 E4885–E4894. 10.1073/pnas.1604135113

728 Siegel M, Buschman TJ, Miller EK (2015) Cortical information flow duringflexible sensorimotor
729 decisions. Science 348:1352–1355.

730 Siegel M., Donner T. H., Oostenveld R., Fries P., Engel A. K. (2008). Neuronal synchronization along
731 the dorsal visual pathway reflects the focus of spatial attention. Neuron 60, 709–
732 71910.1016/j.neuron.2008.09.010

733 Spitzer, B., & Blankenburg, F. (2011). Stimulus-dependent EEG activity reflects internal updating of
734 tactile working memory in humans. Proceedings of the National Academy of Sciences, U.S.A., 108,
735 8444–8449.

736 Spitzer, B., and Blankenburg, F. (2012). Supramodal parametric working memory processing in
737 humans. J. Neurosci. 32, 3287–3295. doi: 10.1523/JNEUROSCI.5280-11.2012

738 Spitzer, B., Gloel, M., Schmidt, T. T., & Blankenburg, F. (2014). Working memory coding of analog
739 stimulus properties in the human prefrontal cortex. Cerebral Cortex, 24, 2229–2236.

740 Spitzer B, Haegens S (2017). Beyond the status quo: A role for beta oscillations in endogenous
741 content (re)activation. eNeuro 4:ENEURO.0170-17.2017.

742 Spitzer, B., Wacker, E., & Blankenburg, F. (2010). Oscillatory correlates of vibrotactile frequency
743 processing in human working memory. Journal of Neuroscience, 30, 4496–4502.

744 Stokes, M. G. (2015). 'Activity-silent' working memory in prefrontal cortex: a dynamic coding
745 framework. Trends Cogn. Sci. 19, 394–405. doi: 10.1016/j.tics.2015.05.004

746 Thut G, Nietzel A, Brandt SA, Pascual-Leone A, (2006). Alpha-band electroencephalographic activity
747 over occipital cortex indexes visuospatial attention bias and predicts visual target detectionJ.
748 Neurosci., 26, pp. 9494-9502

749 Twomey DM, Murphy PR, Kelly SP, O'Connell RG, (2015). The classic P300 encodes a build-to-
750 threshold decision variable. Eur J Neurosci42:1636–1643

751 Urai AE, Braun A, Donner TH (2017). "Pupil-linked arousal is driven by decision uncertainty and alters
752 serial choice bias." Nature communications 8, 14637

753 Wang XJ. (2012) Neural dynamics and circuit mechanisms of decision-making. Curr Opin Neurobiol
754 22:1039–1046. 10.1016/j.conb.2012.08.006

755 Wimmer K, Ramon M, Pasternak T, Compte A (2016). "Transitions between Multiband Oscillatory
756 Patterns Characterize Memory-Guided Perceptual Decisions in Prefrontal Circuits." The Journal of
757 neuroscience. 13; 36(2):489-505.

758 Woodrow, H. (1935). The effect of practice upon time-order errors in the comparison of temporal
759 intervals. Psychological Review, 42, 127–152.

760 Wu Y, Uluç I, Schmidt TT, Tertel K, Kirilina E, Blankenburg F (2018). Overlapping frontoparietal
761 networks for tactile and visual parametric working memory representations. NeuroImage 166, 325-
762 334

Supplementary figure

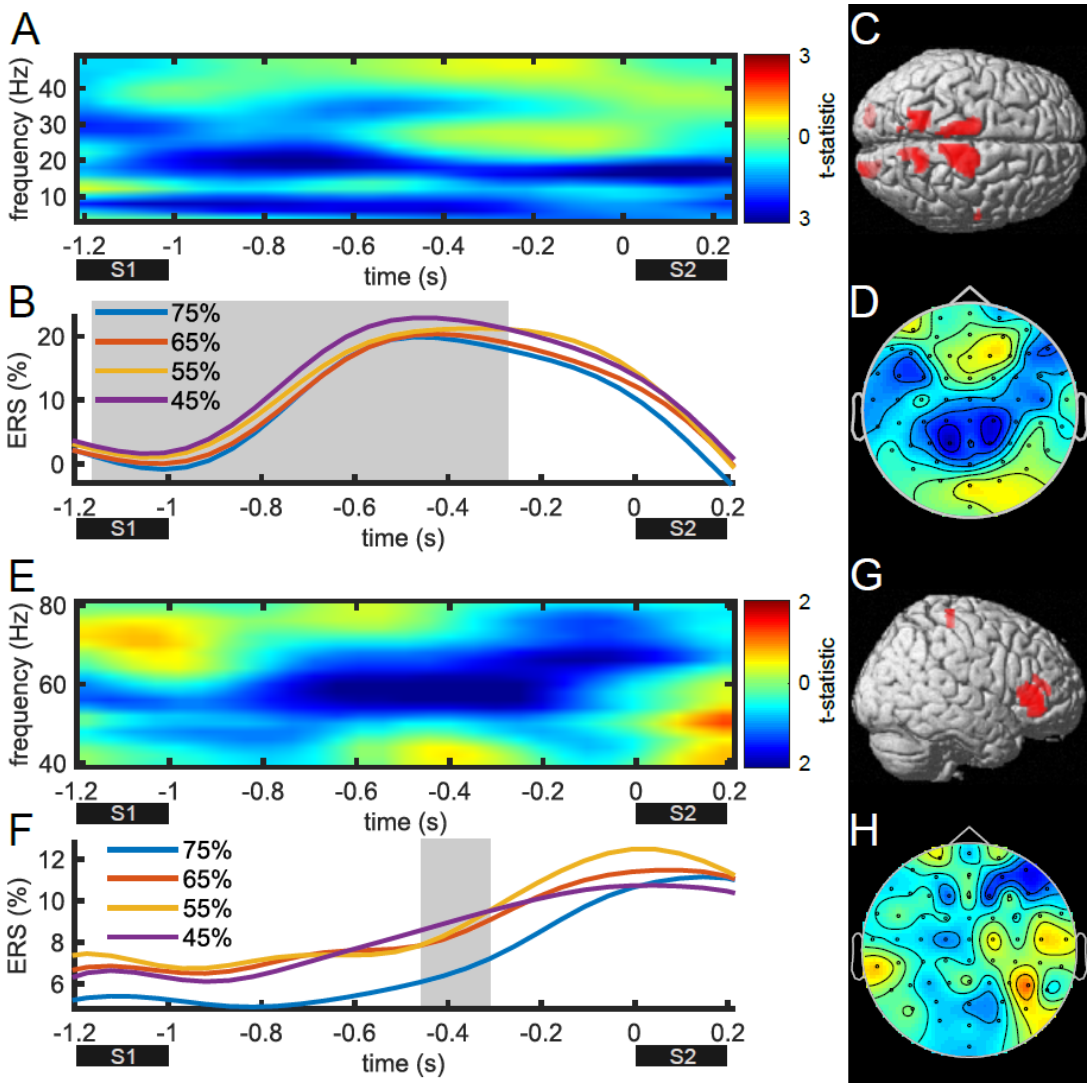

Supplementary Figure 1: Parametric working memory in low central beta and in prefrontal gamma. (A-D) Negative modulation of central low beta power throughout perception of S2 and working memory. (A) Time-frequency map of zero-mean contrast of S1 coherence level (45-75%). (B) Timecourse of low beta power (16-22Hz) for each S1 coherence level, grey area marks significant time points (p_FWE<0.05). (C) Source reconstruction of significant time-frequency window, 3D rendered on a standard brain with red marking of threshholded effect at p<0.05, uncorrected. (D) Topography of negative cluster, the same as used for C. (E-H) Negative modulation of prefrontal low beta power during working memory, same as in A-D.

5 Anlagen

Anlage A – Lebenslauf

2014 - 2018	**PhD Student** Bernstein Center for Computational Neuroscience, Charité Berlin, Neurocomputation and Neuroimaging Unit (NNU), Freie Universität Berlin
2012 - 2014	**Master Student** Cognitive Neuroscience, Donders Institute for Brain and Cognition, Radboud University Nijmengen Oxford Centre for Human Brain Activity, Warneford Hospital, Oxford
2008 - 2012	**Bachelor Student** Institute of Psychology, Saarland University

Anlage B –Eidesstattliche Erklärung

Hiermit erkläre ich an Eides statt,

- dass ich die vorliegende Arbeit eigenständig und ohne unerlaubte Hilfe verfasst habe,
- dass Ideen und Gedanken aus Arbeiten anderer entsprechend gekennzeichnet wurden,
- dass ich mich nicht bereits anderwärtig um einen Doktorgrad beworben habe und keinen Doktorgrad in dem Promotionsfach Psychologie besitze, sowie
- dass ich die zugrundeliegende Promotionsordnung vom 08.08.2016 anerkenne.

Ort, Datum Unterschrift

Anlage C

Erklärung gemäß § 7 Abs. 3 Satz 4 der Promotionsordnung über den Eigenanteil an den veröffentlichten oder zur Veröffentlichung vorgesehenen eingereichten wissenschaftlichen Schriften im Rahmen meiner publikationsbasierten Arbeit

I.

Name, Vorname:	von Lautz, Alexander Horst
Institut:	Arbeitsbereich Neurocomputation and Neuroimaging
Promotionsfach:	Psychologie
Titel:	Master of Science (M.Sc.)

II. Nummerierte Aufstellung der eingereichten Schriften (Titel, Autoren, wo und wann veröffentlicht bzw. eingereicht):

1. **von Lautz AH**, Herding J, Ludwig S, Nierhaus T, Maess B, Villringer A and Blankenburg F (2017): Gamma and Beta Oscillations in Human MEG Encode the Contents of Vibrotactile Working Memory. Front. Hum. Neurosci. 11:576. doi: 10.3389/fnhum.2017.00576

2. **von Lautz AH**, Herding J and Blankenburg F (under review): Neuronal Signatures of a Random-Dot Motion Comparison task. Neuroimage

3. Herding J, Ludwig S, **von Lautz AH**, Spitzer B and Blankenburg F (under review): Centro-parietal EEG potentials index subjective evidence and difficulty during perceptual decision making. Neuroimage

III. Darlegung des eigenen Anteils der Schriften:

Die Bewertung des Eigenanteils richtet sich nach der Skala: “vollständig – überwiegend – mehrheitlich – in Teilen” und enthält nur für den jeweiligen Artikel relevante Arbeitsbereiche.

Zu II.1.: Konzeption (mehrheitlich), Versuchsdesign (mehrheitlich), Programmierung (überwiegend), Datenerhebung (mehrheitlich), Datenauswertung (überwiegend), Ergebnisdiskussion (überwiegend), Erstellen des Manuskriptes (überwiegend).

Zu II.2.: Konzeption (mehrheitlich), Versuchsdesign (überwiegend), Programmierung (vollständig), Datenerhebung (vollständig), Datenauswertung (überwiegend), Ergebnisdiskussion (überwiegend), Erstellen des Manuskriptes (überwiegend).

Zu II.3.: Konzeption (in Teilen), Versuchsdesign (in Teilen), Programmierung (in Teilen), Datenerhebung (in Teilen), Datenauswertung (in Teilen), Ergebnisdiskussion (in Teilen), Erstellen des Manuskriptes (in Teilen).

IV. Die Namen und Anschriften nebst E-Mail oder Fax der jeweiligen Mitautorinnen oder Mitautoren:

zu II.1.: Felix Blankenburg, Arbeitsbereich Neurocomputation and Neuroimaging, Fachbereich für Erziehungswissenschaft und Psychologie, Freie Universität Berlin, Habelschwerdter Allee 45, 14195 Berlin.
E-Mail: felix.blankenburg@fu-berlin.de

Simon Ludwig, Arbeitsbereich Neurocomputation and Neuroimaging, Fachbereich für Erziehungswissenschaft und Psychologie, Freie Universität Berlin, Habelschwerdter Allee 45, 14195 Berlin.
E-Mail: simonludwig@gmail.com

Jan Herding, Arbeitsbereich Neurocomputation and Neuroimaging, Fachbereich für Erziehungswissenschaften und Psychologie, Freie Universität Berlin, Habelschwerdter Allee 45, 14195 Berlin
jan.herding@bccn-berlin.de

Burkhard Maess, Max Planck Institute for Human Cognitive and Brain Sciences, Stephanstraße 1a, 04103 Leipzig
maess@cbs.mpg.de

Arno Villringer, Max Planck Institute for Human Cognitive and Brain Sciences, Stephanstraße 1a, 04103 Leipzig
villringer@cbs.mpg.de

Till Nierhaus, Arbeitsbereich Neurocomputation and Neuroimaging, Fachbereich für Erziehungswissenschaft und Psychologie, Freie Universität Berlin, Habelschwerdter Allee 45, 14195 Berlin.
till.nierhaus@fu-berlin.de

zu II.2.:

Felix Blankenburg, s.o.
Jan Herding, s.o.

zu II.3.:

Felix Blankenburg, s.o.
Simon Ludwig, s.o.
Jan Herding, s.o.

Bernhard Spitzer, Max-Planck-Institute für Bildungsforschung, Max Planck Institute for Human Development, Lentzeallee 94, Raum 130, 14195 Berlin
spitzer@mpib-berlin.mpg.de

Datum, Unterschrift des Doktoranden